UNIVERSITY OF LIVERPOOL

Isomerisation of alkanes over bifunctional Pt-heteropoly acid catalysts

Thesis submitted in accordance with the requirements of the University of Liverpool for the degree of Doctor of Philosophy by

Abdulrahman Abdullatif Alazman

April 2020

Abstract

Isomerisation of n-hexane was studied in the presence of acid and bifunctional metal-acid catalysts based on Keggin-type heteropoly acids (HPA), in particular focusing on $Cs_{2.5}H_{0.5}PW_{12}O_{40}$ (CsPW) and Pt/CsPW as the catalysts, using a fixed-bed microreactor under differential conditions (n-hexane conversion ≤ 10%) at 180-220 °C, ambient pressure and a ratio of n-hexane and H_2 partial pressures of 0.06-0.24. The turnover rate of HPA-catalysed isomerisation was found to correlate with the acid strength of HPA (initial enthalpy of ammonia adsorption). Bifunctional Pt-HPA catalysts were more efficient than monofunctional HPA catalysts. In the isomerisation over Pt/CsPW bifunctional catalyst, n-hexane dehydrogenation step was found to equilibrate at a molar ratio of Pt and H^+ surface sites $Pt_s/H^+ \geq 0.8$, corresponding to a Pt loading ≥ 6%. Bimetallic PtAu/CsPW catalyst showed higher activity in n-hexane isomerisation than Pt/CsPW, although the Au alone without Pt was inert. In the presence of Au, the turnover rate at Pt sites increased more than twofold. The effect of Au is attributed to PtAu alloying. Scanning transmission electron microscopy–energy dispersive X-ray spectroscopy (STEM-EDX) and X-ray diffraction (XRD) analyses of PtAu/CsPW indicated the presence of bimetallic PtAu nanoparticles with a wide range of Pt/Au atomic ratios.

Alongside, isomerisation of cyclohexane was investigated in the presence of monofunctional acid and bifunctional metal-acid catalysts based on Keggin-type heteropoly acid $H_3PW_{12}O_{40}$ and Pt and Au as the metal components using a differential fixed-bed microreactor at 180-300°C, ambient pressure and a C_6H_{12}/H_2 partial pressure ratio of 0.04-0.14. Particular emphasis was placed on the acidic Cs salt,

$Cs_{2.5}H_{0.5}PW_{12}O_{40}$ (CsPW) as the acid catalyst and Pt/CsPW, Au/CsPW and PtAu/CsPW as the bifunctional catalysts. Pt/CsPW and Au/CsPW were more efficient than the monofunctional acid catalyst CsPW, and Pt/CsPW more active than Au/CsPW, both giving >99% selectivity to methylcyclopentane. It was found that with Pt/CsPW, cyclohexane dehydrogenation step equilibrated at a molar ratio of Pt and H^+ surface sites $Pt/H^+ \geq 0.7$, which is much higher than for Pt/zeolite. PtAu/CsPW bimetallic catalyst exhibited a 2-fold higher activity in cyclohexane isomerization and a 3.5-fold higher activity in the accompanying dehydrogenation of cyclohexane to benzene than the mixture of Pt/CsPW and Au/CsPW with the same metal loading. The enhancing effect of gold is assigned to PtAu bimetallic particles, which had a higher Pt dispersion than the Pt in Pt/CsPW. STEM-EDX revealed bimetallic PtAu particles in PtAu/CsPW with a wide range of Pt/Au atomic ratios. No enhancing effect of gold was found in the case of carbon-supported catalyst PtAu/C physically mixed with CsPW, and the STEM-EDX analysis revealed no modification of Pt sites by Au in this catalyst.

Published papers:

1. A. Alazman, D. Belic, E.F. Kozhevnikova, I.V. Kozhevnikov, Journal of Catalysis 357 (2018) 80–89.
2. A. Alazman, D. Belic, A. Alotaibi, E.F. Kozhevnikova, I.V. Kozhevnikov, ACS Catalysis 9 (2019) 5063−5073.

Presentations:

1. A. Alazman, E. F. Kozhevnikova, I. V. Kozhevnikov, The UK Catalysis Conference (UKCC2018), Loughborough, UK, 2018.
2. A. Alazman, E. F. Kozhevnikova, I. V. Kozhevnikov, The UK Catalysis Conference (UKCC2019), Loughborough, UK, 2019.

Acknowledgment

I express personal gratitude to my supervisor Professor Ivan V. Kozhevnikov. Throughout my studies he has provided me with clear guidance, advice and support for the monitoring and accurate formulation of this thesis. I thank Dr. Elena F. Kozhevnikova, who without hesitation throughout my research assisted me to overcome any issues which I faced whilst running the laboratory work. I also extend my gratitude to the technical staff in the Department of Chemistry and to my wider colleagues at the University of Liverpool.

I am forever thankful to my parents who, from my earliest years to the present, have pushed me on this road to reach this level of study. I give a special thankyou to my lovely wife for her patience and her caring for our children when I was away from home.

Additionally, I thank *The Custodian of the Two Holy Mosques' Overseas Scholarship Program* of the Saudi Arabia government, which sponsored me to attend the University of Liverpool.

List of abbreviations

HPA	Heteropoly acid
HPW	$H_3[PW_{12}O_{40}]$
HSiW	$H_4[SiW_{12}O_{40}]$
CsPW	$Cs_{2.5}H_{0.5}[PW_{12}O_{40}]$
2MP	2-Methylpentane
3MP	3-Methylpentane
MCP	Methylcyclopentane
BET	Brunauer-Emmett-Teller method
BJH	Barrett-Joyner-Halenda method
TEM	Transmission electron microscopy
SEM	Scanning electron microscopy
STEM	Scanning transmission electron microscopy
XRD	X-ray diffraction
ICP-AES	Inductively coupled plasma atomic emission spectroscopy
TPR	Temperature programmed reduction
GC	Gas chromatography
GC-MS	Gas chromatography-mass spectroscopy
FID	Flame ionization detector
TCD	Thermal conductivity detector
TOS	Time on stream
TOF	Turnover frequency

Contents

Chapter 1. Introduction

1.1 Importance of catalysis

The root of the word catalysis comes from two Greek words: the prefix *cata* which means ‘down’ and the verb *lysein* which means ‘split’. A catalyst splits down the forces preventing the molecules from reacting [1].

The term catalysis was first used in 1836 by Berzelius [2] to explain the effect of porous platinum on the combustion of hydrogen and oxygen at a moderate temperature. He observed that certain components could speed up the reaction whilst remaining potentially unchanged. Further work on such substances has led to more definitions such as by Ostwald in 1894 [3], who defined the catalysts as “agents which accelerate chemical reactions without affecting the chemical equilibrium”. As the concept of catalysis became more developed, Bond [4] defined the catalyst as “a substance that increases the rate at which a chemical system approaches equilibrium, without being consumed in the process”.

The influences of catalysis are based on changing the reaction rate by lowering the energy of transition states or intermediates, through minimising the activation energy of the reaction that is required to convert the reactants to the products (Figure 1.1). Nevertheless, the thermodynamics of the reaction remains unchanged.

The interest in catalysis has recently grown as it is widely used in most chemical manufacturing processes with the increasing demand for new catalysts and catalytic processes, taking into account the desire for environmentally friendly technologies. This is driving significant research into this field.

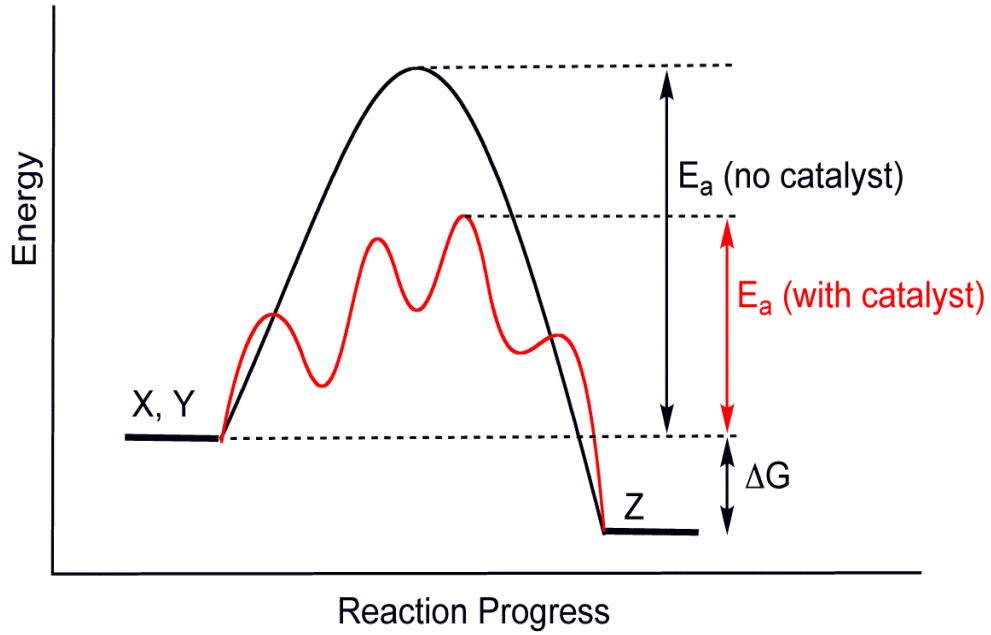

Figure 1.1 Activation energy for catalysed and uncatalysed reaction [5].

Catalysis can be grouped into three different classes depending on the nature of the catalyst and the reactants: homogeneous, heterogeneous and enzymatic or bio-catalysis. Homogeneous catalysis is where both the catalyst and the reactant are in the same phase. In homogeneous catalysis high selectivity of products can be easily achieved as the active sites of the catalysts are readily accessible. However, the separation of homogeneous catalysts from the reaction medium can be challenging, making such catalysts industrially less favourable [6].

1.2 Heterogeneous catalysis

In heterogeneous catalysis, both catalysts and reactants are in different phases, typically a solid catalyst with a liquid or gas reactant, for instance, a solid Fe catalyst employed in the production of ammonia from N_2 and H_2 [7]. The core differences between homogenous and heterogeneous catalysis are illustrated in Table 1.1.

Table 1.1 Comparison of homogeneous and heterogeneous catalysts [8].

Property	Heterogeneous	Homogeneous
Catalyst phase	Usually solid	Dissolved complex
Activity	Variable	High
Selectivity	Variable	High
Stability	Higher stability	Lower stability
Recovery	Easy	Difficult and expensive
Application	Wide	Limited

Heterogeneous catalysts can be bulk and supported. Examples of bulk catalysts are bulk metals, metal oxides and zeolites. Supported catalysts contain an active component immobilised on a support, for example Pt/Al_2O_3, where alumina support serves to increase Pt dispersion and, in addition, provides acid functionality.

Heterogeneous metal-containing catalysts are mainly defined by three different types: metals, metal oxides and metal sulphides. Metals are widely used in many industrial processes with such reactions as hydrogenation, oxidation and reduction of NO_X with hydrocarbons. Metal oxides are broadly utilised in oxidation reactions of hydrocarbons. Metal sulphides are mostly employed in the hydrodesulfurization of petroleum feedstocks.

Generally, heterogeneous catalytic reactions at the gas-solid interface include the following steps, as illustrated in Figure 1.2 [7, 8, 9]:

1. Diffusion of substrate molecules from the gas phase to the active sites on the catalyst surface.
2. Adsorption of substrate molecules on the surface.
3. Chemical reaction of substrate molecules to form products adsorbed on the catalyst surface.
4. Desorption of the products into the gas phase.

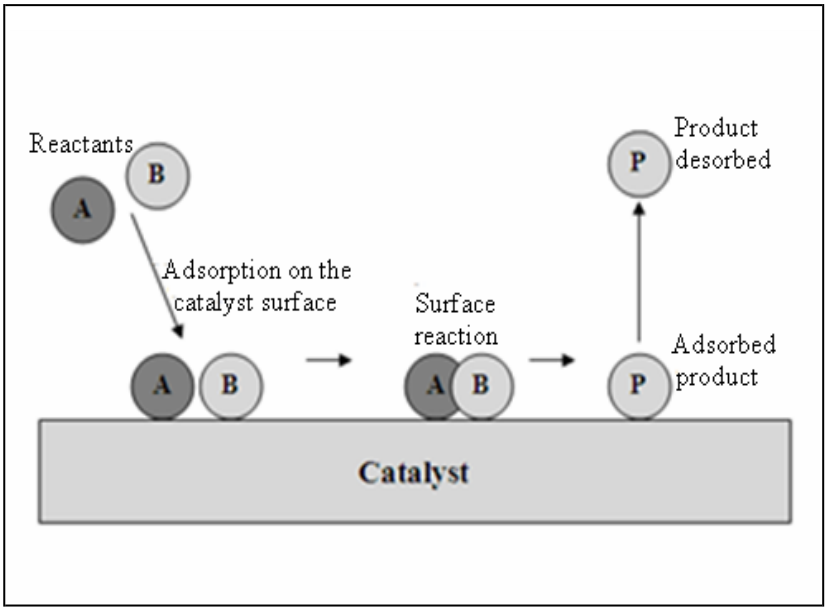

Figure 1.2 Typical steps of heterogeneous catalytic reactions [7].

1.3 Gold catalysis

Since the early days of catalysis, metals have been broadly used as catalysts. The most frequently used metals for catalysis are the 3d transition metals (Cu, Fe, Ni, and Co), the 4d transition metals (Ag, Pd, Rh and Ru) and the 5d transition metals (Pt, Ir, Re and W). Their catalytic activity can be attributed to orbital vacancies in the d-band. For group IB elements (Au, Ag, and Cu), in spite of having occupied orbitals, Ag and Cu have low ionisation potentials that make it easy to lose electrons to make vacancies in d-bands. In the case of gold, the ionisation potential is relatively high so that losing electrons is difficult, which leads to a low reactivity towards other elements [11, 12].

Accordingly, gold has been considered catalytically inactive and has attracted less attention in comparison to other prominent metals such as rhodium, platinum and

palladium which are large scale industrial catalysts, or silver and copper that are used in many large manufacturing processes such as the production of ethylene oxide and methanol, respectively [12].

This view about gold remained prevalent until Thendard and Dulong found that gold was a good catalyst for the decomposition of ammonia [13]. Chambers and Boudart used gold to dehydrogenate cyclohexane [14], which supported the work of Erkelens et al. [15]. In spite of all the previous studies, gold remained unpopular in catalysis field until the 1980s when Haruta discovered that gold was a highly effective catalyst for the oxidation of CO at very low temperature [16, 17]. First nanoparticle gold catalysts prepared by Haruta and co-workers were supported on iron oxide. Sermon et al. [18] had also a positive achievement when prepared supported gold on silica by the impregnation of $HAuCl_4$ solution on silica, then dried it and reduced under hydrogen thus producing a catalyst, which had small particles of gold that effectively catalysed the hydrogenation of olefins. These research proved that gold could be a suitable catalyst for certain reactions when dispersed in tiny particles on the surface of support. The preparation methods were found to play a significant role in controlling the size of gold particles, which was crucial to the activity of gold catalysts [19].

Prati and Porta used gold catalysts in the presence of molecular oxygen for the selective oxidation of alcohols [20]. In addition, Haruta and co-workers utilized gold supported on titania for the selective oxidation of propene to propylene oxide [12, 21]. Hutchings et al. reported that supported gold could be employed for direct production of hydrogen peroxide under mild conditions [22].

Particle size is essential in gold catalysis and it has been found that catalysts with relatively large gold particles are poorly active for reactions such as CO oxidation. The catalytic activity depends on three main factors: the size of the metal particles or the metal-alloy nanoparticles, the nature of the support carrying the metal and the interaction between the metal and the support or between the metals if there is more than one metal [23, 24]. There are other factors, such as the preparation method and chosen support, that must be taken into consideration for the synthesis of gold nanoparticles to guarantee high activity of the catalyst.

Impregnation is a simple and straightforward method that can be used to prepare supported gold catalysts where the pores of the support are filled by the gold precursor solution. In this method, a solution of the gold precursor is stirred with the support and forms particles of gold that have a size between 10 to 35 nm. The gold precursors used are commonly chloroauric acid ($HAuCl_4$) and gold chloride ($AuCl_3$). These catalysts have been successfully applied for the oxidation of alcohols and the direct synthesis of hydrogen peroxide. However such catalysts are poor for CO oxidation due to the presence of chloride ions that poison them. Chloride ions can be removed as HCl by reduction with H_2 [25, 26].

The support plays a crucial role in obtaining the required nanoparticle size and morphology. There are various types of supports such as Al_2O_3, SiO_2, TiO_2, CeO_2, zircona, graphite and activated carbon, which have all been employed for gold catalysts. Choosing the support and observing the relationship between the support and the method of preparation are vital in determining the features of the catalysts produced [23].

Gold, palladium and gold-palladium alloy catalysts have been studied widely in recent decades. The efficiency of a catalyst relies on the degree of activity, selectivity and stability towards forming the main product in chemical reactions. The effect of the support on catalyst activity can clearly be observed in case of the oxidation of benzyl alcohol and glycols [26]. Paalanen, Weckhuysen and Sankar [27] have reported that three crucial parameters play a central role in determining the selectivity, activity and stability of AuPd supported nanoparticle catalysts, namely: the dimension of metal particles, the constitutional alteration within the two metals and the combination of the matrix of the two metal nanoparticles.

Generally, catalytic activity significantly increases when bimetallic catalysts are used, compared to monometallic ones. For example, supported gold-palladium alloys have been reported to be very efficient catalysts for redox reactions due to the specific selectivity coming from the gold particles and the high activity from palladium particles. Au-Pd catalysts often have activity, selectivity and stability that are higher compared to monometallic counterparts, for example, for the oxidation of alcohols and polyols [28].

1.4 Multifunctional catalysis

The drive for sustainable development, which takes into consideration both economic and environmental issues, stimulates catalysis researchers to improve catalytic processes and enhance catalyst synthesis. A cascade reaction (domino reaction or tandem reaction) is a key concept in the chemical processes that assists reducing the number of operations to provide time and cost advantages [29].

Applying cascade conversions to reduce the intermediate recovery steps by combining catalytic reactions in a one-pot process is the current trend to carry out sustainable organic synthesis with high efficiency. The concept of cascade conversions implies that the final product can be obtained without passing through a multistep traditional organic reaction [30].

In the step-by-step process, separation and purification of intermediates in every single step can cost a considerable expense to remove waste, along with the time consumed for every step. Figure 1.3 shows the conversion and recovery steps in a traditional organic system (solid arrows) and in a cascade one-pot process (broken arrows) [30, 31].

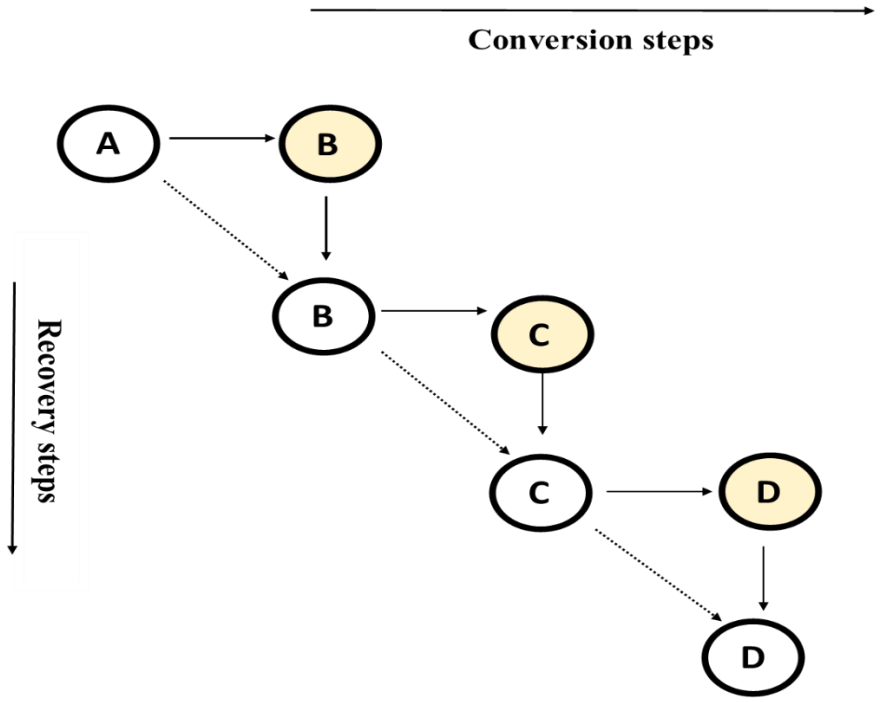

Figure 1.3 The conversion and recovery steps in traditional organic system (solid arrows) and cascade process (broken arrows).

The design of multifunctional catalysts is an important step in the development of cascade processes. Multifunctional catalysts have two or more types of active sites, which can catalyse simultaneously different reactions in a one-pot process. A variety of multifunctional catalysts have been developed to be used in many organic and petrochemical syntheses [32].

In addition, the cascade systems can overcome thermodynamic barriers in the multistep processes (Figure 1.4) [30]. Combining equilibrium-limited endothermic (uphill in energy) steps A → B and B → C with exothermic (downhill) step C → D can drive the cascade process A → D forward.

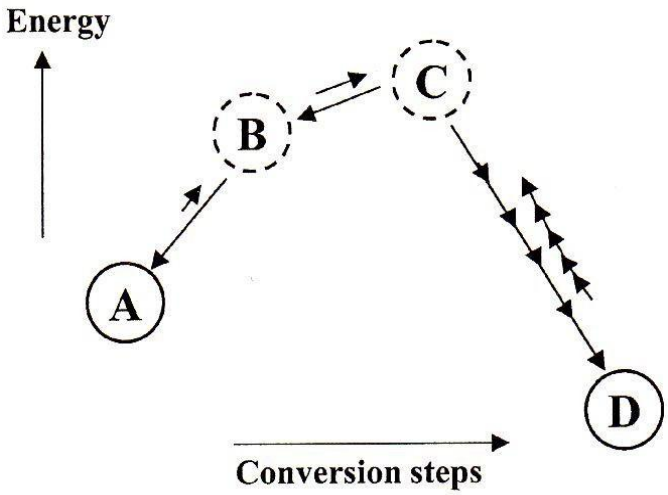

Figure 1.4 Potential energy diagram of the cascade process to tackle thermodynamic barriers in multistep synthesis.

The design of multifunctional catalysts is often based on utilising one or more noble metals supported on an acidic or basic support. The choice of metals and supports depends mainly on the nature of reaction. The major challenge in preparing such catalysts is the precision needed to retain the active sites unaffected by various reaction conditions over time [33].

1.5 Heteropoly acids

1.5.1 Introduction to heteropoly acids

Heteropoly acids (HPA) can be defined as a type of Brønsted acid composed of polyoxometalate anions, which contain oxygen with specific metals and non-metals. The polyoxometalate anions have a general formula $[X_xM_mO_y]^{q-}$ ($x \leq m$), where X is the heteroatom such as Si^{4+}, Ge^{4+}, P^{5+}, B^{3+} and As^{5+} and M is a metal ion referred to as the addenda atom such as W (VI), Mo (VI) and V (V) or a combination of these metals. Due to the various combinations of X and M being formed, there is a wide variety of HPAs adopting different structures [34].

The first heteropoly acid was discovered in 1826 by Berzelius. Subsequently, various heteropoly compounds were synthesised and their structures determined. In 1934, Keggin solved the structure of the most important type of HPA [24], which was named after him. There are also other structural types such as Wells-Dawson, Dexter-Silverton, Anderson-Evans and others [35].

Heteropoly acids have been used in many different applications, particularly in catalysis, due to their strong Brønsted acidity. HPAs are stronger acids than conventional acids like zeolites and metal oxides. In addition to having strong acidity, HPAs have unique structural mobility and multifunctionality that have led to a great number of applications. The most common type of HPA used in commercial applications are the Keggin HPAs $H_3PW_{12}O_{40}$ and $H_4SiW_{12}O_{40}$ which are fairly stable and easily available [34].

1.5.2 Keggin structure

The Keggin structure is adopted by the most common and most important for catalysis heteropoly acids. These are the most stable and easily available HPAs. The Keggin structure was the first HPA structure determined using x-ray diffraction by Keggin in 1934 [29]. The Keggin heteropolyanions are represented by the formula $[XM_{12}O_{40}]^{x-8}$, where X is the central atom (commonly Si^{4+}, P^{5+}, etc.), *x* its oxidation state and M is the metal ion (most commonly W^{6+} and Mo^{6+}). The structure of the Keggin heteropolyanion $PW_{12}O_{40}^{3-}$ is shown in Figure 1.5 [36, 37].

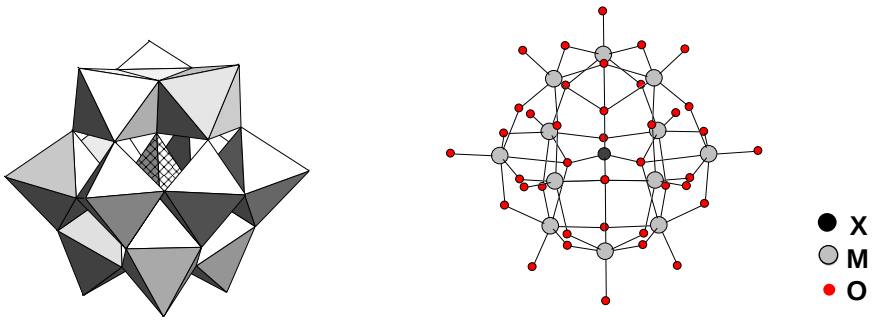

Figure 1.5 The Keggin structure of $PW_{12}O_{40}^{-3}$.

1.5.3 Thermal stability of HPAs

The thermal stability of heteropoly acids is an important feature, which enables them to be used extensively as heterogeneous catalysts. HPAs are relatively stable and usable at moderately high temperatures up to 300-350 °C. Nevertheless, their use is challenged during catalyst regeneration via decoking process, which requires high temperature treatment (about 500 °C) to burn coke formed on the catalyst surface [35].

There are many techniques to estimate the thermal stability of HPAs such as thermogravimetric analysis (TGA), differential thermal analysis (DTA), differential scanning calorimetry (DSC), infrared spectroscopy (IR), X-ray diffraction (XRD) and solid state NMR. One way to analyse thermal stability is by measuring the thermal decomposition temperature at which all acidic protons are released in a multistage process, as presented in Scheme 1.3 [29].

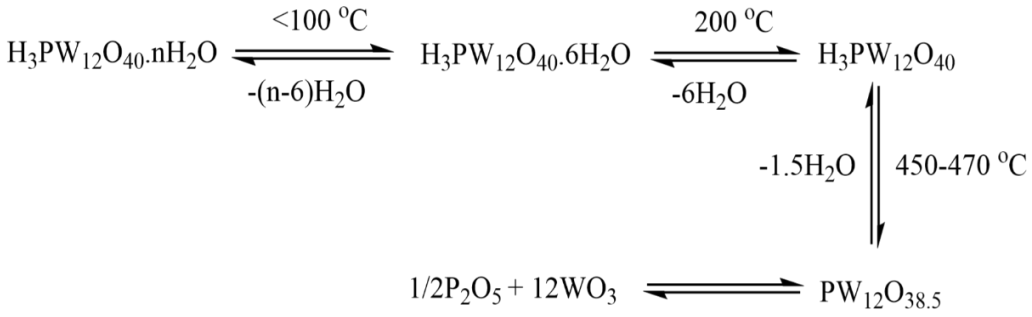

Scheme 1.3 Thermal decomposition of $H_3PW_{12}O_{40}$ hydrate.

Generally, the Keggin acids are the most thermally stable compounds among different HPAs. Here is the order of stability for some common Keggin HPAs in terms of the decomposition temperature (°C), as estimated from TGA [29, 38]:

$H_3PW_{12}O_{40} > H_4SiW_{12}O_{40} > H_3PMo_{12}O_{40} > H_4SiMo_{12}O_{40}$

(465 °C) (445 °C) (375 °C) (350 °C)

1.5.4 Acidity of HPAs

Hetropoly acids are very strong Brønsted acids when compared to conventional solid acids like H_3PO_4/SiO_2 or metal oxides and zeolites. The proton sites in HPA are responsible for their high catalytic activity. The acidity of HPAs mostly comes from the following sources [29, 39, 40]:

- Proton sites in the HPA ($H_3PW_{12}O_{40}$) or its salts ($Cs_{2.5}H_{0.5}PW_{12}O_{40}$).
- Lewis acid sites in the metal counter cations like ($La^{III}[PMo_{12}O_{40}]$).
- Proton sites produced on salt reduction:

$$Pd_2[SiW_{12}O_{40}] + 4\,[H] \rightarrow 2\,Pd^0 + H_4[SiW_{12}O_{40}]$$

- Proton sites produced by a partial hydrolysis of polyanions:

$$[PW_{12}O_{40}]^{3-} + 2\,H_2O \rightarrow [PW_{11}O_{39}]^{7-} + [WO_3] + 4\,H^+$$

- Proton sites formed from dissociation of water coordinated to counter cation:

$$Ln(H_2O)_n^{3+} \rightarrow Ln(H_2O)_n(OH)^{2+} + H^+$$

Two types of proton sites exist in solid HPAs. These are hydrated protons and non-hydrated protons (Figure 1.6) [34]. The hydrated protons have a very high mobility

and are responsible for very high conductivity of HPA hydrates. In contrast, the non-hydrated protons are firmly localised on the peripheral oxygen atoms in the polyanion.

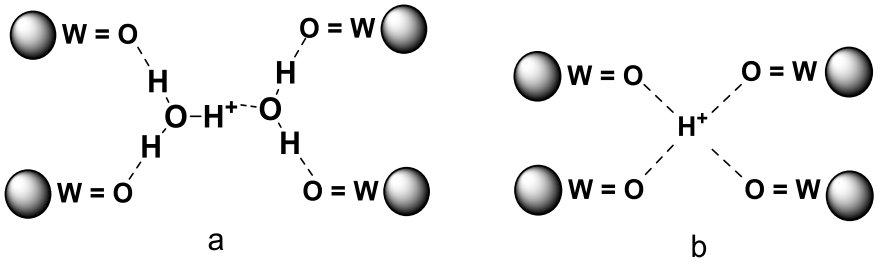

Figure 1.6 Schematic structures of (a) bulk proton sites in $H_3PW_{12}O_{40}.6H_2O$ and (b) in anhydrous $H_3PW_{12}O_{40}$.

Proton sites localised on the surface of HPAs are responsible for high activity of HPAs as heterogeneous acid catalysts. Crystalline HPAs in general have low surface area (usually 1-5 $m^2\ g^{-1}$) and low porosity (<0.1 $cm^3\ g^{-1}$). To extend the surface area they are supported on a neutral porous support like silica and carbon, which can expose the proton sites localised on the oxygen bridges [29, 39, 41].

The acid properties of HPAs and their salts can be characterised by thermal desorption of basic molecules such as pyridine and ammonia. For example, the adsorbed pyridine molecules on the surface of SiO_2-Al_2O_3 are fully desorbed at 300 °C, whereas they stay adsorbed as pyridinium ions on the surface of $H_3PW_{12}O_{40}$ at much higher temperatures. This shows the strength of acidity of $H_3PW_{12}O_{40}$ compared to SiO_2-Al_2O_3 [36].

Izumi et al. have reported the order of acid strength for Keggin heteropoly acids using temperature-programmed desorption (TPD) of ammonia [42]:

$H_3PW_{12}O_{40}$ > $H_4SiW_{12}O_{40}$ > $H_3PMo_{12}O_{40}$ > $H_4SiMo_{12}O_{40}$

592 °C 532 °C 463 °C 423 °C

The nature of counter cations in HPA salts have significant effect on their properties such as acidity, solubility, porosity and thermal stability. The salts with smaller cations, such as Li^+ (0.68 Å) and La^{3+} (1.02 Å), are non-porous, highly soluble in water and have lower surface area (commonly < 10 $m^2 g^{-1}$), whereas the salts with larger cations, such as Cs^+ (1.67 Å) and NH_4^+ (1.43 Å), have bimodal porosity, are poorly soluble in water and have higher surface areas (> 100 $m^2 g^{-1}$) [34, 35].

Okuhara et al. have found that $Cs_{2.5}H_{0.5}PW_{12}O_{40}$ has a comparatively high surface area (100-200 $m^2 g^{-1}$) and strong acid sites, which makes it efficient solid acid catalyst [36, 42, 43]. Figure 1.7 shows the effect of composition of $Cs_{3-x}H_xPW_{12}O_{40}$ salts on their surface area and acidity.

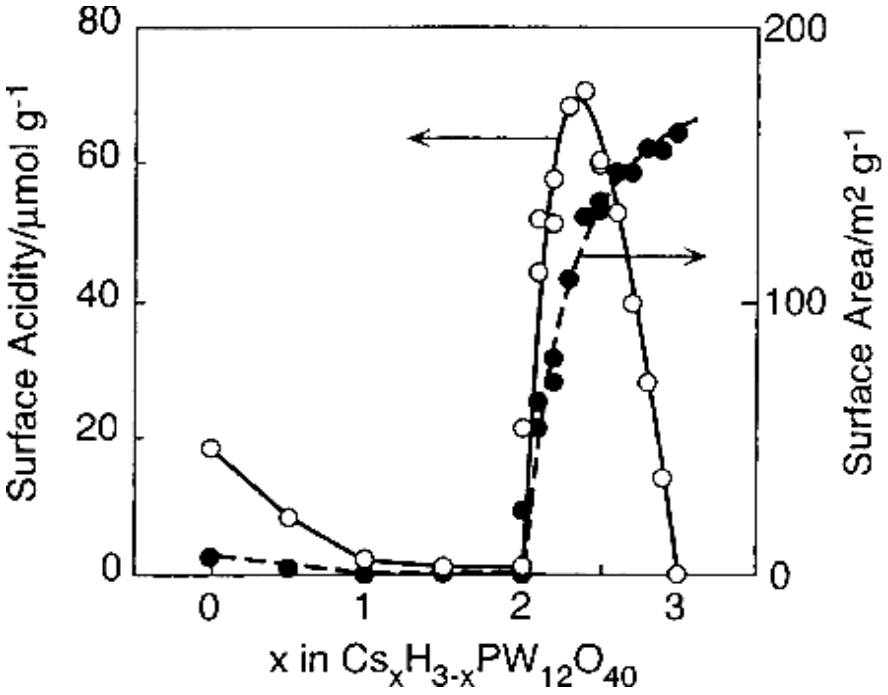

Figure 1.7 Surface acidity and surface area of $Cs_xH_{3-x}PW_{12}O_{40}$ as a function of Cs content, *x* [37].

1.5.5 HPAs in multifunctional catalysts

The diversity of properties of HPAs and their salts allows them to be part of many multifunctional catalysts. For instance, the HPA salt $Cs_{2.5}H_{0.5}PW_{12}O_{40}$ has strong acid sides and a relatively high surface area, which permit it to be widely used as an acidic carrier of transition metals to form multifunctional catalysts to be employed in multistage reactions.

Okuhara and co-workers studied the isomerisation of n-alkanes over multifunctional catalysts, consisting of $Cs_{2.5}H_{0.5}PW_{12}O_{40}$ and noble metals [37]. Hetterley et al. showed that when $Cs_{2.5}H_{0.5}PW_{12}O_{40}$ is combined with Pd metal it becomes an efficient bifunctional catalyst, which converts acetone to methyl isobutyl ketone (MIBK) in the multistage reaction (Figure 1.9) [45]. Alhanash et al. reported an efficient bifunctional catalyst Ru–$Cs_{2.5}H_{0.5}PW_{12}O_{40}$ for the formation of 1,2- propanediol from glycerol hydrogenolysis [46]. Both Pd-loaded and Pt-loaded solid HPAs are employed in n-alkane isomerisation [47]. In an investigation into deactivation and regeneration of HPAs in organic reactions, Kozhevnikov et al. found that doping HPAs with Pt group metals can reduce the temperature of coke burning to 350 °C, which is lower than the decomposition temperature of HPAs (about 500 °C) [48, 49].

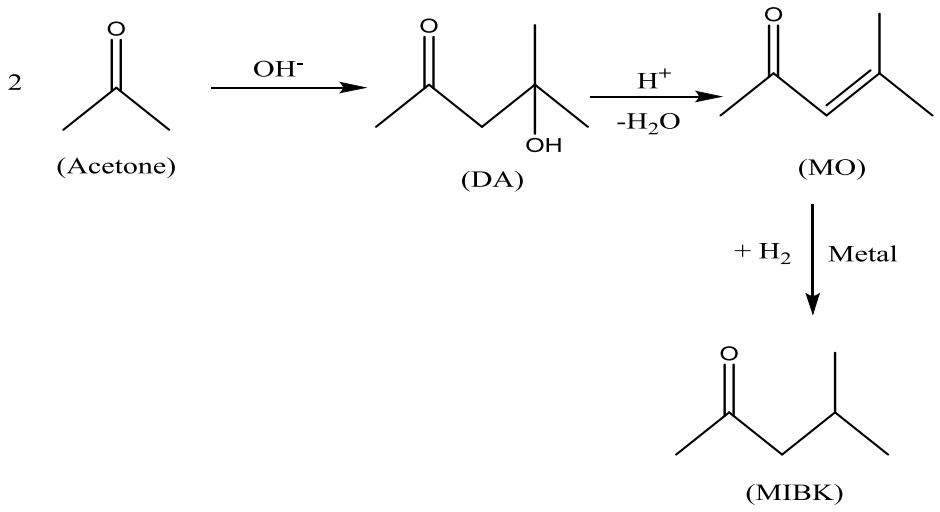

Scheme 1.8 MIBK formation over multifunctional catalysts.

1.6 Alkane isomerisation

The petrochemical industry is almost entirely catalysis oriented. The key reason for this is that in petrochemical syntheses catalytic paths are more effective for the control of selectivity than direct thermal reactions. The increasing usage of gasoline with projected future shortages of crude oil has forced the refinery industries to find processes and methods to maximise the benefits of the oil. This includes the need for improving burning efficiency in fuel combustion engines by using high-octane gasoline [50].

The octane number has been constructed by comparing a gasoline with a blend of iso-octane and n-heptane. This showed that compounds with branched-chain hydrocarbon molecules have a high octane number and ones with straight-chain molecules have a low octane number. The quality of gasoline is now based on the availability of the high-octane constituents. Therefore, the best gasoline could be obtained from crude oil through catalytic processes such as cracking, alkylation, reforming and isomerisation [51].

Interest in isomerisation within the refinery industry started relatively late as the efficiency of gasoline in automobiles had long been improved by adding certain additives, such as tetraethyl lead (TEL) and tetramethyl lead (TML), to the refined gasoline, which increased the octane number. However, such additives caused harm on the environment through emissions released by the burning processes in automobiles. The increasing demand for high-octane gasoline and finding dual-purpose catalysts for naphtha reforming, taking into account environmental protection, have increased interest in isomerisation processes. Hence, the production of branched-chain

hydrocarbons from straight-chain ones via catalysis became essential and integral for the petroleum industry [50-53].

The term isomerisation was brought into organic chemistry by Berzelius in the early eighteenth century, and the reaction was further developed by Markovnikov in 1865. Isomerisation is a chemical reaction that occurs through rearranging atomic bonds within the molecules. In this reaction straight-chain molecules are converted to branched forms whilst keeping the same molecular formula. In skeletal isomerisation, linear paraffins are converted into branched paraffins with the same carbon numbers and cycloparaffins are converted to more branched naphthenes. Such compounds are called isomers [54, 55].

Isomerisation reactions are dependent upon a number of parameters, including temperature, flow rate, pressure, hydrogen/hydrocarbon molar ratio, catalyst activity, substrate composition and impurity content [56].

Improving octane number of C_5-C_6 hydrocarbons requires an isomerisation process to convert the straight-chain alkanes to the branched isomers. To achieve this, a highly effective catalyst is required operating at the lowest possible temperature. Isomerisation of n-alkanes occurs on bifunctional metal-acid catalysts. It starts with alkane dehydrogenation on the metal sites, followed by isomerisation of the olefin formed on the acid sites via a carbocation (carbenium ion) intermediate. The iso-olefin formed is then hydrogenated on the metal sites to produce the branched alkane. Platinum is generally used as the metal component and acidic supports such as chlorinated alumina and zeolite are used as the acid component in bifunctional

isomerisation catalysts. Hydrogen is often supplied to minimise coke formation in this process.

The isomerisation of alkanes can also be catalysed by strong acids in the absence of the metal. The mechanism of alkane isomerisation on monofunctional acid catalysts involves chain initiation to form active carbocations, which rearrange toward the chain propagation. This transformation may involve other possible side reactions such as alkylation or cracking [57]. In liquid superacids, the initial step proceeds by eliminating a H^- from the alkane molecule. The isomerisation reaction does not occur in the absence of a strong enough acid [58, 59]. The second step in the cycle is skeletal isomerisation of carbenium ions, which occurs via protonated cyclopropane (PCP) rearrangement. Only n-alkanes, having longer than the C_4 chain, can be rearranged through the PCP intermediate. In the chain propagation step, the rearranged carbenium ions can abstract a H^- from an alkane to form the isoalkane and a fresh carbenium ion [60].

The isomerisation of alkanes on bifunctional metal-acid catalysts occurs through dehydrogenation of alkane on the metal sites to form an olefin intermediate (Equation 1.1) [60, 61].

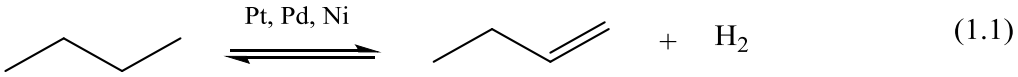

(1.1)

Then the olefin is protonated to form carbenium ion on acid sites (Equation 1.2).

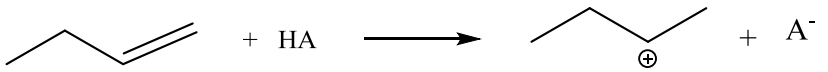

(1.2)

Next, the carbenium ion undergoes skeletal isomerisation via cyclopropyl intermediate (Equation 1.3).

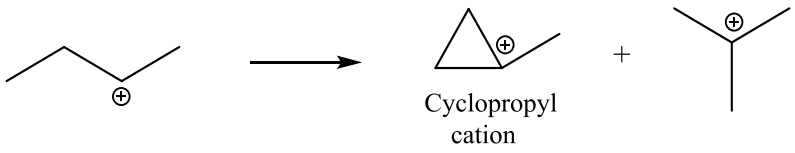

(1.3)

The iso-alkyl carbenium ion is then converted to iso-olefin intermediate through proton elimination (Equation 1.4).

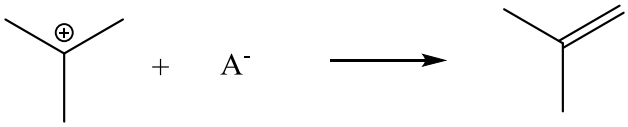

(1.4)

In the last step, the formed iso-olefin intermediate is hydrogenated to form iso-alkane on the catalyst metal sites (Equation 1.5).

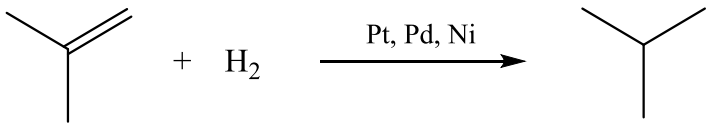

(1.5)

The key in the development of isomerisation catalysts is choosing appropriate acid. Bulk HPAs and their acidic salts have very strong acid sites. $H_3PW_{12}O_{40}$ is the strongest HPA and it is most often used in catalytic applications [35].

Misono and co-workers examined the effectiveness of Pt-doped $Cs_{2.5}H_{0.5}PW_{12}O_{40}$ as a catalyst for the isomerisation of n-pentane [62]. Essayem et al. found that under certain conditions the activity and selectivity of Pt + $Cs_{2.5}H_{0.5}PW_{12}O_{40}$ were noticeably higher than those of Pt-doped H-ZSM-5 or SO_4^{2-}/ZrO_2 [64].

1.7 Cycloalkane isomerisation

Cycloalkane isomerisation was first studied at the end of the eighteenth century by Markovnikov and co-workers [54, 55]. Cycloalkane isomerisation contributes significantly to the improvement of the quality of gasoline production. Naphthene isomerisation reactions, for instance cyclohexane isomerisation, is a process prevalent in oil refinery to produce branched products [51].

Initially, the isomerisation of cyclohexane to methylcyclopentane was carried out using only acid catalysts such as aluminium chloride, boron trifluoride and others. This process, however, was restricted to the temperatures below 150 °C due to catalyst volatility and activity towards cracking as well as catalyst corrosiveness. Bifunctional

metal-acid catalysts are efficient for the isomerisation of cycloalkanes at relatively high temperatures between 340 °C to 540 °C. However, at these temperatures, cyclohexane isomerisation is accompanied by dehydrogenation to form benzene and hydrocracking, which reduce the yield of methylcyclopentane [65].

The bifunctional metal-acid catalysts allow overcoming costly conditions that are required in the cycloalkane isomerisation process, such as high pressure and temperature and to minimise the formation of side products. Platinum/zeolite and platinum on chlorinated alumina are highly effective isomerisation catalysts. But these catalysts have some defects: Pt/zeolite requires a high temperature and $Pt/Al_2O_3(Cl)$ is highly sensitive to the feed contaminants. Zirconium dioxide is also used for the isomerisation processes, although it has a high rate of deactivation [66].

The bifunctional mechanism for the isomerisation of cycloalkanes has been proposed by Keulemans and Voge (1959) [66] and Sinfelt (1964) [68]. This mechanism will be discussed later in this thesis (Chapter 4 and 5).

1.8 Objectives and thesis outline

The need for a substantial improvement of alkane and cycloalkane isomerisation for the benefit of petroleum industry to lower the consumption of oil and to protect the environment is a challenge for both industrial and academic research.

The aim of our study is to gain a better understanding of bifunctional metal-acid catalysis for the isomerisation of n-hexane and cyclohexane. Here, we investigate vital reaction pathways of the gas-phase isomerisation of n-hexane and cyclohexane in

the presence of bifunctional metal-acid catalysts based on Keggin heteropoly acids using a fixed-bed continuous flow reactor. The selected HPAs, which are chosen as acid components for this study, are tungstophosphoric heteropoly acid $H_3PW_{12}O_{40}$ and its acidic caesium salt $Cs_{2.5}H_{0.5}PW_{12}O_{40}$. Pt, Au and AuPt bimetallics are the chosen metal components. In addition, this study investigates the effect of Au additives to Pt in the bifunctional metal-acid catalysts on the performance stability, selectivity and turnover reaction rate. Furthermore, kinetics of n-hexane and cyclohexane isomerisation over bifunctional metal-acid catalysts is studied to elucidate the effect of diverse reaction parameters such as the temperature, pressure and catalyst loading.

The catalysts are prepared following conventional procedures and characterised using various techniques such as X-ray diffraction (XRD), surface area and porosity measurements (BET), inductively coupled plasma atomic emission spectroscopy (ICP-AES), hydrogen chemisorption, temperature programmed desorption (TPD) and scanning transmission electron microscopy (STEM).

Chapter 1 presents a literature review focussing on the importance of catalysts, the principle mechanism of heterogeneous catalysis, a brief background of catalysis by gold and a concept of multifunctional catalysis. This chapter also discusses the chemistry of heteropoly acids and their catalytic properties, along with alkane and cycloalkane hydroisomerisation.

Chapter 2 provides the preparation procedures for the catalysts used in this work. It also outlines the methods and techniques which are utilised to characterise the prepared catalysts. The fixed-bed reactor setup with on-line GC analysis, reaction conditions and methodology for the catalyst testing are also described.

Chapter 3 contains the results of catalyst characterisation using BET, XRD, ICP-AES, STEM, TPD and other techniques.

Chapter 4 describes the investigation of n-hexane isomerisation in the gas phase over bifunctional Pt-hetropoly acid catalysts and the enhancing effect of gold additives.

Chapter 5 describes the investigation of cyclohexane isomerisation in the gas phase over Pt-, Au- and PtAu-hetropoly acid catalysts.

Chapter 6 summarizes the results obtained and gives some ideas for the future work.

References

[1] B. Lindström, L.J. Pettersson, A brief history of catalysis, Cattech, 7 (2003) 130-138.

[2] J. Berzelius, Considerations respecting a new power which acts in the formation of organic bodies, Edinburgh New Philosophical Journal, 21 (1836) 223-228.

[3] W. Ostwald, Definition der katalyse, Zeitschrift für Physikalische Chemie, 15 (1894) 705-706.

[4] G.C. Bond, Heterogeneous catalysis: principles and applications 2nd Ed, Oxford Science, 1987.

[5] https://en.wikipedia.org/wiki/Catalysis

[6] I. Chorkendorff, J.W. Niemantsverdriet, Concepts of modern catalysis and kinetics, John Wiley & Sons, 2017.

[7] M. Bowker, The basis and applications of heterogeneous catalysis, Oxford Science Publication, 1998.

[8] B. Cornils, W.A. Herrmann, Aqueous-phase organometallic catalysis: concepts and applications, John Wiley & Sons, 2004.

[9] D.J. Cole-Hamilton, Homogeneous catalysis new approaches to catalyst separation, recovery, and recycling, Science, 299 (2003) 1702-1706.

[10] G. Rothenberg, Catalysis: concepts and green applications, John Wiley & Sons, 2017.

[11] A.G. Sault, R.J. Madix, C.T. Campbell, Adsorption of oxygen and hydrogen on Au (110)-(1× 2), Surface science, 169 (1986) 347-356.

[12] M. Haruta, When gold is not noble: catalysis by nanoparticles, The chemical record, 3 (2003) 75-87.

[13] P. Dulong, L. Thenard, Note sur la Propriété que Possèdent Quelques Métaux de faciliter la combinaison des fluides élastiques, Annales de Chimie, 2 (1823) 440-444.

[14] R.P. Chambers, M. Boudart, Selectivity of gold for hydrogenation and dehydrogenation of cyclohexene, Journal of Catalysis, 5 (1966) 517-528.

[15] J. Erkelens, C. Kemball, A. Galwey, Some reactions of cyclohexene with hydrogen and deuterium on evaporated gold films, Transactions of the Faraday Society, 59 (1963) 1181-1191.

[16] M. Haruta, T. Kobayashi, H. Sano, N. Yamada, Novel gold catalysts for the oxidation of carbon monoxide at a temperature far below 0 C, Chemistry Letters, 16 (1987) 405-408.

[17] M. Haruta, N. Yamada, T. Kobayashi, S. Iijima, Gold catalysts prepared by coprecipitation for low-temperature oxidation of hydrogen and of carbon monoxide, Journal of Catalysis, 115 (1989) 301-309.

[18] P.A. Sermon, G.C. Bond, P.B. Wells, Hydrogenation of alkenes over supported gold, Journal of the Chemical Society, 75 (1979) 385-394.

[19] J. Regalbuto, Catalyst preparation: science and engineering, CRC Press, 2016.

[20] L. Prati, F. Porta, Oxidation of alcohols and sugars using Au/C catalysts: Part 1. Alcohols, Applied Catalysis A: General, 291 (2005) 199-203.

[21] M. Chen, D.W. Goodman, The structure of catalytically active gold on titania, Science, 306 (2004) 252-255.

[22] G.J. Hutchings, Nanocrystalline gold and gold palladium alloy catalysts for chemical synthesis, Chemical Communications, (2008) 1148-1164.

[23] P.J. Miedziak, Q. He, J.K. Edwards, S.H. Taylor, D.W. Knight, B. Tarbit, C.J. Kiely, G.J. Hutchings, Oxidation of benzyl alcohol using supported gold–palladium nanoparticles, Catalysis Today, 163 (2011) 47-54.

[24] J.A. Lopez-Sanchez, N. Dimitratos, P. Miedziak, E. Ntainjua, J.K. Edwards, D. Morgan, A.F. Carley, R. Tiruvalam, C.J. Kiely, G.J. Hutchings, Au–Pd supported nanocrystals prepared by a sol immobilisation technique as catalysts for selective chemical synthesis, Physical Chemistry Chemical Physics, 10 (2008) 1921-1930.

[25] D.I. Enache, J.K. Edwards, P. Landon, B. Solsona-Espriu, A.F. Carley, A.A. Herzing, M. Watanabe, C.J. Kiely, D.W. Knight, G.J. Hutchings, Solvent-free oxidation of primary alcohols to aldehydes using Au-Pd/TiO_2 catalysts, Science, 311 (2006) 362-365.

[26] D.I. Enache, D.W. Knight, G.J. Hutchings, Solvent-free oxidation of primary alcohols to aldehydes using supported gold catalysts, Catalysis Letters, 103 (2005) 43-52.

[27] P. Paalanen, B.M. Weckhuysen, M. Sankar, Progress in controlling the size, composition and nanostructure of supported gold–palladium nanoparticles for catalytic applications, Catalysis Science & Technology, 3 (2013) 2869-2880.

[28] L. Prati, A. Villa, C.E. Chan-Thaw, R. Arrigo, D. Wang, D.S. Su, Gold catalyzed liquid phase oxidation of alcohol: the issue of selectivity, Faraday Discussions, 152 (2011) 353-365.

[29] I.V. Kozhevnikov, Sustainable heterogeneous acid catalysis by heteropoly acids, Handbook of Green Chemistry: Online, (2010) 153-174.

[30] A. Bruggink, R. Schoevaart, T. Kieboom, Concepts of nature in organic synthesis: cascade catalysis and multistep conversions in concert, Organic Process Research & Development, 7 (2003) 622-640.

[31] D.E. Fogg, E.N. dos Santos, Tandem catalysis: a taxonomy and illustrative review, Coordination Chemistry Reviews, 248 (2004) 2365-2379.

[32] J. C. Wasilke, S.J. Obrey, R.T. Baker, G.C. Bazan, Concurrent tandem catalysis, Chemical Reviews, 105 (2005) 1001-1020.

[33] M.J. Climent, A. Corma, S. Iborra, Heterogeneous catalysts for the one-pot synthesis of chemicals and fine chemicals, Chemical Reviews, 111 (2010) 1072-1133.

[34] I.V. Kozhevnikov, Catalysis by heteropoly acids and multicomponent polyoxometalates in liquid-phase reactions, Chemical Reviews, 98 (1998) 171-198.

[35] I.V. Kozhevnikov, Catalysts for fine chemical synthesis, catalysis by polyoxometalates, John Wiley & Sons, 2002.

[36] S.P. Jiang, Functionalized mesoporous structured inorganic materials as high temperature proton exchange membranes for fuel cells, Journal of Materials Chemistry A, 2 (2014) 7637-7655.

[37] T. Okuhara, N. Mizuno, M. Misono, Catalytic chemistry of heteropoly compounds, Advances in Catalysis, 41 (1996) 113-252.

[38] R. Prins, A. Wang, X. Li, Introduction to Heterogeneous Catalysis, World Scientific Publishing Company, 2016.

[39] N. Mizuno, M. Misono, Heterogeneous catalysis, Chemical Reviews, 98 (1998) 199-218.

[40] M.T. Pope, Heteropoly and isopoly oxometalates, Springer-Verlag, 1983.

[41] J.B. Moffat, Metal-oxygen clusters: the surface and catalytic properties of heteropoly oxometalates, Springer Science & Business Media, 2006.

[42] Y. Izumi, R. Hasebe, K. Urabe, Catalysis by heterogeneous supported heteropoly acid, Journal of Catalysis, 84 (1983) 402-409.

[43] T. Okuhara, T. Nishimura, H. Watanabe, M. Misono, Insoluble heteropoly compounds as highly active catalysts for liquid-phase reactions, Journal of Molecular Catalysis, 74 (1992) 247-256.

[44] T. Okuhara, T. Nishimura, H. Watanabe, K. Na, M. Misono, Novel catalysis of cesium salt of heteropoly acid and its characterization by solid-state NMR, Studies in Surface Science and Catalysis, 90 (1994) 419-428.

[45] R.D. Hetterley, E.F. Kozhevnikova, I.V. Kozhevnikov, Multifunctional catalysis by Pd-polyoxometalate: one-step conversion of acetone to methyl isobutyl ketone, Chemical Communications, (2006) 782-784.

[46] A. Alhanash, E.F. Kozhevnikova, I.V. Kozhevnikov, Hydrogenolysis of glycerol to propanediol over Ru: polyoxometalate bifunctional catalyst, Catalysis Letters, 120 (2008) 307-311.

[47] K. Na, T. Okuhara, M. Misono, Skeletal isomerization of n-butane over caesium hydrogen salts of 12-tungstophosphoric acid, Journal of the Chemical Society, Faraday Transactions, 91 (1995) 367-373.

[48] M. Musawir, E.F. Kozhevnikova, I.V. Kozhevnikov, Fries rearrangement of phenyl acetate catalysed by platinum-doped heteropoly salt: Catalyst regeneration and reuse, Journal of Molecular Catalysis A: Chemical, 262 (2007) 93-97.

[49] M. Siddiqui, S. Holmes, H. He, W. Smith, E. Coker, M. Atkins, I. Kozhevnikov, Coking and regeneration of palladium-doped $H_3PW_{12}O_{40}/SiO_2$ catalysts, Catalysis Letters, 66 (2000) 53-57.

[50] L. Lloyd, Handbook of industrial catalysts, Springer Science & Business Media, 2011.

[51] R.A. Meyers, R.A. Meyers, Handbook of petroleum refining processes, McGraw-Hill New York, 2004.

[52] B. Leach, Applied industrial catalysis, Elsevier, 2012.

[53] N. Musselwhite, S. Alayoglu, G. Melaet, V.V. Pushkarev, A.E. Lindeman, K. An, G.A. Somorjai, Isomerization of n-hexane catalyzed by supported monodisperse PtRh bimetallic nanoparticles, Catalysis Letters, 143 (2013) 907-911.

[54] D.Y. Murzin, T. Salmi, Catalytic kinetics, Elsevier, 2005.

[55] F. Hartley, P. Vezey, Supported transition metal complexes as catalysts, Advances in Organometallic Chemistry, 15 (1977)189-234.

[56] A. Ibragimov, R. Shiriyazdanov, A. Davletshin, M. Rakhimov, Isomerization of light alkanes catalyzed by ionic liquids: an analysis of process parameters, Theoretical Foundations of Chemical Engineering, 47 (2013) 66-70.

[57] G.A. Olah, G.S. Prakash, J. Sommer, A. Molnar, Superacid chemistry, John Wiley & Sons, 2009.

[58] A. Dhar, A. Dutta, C.O. Castillo-Araiza, V. Suárez-Toriello, D. Ghosh, U. Raychaudhuri, One-pot isomerization of n-alkanes by super acidic solids: Sulfated aluminum-zirconium binary oxides, International Journal of Chemical Reactor Engineering, 14 (2016) 795-807.

[59] M. Nava, I.V. Stoyanova, S. Cummings, E.S. Stoyanov, C.A. Reed, The Strongest brønsted acid: protonation of alkanes by $H(CHB_{11}F_{11})$ at room temperature, Angewandte Chemie International Edition, 53 (2014) 1131-1134.

[60] G.A. Olah, Á. Molnár, Hydrocarbon chemistry, John Wiley & Sons, 2003.

[61] A. Dhar, R.L. Vekariya, P. Sharma, Kinetics and mechanistic study of n-alkane hydroisomerization reaction on Pt-doped g-alumina catalyst, (2017).

[62] A. Dhar, R.L. Vekariya, P. Bhadja, n-Alkane isomerization by catalysis a method of industrial importance: an overview, Cogent Chemistry, 4 (2018) 1514686.

[63] Y. Liu, K. Na, M. Misono, Skeletal isomerization of n-pentane over Pt-promoted cesium hydrogen salts of 12-tungstophosphoric acid, Journal of Molecular Catalysis A: Chemical, 141 (1999) 145-153.

[64] N. Essayem, Y.B. Taârit, C. Feche, P. Gayraud, G. Sapaly, C. Naccache, Comparative study of n-pentane isomerization over solid acid catalysts, heteropolyacid, sulfated zirconia, and mordenite: dependence on hydrogen and platinum addition, Journal of Catalysis, 219 (2003) 97-106.

[65] R.H. Elkins, Isomerization of alkanes and cycloalkanes, Google Patents, 1956.

[66] S. Triwahyono, A.A. Jalil, H. Hamdan, Isomerisation of cyclohexane to methylcyclopentane over $Pt/SO_4^{2-}–ZrO_2$ Catalyst, The Institution of Engineers, 67 (2006) 30-35.

[67] A. Keulemans, H. Voge, Reactivities of naphthenes over a platinum reforming catalyst by a gas chromatographic technique, The Journal of Physical Chemistry, 63 (1959) 476-480.

[68] J. Sinfelt, Bifunctional catalysis, Advances in Chemical Engineering, (1964) 37-74.

Chapter 2. Experimental

This chapter focuses on the key experimental techniques applied in this study, starting from chemicals used in the catalyst preparation, preparation procedures to prepare the catalyst, characterisation techniques to examine catalyst properties and catalyst evaluation by testing the activity on both isomerisation of n-hexane and cyclohexane over metal-acid bifunctional catalysts in the gas phase using a fixed-bed reactor.

2.1 Chemicals and catalysts

n-Hexane (>99%), H_2PtCl_6 hydrate, $HAuCl_4 \cdot 3H_2O$, $H_3PW_{12}O_{40}$ (HPW, 99%) and $H_4SiW_{12}O_{40}$ (HSiW, 99.9%) hydrates, cyclohexane (>99%), activated carbon Darco KB-B (150 μm particle size) were all purchased from Sigma-Aldrich. Catalyst supports P25 titania (anatase/rutile = 3:1) and Aerosil 300 silica (surface area S_{BET} = 300 m^2g^{-1}) was from Degussa; it was wetted and calcined at 400 °C prior to use. H_2 gas cylinders (>99%) were supplied by the British Oxygen Company. All reagents were used without further purification.

2.2 Catalyst preparation

Cesium tungstophosphate $Cs_{2.5}H_{0.5}PW_{12}O_{40}$ (CsPW) was prepared according to the literature procedure [1, 2] by adding aqueous caesium carbonate (0.47 M) dropwise to an aqueous solution of $H_3PW_{12}O_{40}$ (0.75 M) at 40 °C with stirring. The precipitate was stirred for further 2 hours then left to age for 24 hours at room temperature. The

mixture was dried using a rotary evaporator at 45 °C/25 Torr to give the CsPW as a white powder. Prior to use, the catalyst was calcined under vacuum at 150 °C/0.5 Torr for 1.5 hours. Surface area and pore size were determined by BET analysis to confirm the stoichiometry of the catalyst.

The catalyst 5% Au supported on carbon was prepared by adding an aqueous solution of $HAuCl_4.3H_2O$ (0.05 g) to Darco KB-B activated carbon (0.45 g) at 50 °C with stirring. The slurry was left for 2 hours then rotary evaporated to dryness. The black powder was reduced under a H_2 flow at 250 °C for 2 hours.

Commercial carbon supported platinum 10%Pt/C (7.1% Pt from ICP analysis) was used to prepare two different gold catalysts, with gold to platinum ratios of 1:1 and 2:1. Aqueous $HAuCl_4.3H_2O$ (0.07 g and 0.13 g) was added to platinum on activated carbon (0.5 g) at 50 °C with stirring. The slurry was left for 2 hours then rotary evaporated to dryness. The resulting powders were reduced with a H_2 flow at 250 °C for 2 hours. 7% Au supported on carbon was prepared by adding aqueous $HAuCl_4.3H_2O$ (0.15 g) to Darco KB-B activated carbon (0.96 g) at 50 °C with stirring. The slurry was left for 2 hours then rotary evaporated to dryness. The resulting powder was reduced with a H_2 flow at 250 °C for 2 hours and utilised to prepare two platinum catalysts with gold to platinum ratios of 1:1 and 2:1. 7% Au/C (0.5 g and 0.25 g) was added to the aqueous solutions of platinum (II) acetylacetonate benzene (0.02 M) with stirring at 50 °C for 2 hours. The slurries were rotary evaporated to dryness then reduced with a H_2 flow at 250 °C for 2 hours.

Catalysts with co-impregnated platinum and gold onto carbon support with metal ratios of 1:1 and 1:2 were prepared by adding an aqueous solution of $H_2[PtCl_6]$ (0.074 g) and $HAuCl_4.3H_2O$ (0.070 g and 0.14 g) to Darco KB-B activated carbon (0.43

g/0.40 g) at 50 °C with stirring. The slurries were left for 2 hours then rotary evaporated to dryness. The resulting powders were reduced with a H_2 flow at 250 °C for 2 hours. Physical mixtures of the bifunctional catalysts with 0.05% Pt loading were prepared by grinding the two components together in the required ratios. 0.32%Pt/CsPW was prepared by adding aqueous solution $H_2[PtCl_6]$ (0.017 g) to an aqueous CsPW precipitate (1.985 g) at 50 °C with stirring. The slurry was left for 2 hours then rotary evaporated to dryness. The resulting powder was reduced with a H_2 flow at 250 °C for 2 hours.

The literature states that the preparation method of gold catalysts can strongly affect their catalytic activity [3-8]. Therefore, various methods of impregnation were used when preparing catalysts containing gold. 0.25%Pt/0.5%Au/CsPW was prepared both with successive impregnation (SI) of Pt then Au and co-impregnation (CI). 0.32%Pt/0.36%Au/CsPW-SI was prepared by adding aqueous $H_2[PtCl_6]$ (0.017 g) to an aqueous CsPW precipitate (1.952 g) at 50 °C with stirring. The slurry was left for 2 hours, rotary evaporated to dryness and reduced with a H_2 flow at 250 °C for 2 hours. The aqueous solution of $HAuCl_4$ (0.032 g) was then added to the aqueous solution of Pt/CsPW with stirring and left for 2 hours. The catalyst was then rotary evaporated to dryness and reduced with a H_2 flow at 250 °C for 2 hours. 0.28%Pt/0.35%Au/CsPW-CI was prepared by adding an aqueous slurry of $H_2[PtCl_6]$ (0.017 g) and $HAuCl_4$ (0.032 g) to an aqueous CsPW precipitate (1.952 g) at 50 °C with stirring then left for 2 hours. The resulting slurry was then rotary evaporated to dryness and reduced with a H_2 flow at 250 °C for 2 hours.

These methods were also employed to prepare 5.26%Pt/3.26%Au/CsPW-CI. This was prepared by adding an aqueous solution of $HAuCl_4$(0.11g) and $H_2[PtCl_6]$

(0.017 g) to an aqueous CsPW precipitate (0.90 g) at 50 °C with stirring. The slurry was left for two hours then rotary evaporated to dryness. The powder was reduced with a H_2 flow at 250 °C for 2 hours.

5.78% Pt/CsPW and 2.62% Au/CsPW were prepared by adding an aqueous solution of the appropriate metal precursor $H_2[PtCl_6]$ (0.80 g) or $HAuCl_4$ (0.11 g) to an aqueous CsPW precipitate (4.75 g and 0.95 g) at 50 °C with stirring. The slurries were both left for 2 hours then rotary evaporated to dryness. The resulting powders were reduced with a H_2 flow at 250 °C for 2 hours. Physical mixtures of the acid supported catalysts and CsPW were prepared in 1:19 and 1:79 dilutions w/w by grinding the two substances together. Similarly, physical mixtures of the acid supported catalysts with SiO_2 into 1:7 w/w dilutions were prepared by grinding the two substances together. Metal loadings quoted are confirmed by a ICP-AES elemental analysis.

2.3 Catalyst characterisation techniques

2.3.1. Surface area measurements (BET)

BET is a common technique used to determine the surface area and porosity of catalysts. It is extremely useful in catalyst characterisation as a larger surface area usually makes a more active catalyst [9, 10]. BET was developed by Brunaur, Emmett, and Teller in 1938 [11]. The BET method is based on the volume of gas adsorbed on the sample surface at a certain temperature and pressure. The gas utilized in this method is N_2 and the concept relies on the following equation, which is called the BET equation (Equation 2.1).

$$\frac{P}{V(P_0 - P)} = \frac{1}{V_m C} + \frac{C-1}{V_m C} \times \frac{P}{P_0} \qquad (2.1)$$

In this equation, V is the volume of adsorbed gas at the equilibrium pressure P, V_m is the volume of adsorbed gas on a monolayer. P_o is the saturation pressure of adsorbate and C is a constant.

When $P/V(P_o-P)$ is plotted against P/P_o, it gives a straight line from which V_m and C can be calculated. Then, the surface area (SA) can be calculated by applying Equation 2.2, assuming every single molecule of adsorbed N_2 occupies the cross section area of adsorbate σ = 0.162 nm^2. N_a is Avogadro's number (6.023 X 10^{23}), V_o is the molar volume of the gas and M is the sample weight [10].

$$SA(m^2/g) = V_m N_a \sigma / M V_o \qquad (2.2)$$

The surface area and porosity of the catalysts prepared were measured on a Micromeritics ASAP 2010 adsorption setup (Figure 2.1). The catalyst had first been outgassed at a specific temperature depending on the nature of the components, usually between 150-200 °C, under vacuum for 2 hours. A sample typically (0.1-0.2 g) was loaded in a physisorption tube and the actual mass was recorded. The tube containing the sample was then put on the degasser after putting it into a heater pad for evacuating under 250 °C for 1.5 h to remove the contaminants or any organics that might be covering the surface. When the course of degassing was complete and the pressure reached 8 mmHg, it was allowed to cool to room temperature. Then the tube was unloaded from the degasser and covered with a stopper and reweighed. The weight was

recorded. A filler rod was inserted into the tube and loaded on the analyser to start the absorption process, using nitrogen as adsorbate at -196 °C. A liquid nitrogen dewar was used for this purpose. After the analyser was set up, the analysis was programmed.

Figure 2.1 Micromeritics ASAP 2010 instrument for the surface area and porosity measurement.

2.3.2 Temperature programmed reduction

Temperature programmed reduction (TPR) is a common technique that investigates the reducibility of catalysts [12]. Typically, in this method a reducing agent used is a gas mixture, usually hydrogen diluted with nitrogen or argon that flows over the catalyst sample with programmed heating. While the gas flows over the sample, a thermal conductivity detector (TCD) indicates thermal conductivity changes of the

reducing gas and records the change as a signal. The outcome signal refers to the amount of hydrogen reacted with the catalyst sample.

Figure 2.2 Micromeritics TPD/TPR 2900 system.

The TPR profile can be identified by plotting the TCD signals versus the temperature. A set of experimental parameters that can affect the TPR profile are gas flow rate, sample weight, heating temperature rate and sample particle size. TPR is a beneficial characterisation method providing useful details by which various catalysts can be compared by their reduction conditions in an effort to elucidate variations in activity and selectivity [13, 14].

TPR analysis was carried out using a Micromeritics TPD/TPR 2900 instrument (Figure 2.2) with a thermal conductivity detector. Catalyst samples (15-20 mg) were

heated up from 25-800 °C at a rate of 10 °C min^{-1} in an H_2-N_2 (5:95) gas flow (60 ml min^{-1}) [33].

2.3.3 Temperature programmed desorption

The investigation of surface structures is important for the optimum design of catalysts as the interaction of reactants with the catalyst surface is an essential step in heterogeneous catalysis. Temperature at which species are desorbed from a surface is indicative of the strength of the surface bond. Prob molecules such as hydrogen molecules are adsorbed at a lower temperature and their desorption or reaction with increased temperature is monitored to characterise surface properties of a catalyst. A carrier gas containing the desired species is used and the reaction is carried out by increasing the temperature. A solid sample after reduction is exposed to adsorbate gas under mild conditions and then heated under inert conditions in a programmed method to desorb it. The gas stream containing desorbed molecules is monitored by a thermal conductivity detector (TCD). The TCD signal is proportional to the quantity of molecules desorbed, while thermal energy released is monitored by a thermocouple. A peak on TPD chromatogram provides information about the binding energy which indicates active sites in the sample [15, 16]. In this work, H_2-TPD for Pt/CsPW and PtAu/CsPW catalysts was measured at 10 °C min^{-1} temperature ramp rate and 50 mL min^{-1} N_2 flow rate using a Micromeritics TPD/TPR 2900 instrument [17].

2.3.4 H_2 chemisorption

Determining metal dispersion on the surface of supported catalysts is a key measure to comprehend the catalyst activity. Pulse hydrogen chemisorption is a typical method used for such a purpose as it has a high sensitivity. The technique works on the basis of H_2/O_2 titration and the oxygen pre-adsorbed on metal sites is titrated by H_2. This is a common technique used to estimate the dispersion for metals like Pt and Pd [17, 18].

The stoichiometry of H_2/O_2 titration is represented by Equation 2.3 [17, 19]:

$$M_s\text{-}O + 3/2H_2 \rightarrow M_s\text{-}H + H_2O \qquad (2.3)$$

The amount of hydrogen adsorbed onto the metal surface was measured by integrating areas of peaks detected by a thermal conductivity detector, which were displayed on the monitor screen. Constant volume of hydrogen was injected repeatedly until there was no further change of the area of the peaks, which represent hydrogen adsorption. The total volume of adsorbed hydrogen was calculated at 75 °C (348 K) based on Equation 2.4:

$$V_{348K} = \sum \{V - [(P_{ads}/P_{av})\} \text{ x } V] \qquad (2.4)$$

where V_{348K} is the total volume of hydrogen absorbed at 75 °C (348 K), V is the hydrogen pulse volume, P_{ads} is the peak area of adsorbed hydrogen and P_{av} is the average peak area for about four to six injections at saturation with no further hydrogen adsorption. Equation 2.5 gives the total adsorbed volume of H_2 at 0 °C (273 K):

$$V_{273K} = V_{348K} \times (273/348) \qquad (2.5)$$

Equation 2.6 shows how the total dispersion is calculated, where D is the metal dispersion, Ar is the atomic weight of metal, M_{cat} is the weight of catalyst analysed (g), 22414 is the molar volume of H_2 under standard conditions, C_M is the loading of metal as a fraction of catalyst weight and 1.5 is the adsorption stoichiometry of H_2:

$$D = \frac{V_{273}\ (\text{ml}) \times Ar\ (\text{g mol}^{-1})}{M_{cat}\ (\text{g}) \times 22414\ (\text{ml mol}^{-1}) \times C_M \times 1.5} \qquad (2.6)$$

The average diameter of metal particles (d) was calculated from the empirical Equation 2.7 [19]:

$$d\ (nm) = 0.9/D \qquad (2.7)$$

The hydrogen-oxygen titration pulse technique was utilised for the hydrogen chemisorption on Pt catalysts by a Micromeritics TPD/TPR 2900 instrument. Samples were exposed to air at room temperature for 24 hours prior to analysis to adsorb oxygen onto the metal surface. The sample (0.05 g) was placed in a glass tube connected to the analysis instrument at room temperature. Pulses of a constant volume of pure H_2 were injected into the N_2 flow at one minute intervals, until the catalyst was saturated with hydrogen.

2.3.5 CO chemisorption

Dispersion is an indication of the percentage of the exposed metal surface area present on the acidic support or the amount of metal available for reaction with the substrate [16, 20]. The technique of pulse chemisorption of CO was used to determine metal dispersion on a Micromeritics TPD/TPR 2900 instrument, in addition to the H_2/O_2 titration described above. A catalyst sample was placed in the sample tube and helium gas at 50 °C was made to flow over the sample. CO was introduced by manual injection (20-50 µl) until saturation was complete. The metal dispersion was calculated assuming the adsorption stoichiometry of CO:M = 1.

2.3.6 Powder X-ray diffraction (XRD)

Power X-ray diffraction is a crucial technique for the investigation of solid crystalline substances as it presents key information about the crystal structure by the diffraction pattern. It is conducted effectively to analyse heterogeneous catalysts. XRD as an analytical method was developed by Bragg, William and Lawrence and the principal equation used in XRD is called the Bragg's law (Equation 2.8) [21]:

$$n\lambda = 2d\,sin\theta \qquad (2.8)$$

where n is an integral value, λ is the incident wavelength of X-ray, d is the difference between the lattice planes and θ is the diffraction angle. The generated X-rays are focused towards the analytical sample. Those that draw the crystal plane show an angle that is equivalent to the diffraction angle (d).

The X-ray diffraction instrument consists mainly of an X-ray source, a vacuum chamber having the sample holder and a detector which analyses the diffracted X-rays.

The information obtained from XRD can guide to the dimensions and the pattern of the unit cell. The average particle size can be computed applying the Scherrer equation (Equation 2.12):

$$t = 0.9\lambda/B\ cos\theta \qquad (2.12)$$

where t is the particle size, λ is the incident wavelength of X-ray, B is the total width at half height of the diffraction peak and θ is the diffraction angle [23]. Powder X-ray diffraction patterns were recorded over a range of 2θ 10-60^o on a PANalytical Xpert diffractometer with a CuKα radiation (λ = 1.542 Å) to deliver information on the crystalline nature of the catalysts. The mean particle size was calculated from the XRD patterns using the Scherrer equation [22].

2.3.7 Transmission electron microscopy (TEM)

Transmission electron microscopy (TEM) is a valuable technique in studying catalyst features. It provides a profile of the size, structure and composition of the substance. In TEM, an electron gun bumps an electron current which is condensed and focused in the shape of a beam by an anode and an electromagnetic lens. The beam of electrons hits the specimen and various types of electron beams are reflected from the surface of the specimen (Figure 2.4). The transmitted segment of the beam which hits a fluorescent screen can be used to shape an enlarged image of the specimen [23].

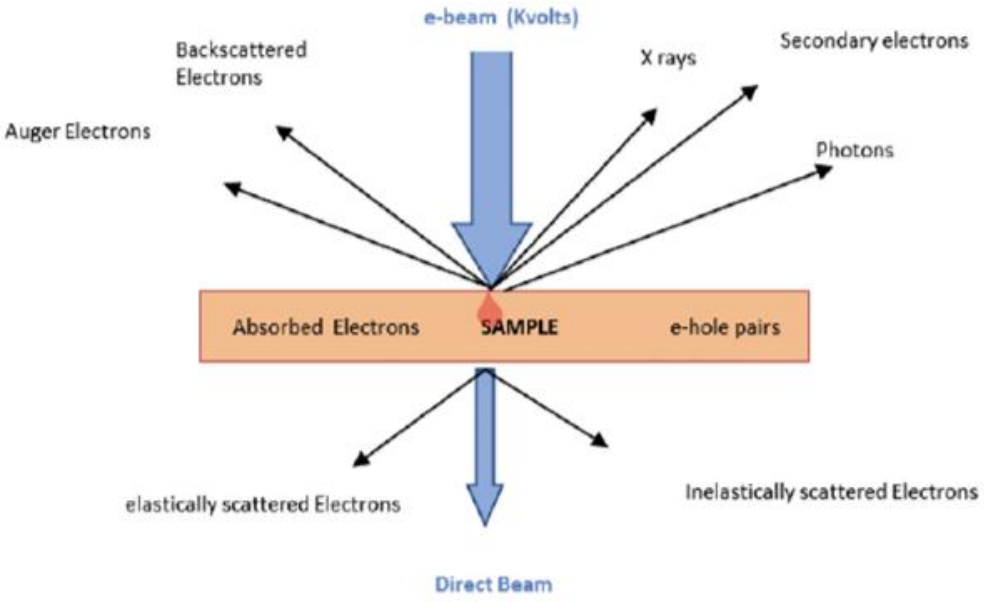

Figure 2.4 Interaction between electrons and the specimen in TEM.

2.3.8 Scanning transmission electron microscopy (STEM)

Scanning transmission electron microscopy (STEM) is one of the principal electron microscopies where a beam of electrons is directed to a very thin sample of the material under a high vacuum. The beam of electrons then passes through a proper shape of electromagnetic field, which access as a focused beam that scans the surface of the sample to transmit signals detected to form an image. The outcomes can be analysed by an Energy Dispersive X-Ray (EDX) detector or annular dark field (ADF) [24].

In this study, STEM and EDX analyses were carried out on a VG HB601 UX scanning transmission electron microscope (STEM), equipped with an energy dispersive x-ray (EDX) spectrometer.

2.3.9 Inductively coupled plasma atomic emission spectroscopy (ICP-AES)

ICP-AES can give data about the elemental and proportional constitution of a sample under analysis. It is an electromagnetic radiation process using an inductively coupled plasma to generate electrons and ions through excitation of atoms of the sample involved. In this process a plasma gas such as argon flows through a coil to cause ionisation of the argon. The argon ions then move with a circular magnetic field generating an intense heat, which can reach 10000 °C. Fume sample atoms pass by the plasma flame to leave the flame in an excited state. When the excited state atoms return to ground state and release photons at a different wavelength, the wavelengths that are produced are conveyed to a signal amplification unit where the intensity of the wavelengths can be detected. Each metal has a respective wavelength which can represent the concentration of metals in the sample [24] .

2.3.10 C analysis

Elemental analysis is a quantitative analysis where the element of a solid sample can be analysed. This sort of analysis is useful to determine the amount of carbon (coke) which might be formed after using the catalyst, in order to help ascertain the effect of deposited coke on the catalyst function. Commonly, a small amount of spent catalyst (about 5 mg) is placed in a burning reactor and heated under flowing

helium at 1000 °C. Pure oxygen is injected to cause a spark combustion to form a CO_2 and H_2O gas combination, which is passed to the GC detector to detect the mixture components. The proportion of each component can then be calculated [25].

2.3.11 Gas chromatography

Gas chromatography is a technique used for the separation and quantitative analysis of volatile compounds. The compound for analysis is heated in an injector until it is in a gas state and mixed with a gaseous mobile medium such as helium, nitrogen or argon. It is transported over a packed column having an inert surface where the substances are separated and following this they are analysed by a suitable detector (Figure 2.5) [25].

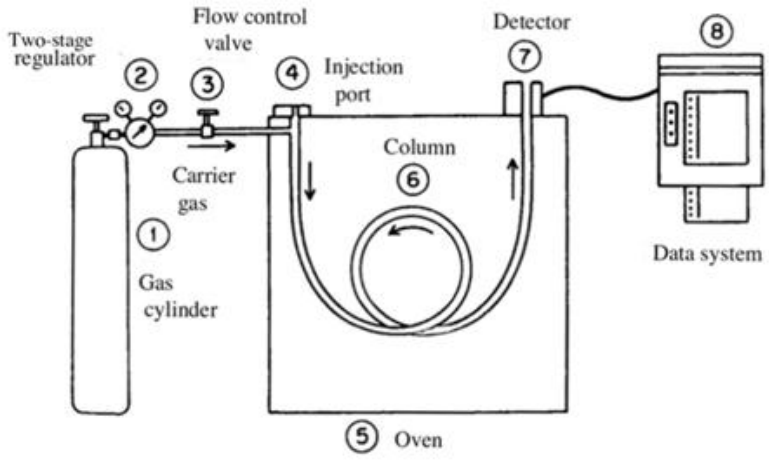

Figure 2.5 Schematic diagram of gas chromatography (GC).

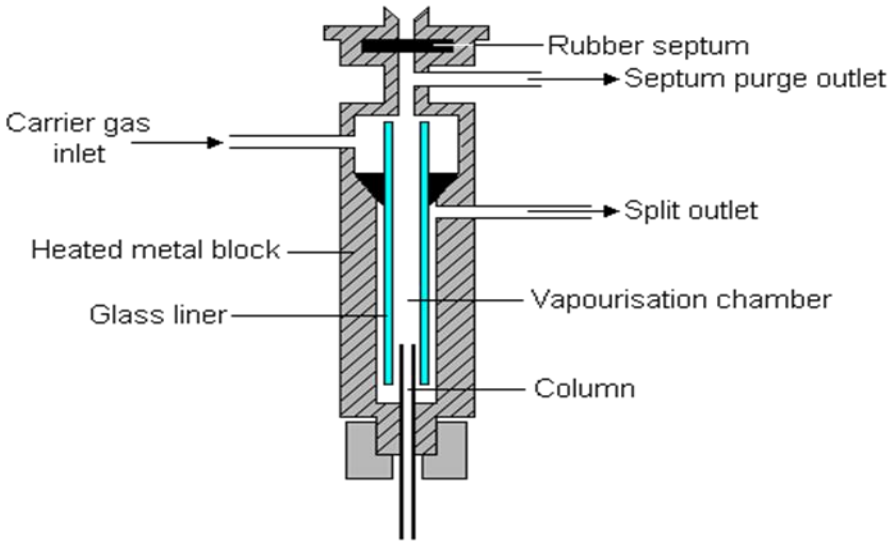

Figure 2.6 Split-splitless vaporising injector [26].

The column used in GC for separation is commonly of two designs: packed or capillary columns. Packed columns are typically composed of a fine inert solid material such as a stainless steel or glass coil, packed with a stationary phase. These are 1.5-10 m in length with a 2-5 mm internal diameter. Capillary columns are composed of fused quartz, which are coated with a thin layer of material such as silicon grease. The capillary tube length is between 10-200 m with a 0.1-1.0 mm internal diameter. Capillary columns give the best separation efficiency, but they are overloaded easily. The column is placed in a chamber so that a uniform temperature (50-300 °C) can be maintained.

Mostly, GCs employ capillary columns which are longer, to achieve a capable separation. Although, they can only use a low sample quantity simplifying the need for a split injector. In a split injector (Figure 2.6) the injected substance is introduced

through the port, where it is heated and interacts with the carrier gas on an inert packing. The merged mixture is then split into two portions using different flow rates of the carrier gas.

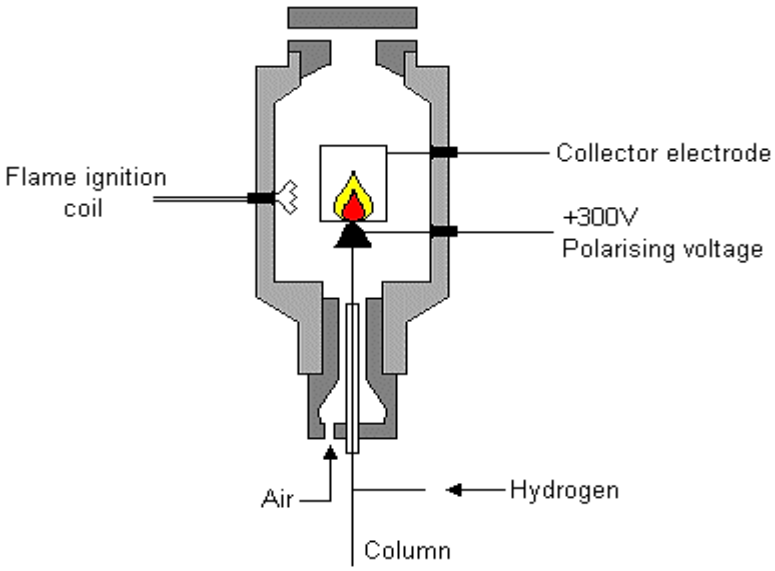

Figure 2.7 Flame ionisation detector [26].

When the various constituents in the column have been split they are measured by a flame ionisation detector (FID), which is highly sensitive to the hydrocarbon content (Figure 2.7). The column is directly connected to the FID. Upon entering the detector, the column load is combined with hydrogen and air and burned in the chamber. When the sample molecules reach the flame, they are ionised and release electrons. Across the flame there are electrodes, one with a negative charge and one with a positive. This induced electric current which is amplified, then detected by the computer and displayed in a graph. The generated ions are proportional to the number of hydrocarbons in the stream. The gaseous exhaust created exits through the exhaust port and the whole waste is heated to prevent condensation in the detector.

For FID, the molar response factors for alkane molecules depend mainly on the number of carbon atoms in the molecule based on the effective carbon number (ECN) concept [27]. Hence these are expected to be close for alkane isomers, for example, n-hexane, 2-methylpentane and 3-methylpentane, i.e., the molar response factors of the alkane isomer products relative to the alkane substrate are close to one, $K_p \approx 1$. Our GC analysis showed that this was indeed the case for the above hexane isomers as well as for cyclohexane and methylcyclopentane within 5-7% accuracy, i.e., K_p = 1.00±0.07. Therefore, for the calculation of alkane conversion, product yields and product selectivities from GC analysis (see below), the value K_p = 1.00 was used.

$$Product\ yield\ (Y_P) = \frac{moles\ of\ a\ product\ formed}{moles\ of\ substrate\ supplied} \times 100 = \frac{(S_P \times K_P \times A)}{S_r + (\sum S_P \times K_P \times A)} \times 100$$

$$Conversion\ (X) = \frac{moles\ of\ substrate\ reacted}{moles\ of\ substrate\ supplied} \times 100 = \sum Y_P$$

$$Selectivity\ (S) = \frac{moles\ of\ a\ product\ formed}{moles\ of\ substrate\ reacted} \times 100 = \frac{Y_P}{X} \times 100$$

where S_p is the peak area of the product, K_p is the response factor of the product relative to the substrate, A is the stoichiometry factor of the product relative to the substrate, S_r is the peak area of the unreacted substrate.

2.3.12 Gas chromatography-mass spectroscopy (GC-MS)

Gas chromatography-mass spectroscopy is used in separating and identifying reaction products to provide further evidence of the compound components. Typically, the reaction products are firstly separated by gas chromatography as explained earlier and then anaylised by MS.

Separated molecules by the GC in which they are in volatile state, interact with the accelerated electrons that generated by an electric field. This interaction commonly produces positive ions due to the loss of an electron as shown in equation 2.13

$$M + e^- \rightarrow M^{+\cdot} + 2e^- \qquad (2.13)$$

where M is the molecule, e^- is the high-energy electron and $M^{+\cdot}$ is the positive molecular ion. The molecular ions (radical cations) are then sorted based on their mass to charge ratio into a mass spectrometer detector [28].

2.4 Catalyst testing

The catalytic activity and selectivity of the prepared catalysts were tested and evaluated over both gaseous n-hexane and cyclohexane isomerisation reactions. The assessment was run in a fixed-bed microreactor setup (Figure 2.8) under optimised reaction conditions of temperature, pressure and flow rate. Prior to the reaction, the catalyst had heat treatment for an hour under hydrogen flow to ensure it was free of any contamination under a similar temperature allocated for the reaction. A hydrogen gas was bypassed through a feed saturator to maintain the partial pressure of the feed to ensure the regulation of the flow rate of the stream. Reaction products were analysed by on-line GC (Figure 2.9 and 2.10). For hexane isomerisation, the reactor was fitted with on-line gas chromatograph Varian Star 3400 CX, for cyclohexane isomerisation with Varian 3800 (Figure 2.8). Both instruments were fitted with 30 m x 0.25 mm HP

INNOWAX capillary columns and flame ionisation detectors. The GC analysis was carried out at a column temperature of 100 ^{o}C, the temperature of injector and detector was 200 and 250 ^{o}C, respectively.

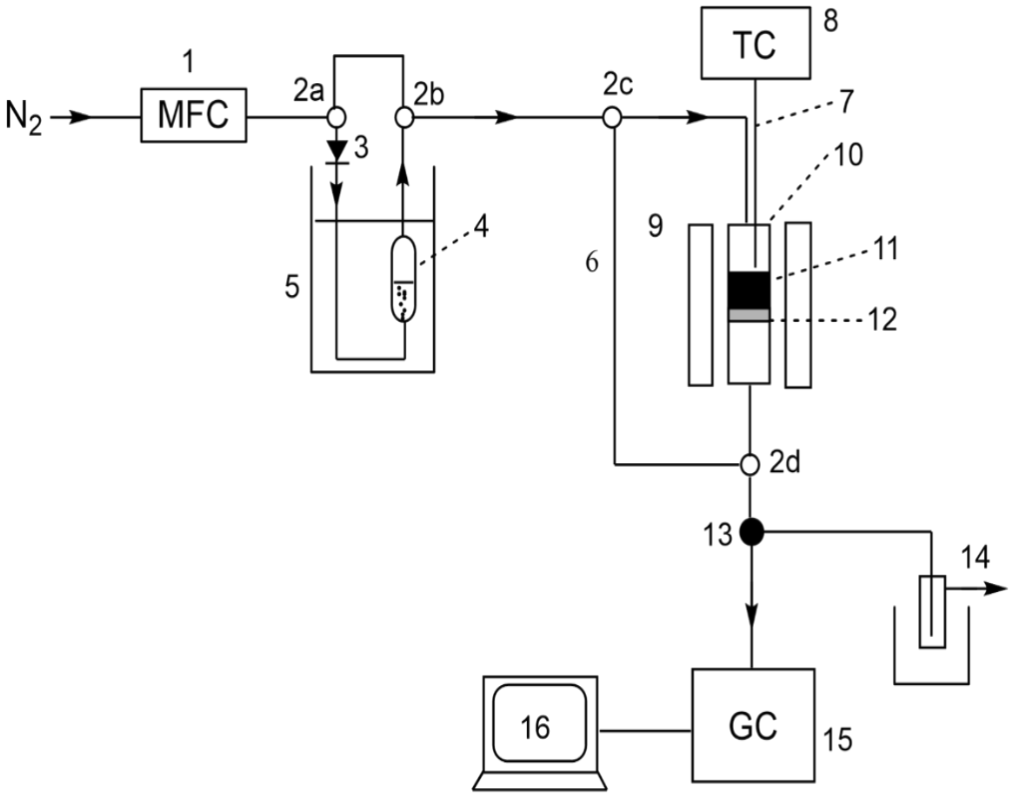

Figure 2.8 Flow fixed-bed microreactor for n-hexane and cyclohexane isomerisation, (1) brooks flow controller, (2) 3-way valve, (3) check valve , (4) saturator for liquid substrate, (5) ice bath, (6) bypass tube, (7) thermocouple, (8) Eurotherm temperature controller, (9) furnace, (10) Pyrex tubular reactor, (11) catalyst bed, (12) glass wool support, (13) multiposition valve with air actuator, (14) product trap, (15) Varian gas chromatograph, (16) computer.

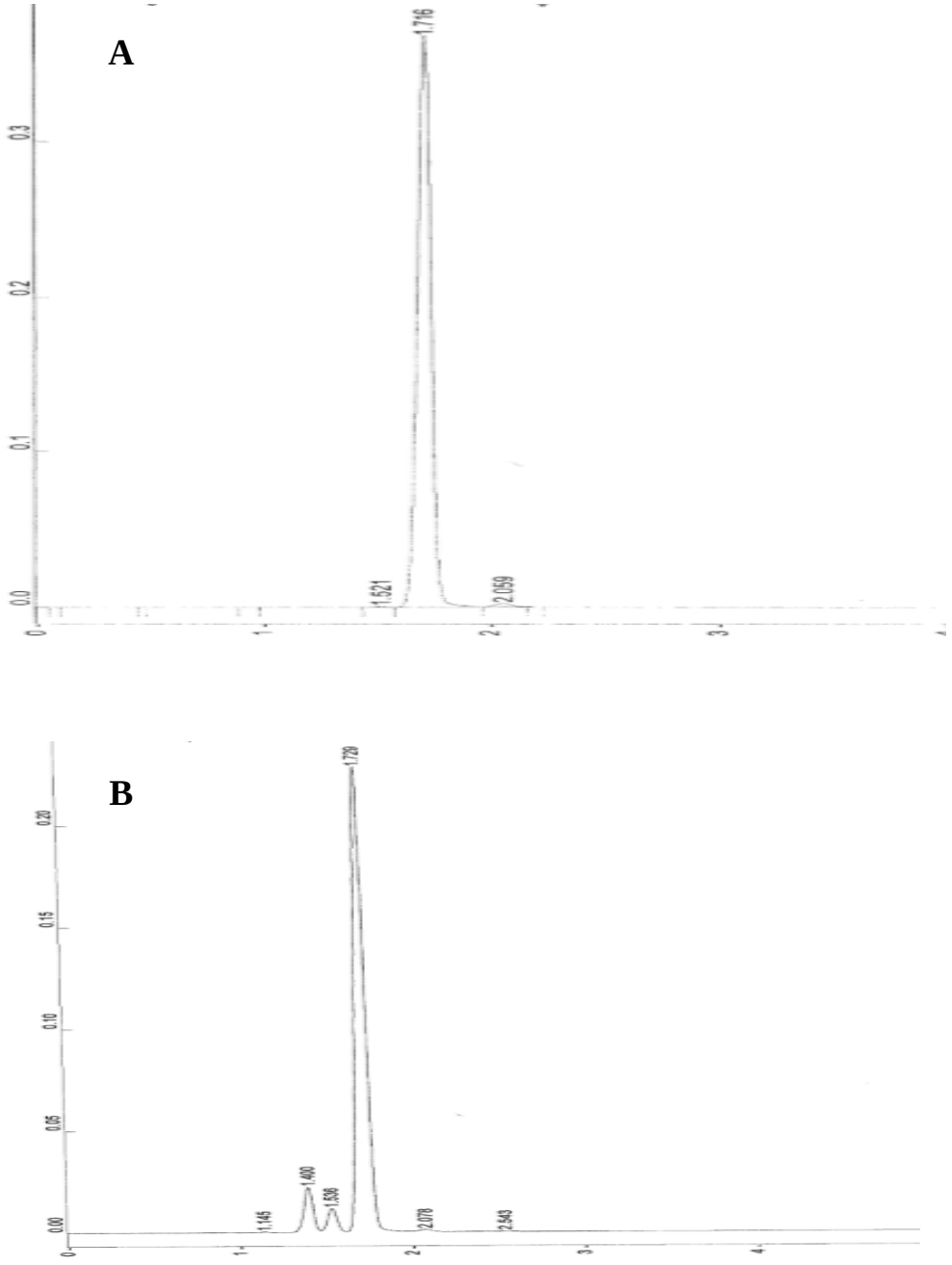

Figure 2.9 (A) GC trace for n-hexane (1.7 min retention time) and (B) for n-hexane isomerisation over 5.6%Pt/4.4%Au/CsPW at 200 °C indicating 2-methylpentane and 3-methylpentane products at 1.40 and 1.53 min retention time, respectively).

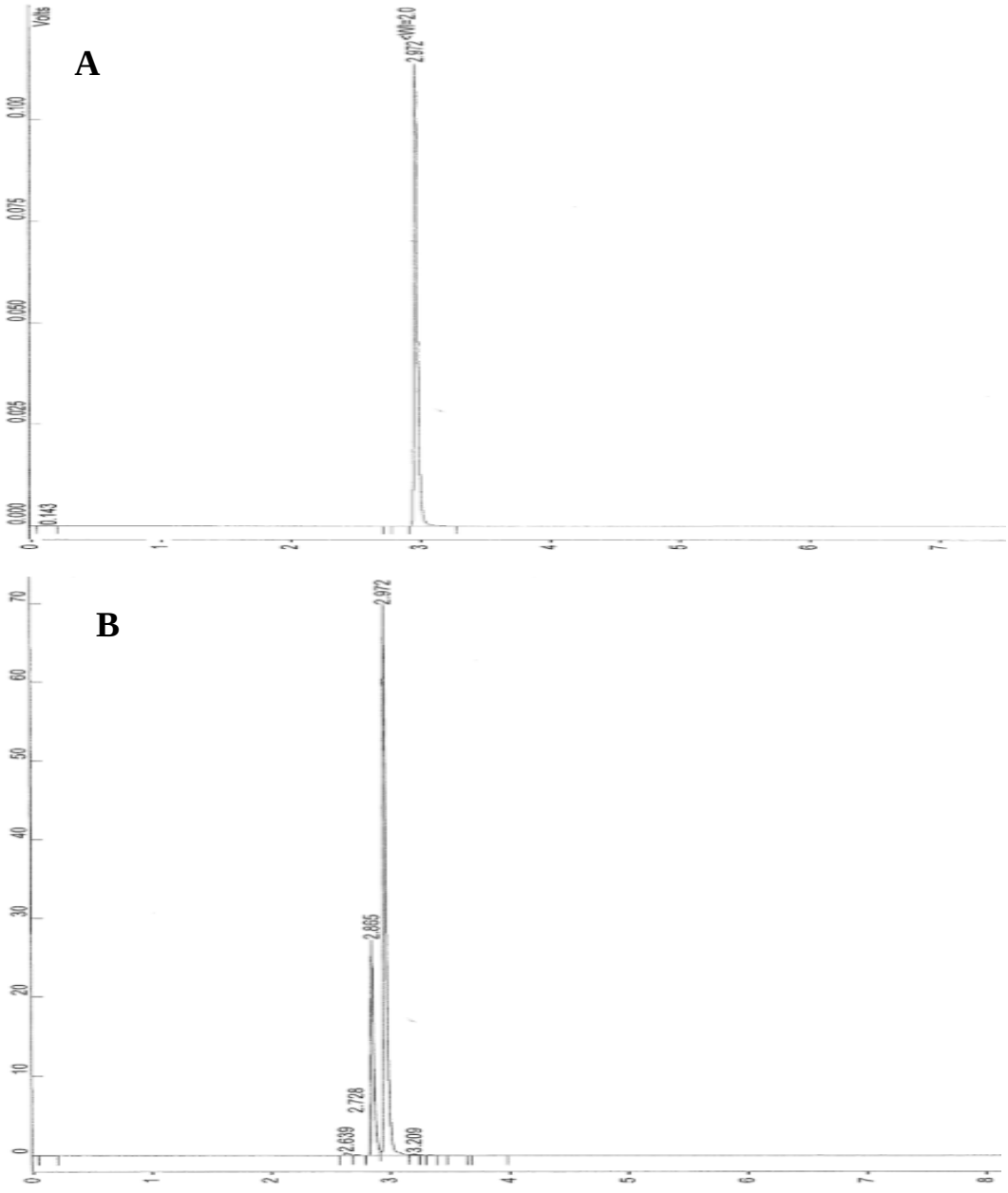

Figure 2.10 (A) GC trace for cyclohexane and (B) for cyclohexane isomerisation over 5.6%Pt/4.4%Au/CsPW at 200 °C indicating methylcyclopentane product (2.9 min retention time).

References

[1] Y. Izumi, M. Ono, M. Ogawa, K. Urabe, Acidic cesium salts of Keggin-type heteropolytungstic acids as insoluble solid acid catalysts for estenfication and hydrolysis reactions, Chemistry Letters, 22 (1993) 825-828.

[2] A. Corma, H. Garcia, Supported gold nanoparticles as catalysts for organic reactions, Chemical Society Reviews, 37 (2008) 2096-2126.

[3] N. Dimitratos, J.A. Lopez-Sanchez, D. Morgan, A.F. Carley, R. Tiruvalam, C.J. Kiely, D. Bethell, G.J. Hutchings, Solvent-free oxidation of benzyl alcohol using Au–Pd catalysts prepared by sol immobilisation, Physical Chemistry Chemical Physics, 11 (2009) 5142-5153.

[4] M. Haruta, Gold as a novel catalyst in the 21st century: Preparation, working mechanism and applications, Gold Bulletin, 37 (2004) 27-36.

[5] H. Sakurai, M. Haruta, Carbon dioxide and carbon monoxide hydrogenation over gold supported on titanium, iron, and zinc oxides, Applied Catalysis A: General, 127 (1995) 93-105.

[6] M. Valden, S. Pak, X. Lai, D. Goodman, Structure sensitivity of CO oxidation over model Au/TiO 2 2 catalysts, Catalysis Letters, 56 (1998) 7-10.

[7] A. Wolf, F. Schüth, A systematic study of the synthesis conditions for the preparation of highly active gold catalysts, Applied Catalysis A, General, 226 (2002) 1-13.

[8] K. Alharbi, W. Alharbi, E.F. Kozhevnikova, I.V. Kozhevnikov, Deoxygenation of Ethers and Esters over Bifunctional Pt–Heteropoly Acid Catalyst in the Gas Phase, ACS Catalysis, 6 (2016) 2067-2075.

[9] G. Leofanti, M. Padovan, G. Tozzola, B. Venturelli, Surface area and pore texture of catalysts, Catalysis Today, 41 (1998) 207-219.

[10] G. Leofanti, G. Tozzola, M. Padovan, G. Petrini, S. Bordiga, A. Zecchina, Catalyst characterization: applications, Catalysis Today, 34 (1997) 329-352.

[11] S. Brunauer, P.H. Emmett, E. Teller, Adsorption of gases in multimolecular layers, Journal of the American Chemical Society, 60 (1938) 309-319.

[12] F. Pinna, Supported metal catalysts preparation, Catalysis Today, 41 (1998) 129-137.

[13] N.W. Hurst, S.J. Gentry, A. Jones, B.D. McNicol, Temperature programmed reduction, Catalysis Reviews Science and Engineering, 24 (1982) 233-309.

[14] D.A. Monti, A. Baiker, Temperature-programmed reduction. Parametric sensitivity and estimation of kinetic parameters, Journal of Catalysis, 83 (1983) 323-335.

[15] J.L. Falconer, J.A. Schwarz, Temperature-programmed desorption and reaction: applications to supported catalysts, Catalysis Reviews Science and Engineering, 25 (1983) 141-227.

[16] R. Cvetanović, Y. Amenomiya, A temperature programmed desorption technique for investigation of practical catalysts, Catalysis Reviews, 6 (1972) 21-48.

[17] J.E. Benson, M. Boudart, Hydrogen-oxygen titration method for the measurement of supported platinum surface areas, Journal of Catalysis, 4 (1965) 704-710.

[18] J.H. Sinfelt, Structure of metal catalysts, Reviews of Modern Physics, 51 (1979) 569.

[19] J. Benson, H. Hwang, M. Boudart, Hydrogen-oxygen titration method for the measurement of supported palladium surface areas, Journal of Catalysis, 30 (1973) 146-153.

[20] D. Cox, K. Reichmann, D. Trevor, A. Kaldor, CO chemisorption on free gas phase metal clusters, The Journal of Chemical Physics, 88 (1988) 111-119.

[21] P.W. Atkins, J. De Paula, J. Keeler, Atkins' physical chemistry, Oxford University Press, 2018.

[22] A.W. Burton, Powder Diffraction in Zeolite Science, Zeolite Characterization and Catalysis, Springer, 2009.

[23] S.L. Flegler, S.L. Flegler, Scanning & Transmission Electron Microscopy, Oxford University Press, 1997.

[24] B. Imelik, J.C. Vedrine, Catalyst characterization: physical techniques for solid materials, Springer Science & Business Media, 2013.

[25] D. Kealey, P.J. Haines, Analytical chemistry, BIOS, Oxford, 2002.[31] H.M. McNair, J.M. Miller, N.H. Snow, Basic gas chromatography, John Wiley & Sons, 2019.

[26] http://teaching.shu.ac.uk/hwb/chemistry/totorials/chrom/gaschrm.htm

[27] J.T. Scanlon, E.W. Donald, Calculation of flame ionisation detector relative response factors using the effective carbon number concept, Journal of Chromatography Science, 23 (1985) 333-340.

[28] F.W. Karasek, R.E. Clement, Basic gas chromatography-mass spectrometry: principles and techniques, Elsevier, 2012.

Chapter 3. Catalyst characterisation

This chapter illustrates the results of catalyst characterisations, which provide features of the catalyst engaged in this research. Based on different techniques described in Chapter 2, the outcomes obtained from them are detailed here.

3.1 Inductively coupled plasma atomic emission spectroscopy (ICP-AES)

To study the effect of Pt loading many catalysts were prepared with different Pt loading. The actual loading of the doped metal was analysed by inductively coupled plasma atomic emission spectroscopy (ICP-AES) method to verify the actual Pt percentage in the catalysts. A small amount of catalyst between 30-50 mg was dissolved in a mixture of concentrated HNO_3 with HCl in 1:3 ratio and heated for about two hours until the solid sample was completely dissolved. The mixture was left to cool overnight to be ready for ICP-AES analysis.

ICP-AES elemental analysis was carried out on a Spiro Ciros optical emission spectrometer to confirm the platinum loadings in the catalyst. It was also used to analyse gold loading in supported Au and PtAu catalysts.

Tables 3.1 and 3.2 show the ICP-AES analysis for the metal components in CsPW-supported and carbon-supported catalysts, respectively. In Table 3.1, it can be seen that the platinum loadings were in agreement with the preparation

stoichiometries, the gold loadings often differed, however. This may be due to water contamination in the gold precursor, reducing the amount of gold in the preparation. In Table 3.2, the calculated and experimental values are almost the same because the preparation procedure did not involve operations such as extraction and washing which may cause metal loss.

Table 3.1 ICP-AES analysis for CsPW-supported metal catalysts.

Catalyst	Element	Calculated (% wt)	Experimental (% wt)
0.11%Pt/CsPW	Pt	0.1	0.11
0.23%Pt/CsPW	Pt	0.2	0.23
0.32%Pt/CsPW	Pt	03	0.32
0.71%Pt/CsPW	Pt	0.7	0.71
2.45%Pt/CsPW	Pt	2.5	2.45
3.56%Pt/CsPW	Pt	3.5	3.56
3.76%Pt/CsPW	Pt	3.8	3.76
5.6%Pt/CsPW	Pt	5.0	5.6
5.78%Pt/CsPW	Pt	5.0	5.78
6.0%Pt/CsPW	Pt	6.0	6.0
11.5%Pt/CsPW	Pt	10.0	11.5
2.62%Au/CsPW	Au	3.0	2.62
4.7%Au/CsPW	Au	5.0	4.7
0.28%Pt/0.35%Au/CsPW	Pt	0.3	0.3
	Au	0.4	0.4

5.57%Pt/4.25%Au/CsPW	Pt	6.0	5.57
	Au	4.5	4.25
5.9%Pt/4.4%Au/CsPW	Pt	5.0	5.9
	Au	5.0	4.4

Table 3.2 ICP-AES analysis for carbon-supported metal catalysts.

Catalyst	Element	Calculated (% wt)	Experimental (% wt)
5.0%Au/C	Au	5.0	5.0
6.2%Pt/C	Pt	6.0	6.2
6.7%Pt/5.0%Au/C	Pt	6.0	6.7
	Au	5.0	5.0

3.2. Surface area measurements (BET)

BET analysis was utilized to provide surface area characterisation of the catalysts tested in this work. The texture of the heteropoly acid catalysts was determined using the BET analysis by a Micromeritics ASAP 2010 instrument, with nitrogen physisorption at -196 °C. Prior to measurement, the samples were pre-treated at 250 °C in vacuum for 2 h. The Barrett, Joyner and Halenda (BJH) method was also used to calculate pore volume and pore size through the adsorption isotherm method. Approximately 0.2 g of catalyst was used in the analysis.

An adsorption isotherm is an extremely helpful tool which can feature the behaviour of the catalyst surface structure. There are six possible types of adsorption isotherms as shown in Figure 3.1. An adsorption isotherm estimates the amount of the gas adsorbed, which is called adsorbate, onto the porous material, which is called adsorbent. The unit used for calculating the amount of adsorption is mole or grams of the adsorbate per gram of adsorbent. An adsorption isotherm plot reflects whether the catalyst is porous or not, along with the volume and the size of the pores. It can indicate whether the catalyst is exposed to physical or chemical adsorption.

The four types of isotherms in Figure 3.1 (I, II, IV and VI) represent most typical types of catalyst texture, namely microporous, macroporous, mesoporous and uniform ultramicroporous, respectively. For the catalysts prepared in this research, adsorption isotherm IV is the common type, which came out from the BJH analysis [1-3].

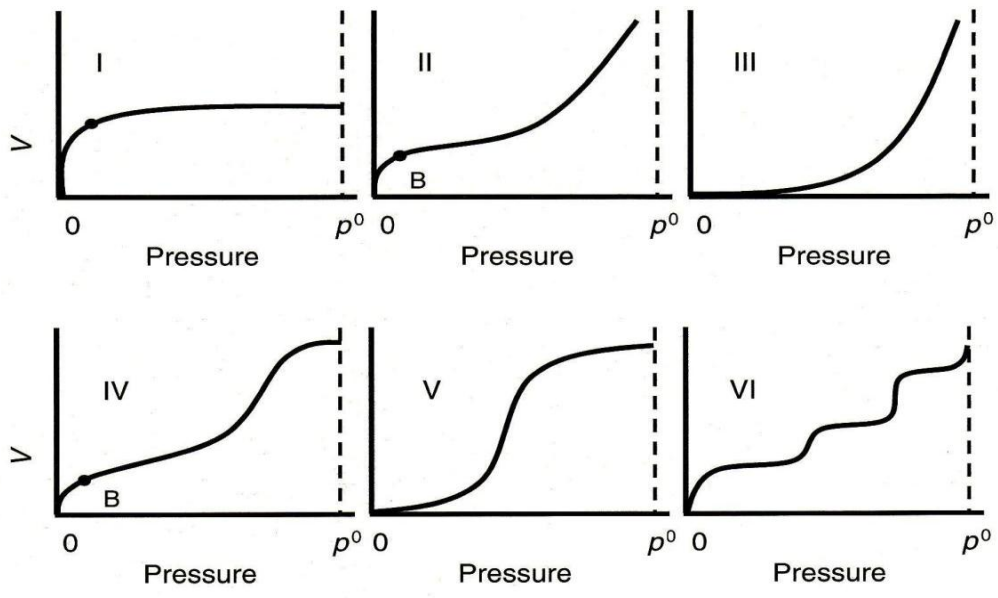

Figure 3.1 The six typical types of nitrogen adsorption isotherms (p^o is the saturation

pressure).

In type I isotherm, there is initially an increase of the amount of gas adsorbed at relatively low gas pressure. After a certain time with increasing pressure, saturation takes place with no more further adsorption and this is independent of any higher pressure. The saturation is caused by the filling of adsorbed molecules in pores. Only a monolayer adsorption with no further layer formation happens here. In this case, the adsorbate is microporous. This type can be exemplified by adsorption of N_2 or H_2 on charcoal at -180 °C.

In type II isotherm, there is an increase of the entire adsorption at low pressure, which indicates the formation of monolayer adsorption. After that, there is continuous formation of adsorption on multilayers with increasing the adsorbate pressure until condensation happens. This is a non-porous adsorbent, and type II can be an example of adsorption of N_2 on Fe or Pt at -195 °C.

In type III, there is a slight increase in the adsorption at lower pressure, which indicates a weak interaction between adsorbate and adsorbent. There is a continuous increase of the saturated pressure, which indicates straightaway a formation of multilayers with a strong adsorbate-adsorbate interaction. This type of adsorption is called clustering and the type of solid can be both porous and nonporous. An example of this is adsorption of Br_2 on silica at 80 °C.

Type IV isotherm is similar to type II up to low pressure, as the first formation of the adsorption monolayer takes place at low pressure. But when the pressure is further increased, the capillary condensation occurs within pores. As a result, there is the formation of a multilayer and the formation of a hysteresis loop upon desorption.

Such adsorbents are mesoporous. This is an example of adsorption of benzene on silica at 50 °C.

In type V, the monolayer adsorption starts condensing inside the pores and when it is completed the formation of multilayer takes place by the capillary condensation. This can be exemplified by adsorption of water vapour on activated charcoal at 100 °C.

Type VI is a multilayer adsorption where first a complete formation of the monolayer on the adsorbent take place, followed by subsequent formation of the multiple layers. This behaviour is typical of nonporous solids.

Type IV isotherm will be exposed more in this work as it is related to the prepared catalysts and it attributes mesoporous substrate.

When the formation of adsorption is completed, the desorption process starts. The desorption measurements occur by lowering the pressure to allow the desorbed gas to release. This step leads to a loop in the graph of the adsorption isotherm. This loop is called a hysteresis loop. According to IUPAC, a hysteresis loop is classified into four types as shown in Figure 3.2 [3, 4].

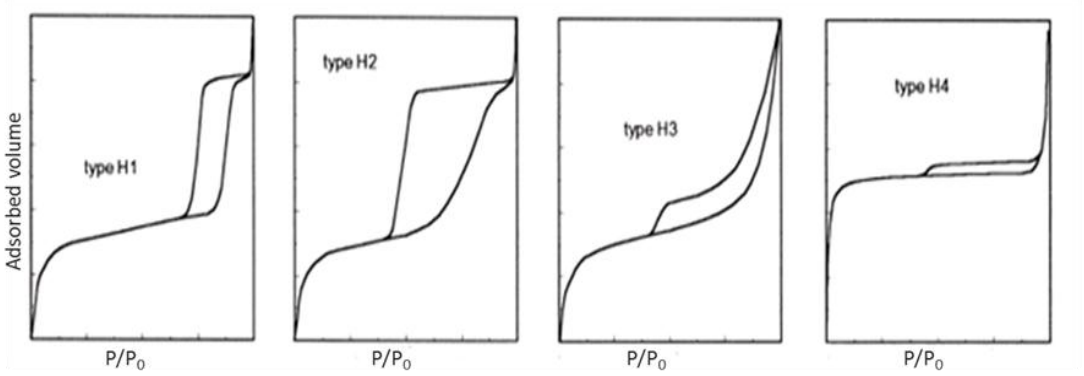

Figure 3.2 The four common shapes of hysteresis loops in N_2 adsorption isotherms.

Type H1 hysteresis is present in the case of solid samples involving particles containing crossed channels, which in shape are either cylindrical or spherical aggregates. When the shape and the size of the pores are identical, they are attributed in H1 hysteresis. Type H2 hysteresis occurs when the size and shape of the particles are different and close in shape to the ink bottle, where the pore body is wider than the pore mouth. These loops are due to the difference in size and shape of the pores, which reflects the behaviour of the adsorption and desorption process of the gas within the sample. These types of loops are common in mesoporous solid substances such as heteropoly acids.

Type H3 hysteresis is commonly characteristic of a solid substance of non-identical particles, which have slit or plate shapes. Zeolite is an example of this type. Type H4 hysteresis is characterised by identical pores in size and shape. Active carbon symbolises this type of hysteresis.

In some cases, the hysteresis loop cannot be included within these four types (Figure 3.3), due to the presence of a variety of shapes of the pores such as interconnected, blind, wedge and funnel pores. These lead to unrecognized loops. Substances with irregular pores may show a much reduced hysteresis loop.

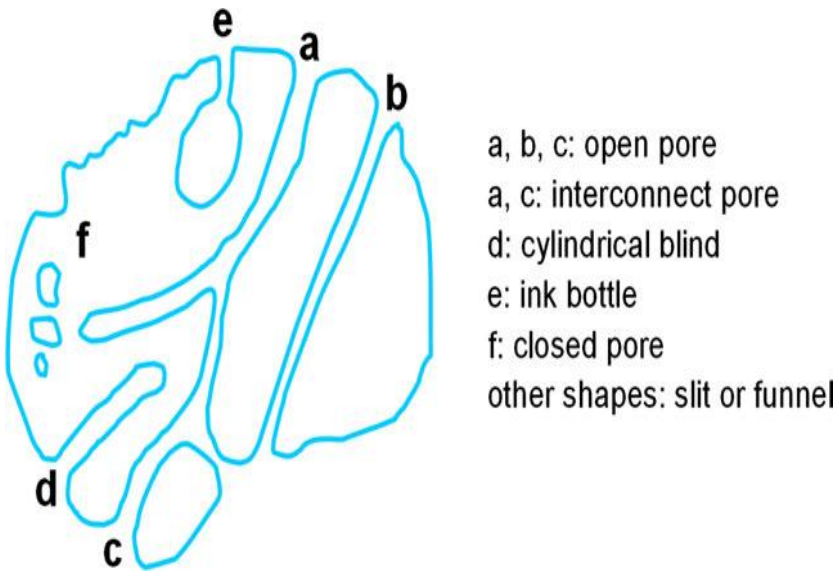

Figure 3.3 Different shapes of pores in a porous solid [5].

Based on IUPAC classification, the size of pores can be classified into one of the following classes: a solid substance that has pores less than 2 nm in diameter is named microporous, the substance having pores within 2 and 50 nm is mesoporous and the one containing pores greater than 50 nm is macroporous [6, 7].

Commonly, the total surface area of the most heterogeneous catalysts is within the range 1-10^3 m^2 g^{-1}, while their external surface area is within 0.01- 10 m^2g^{-1}. This demonstrates the importance of pores to increase the total surface area due to the contribution of pore walls. In general, porous solids are more favourable as catalysts in chemical reactions [8-10].

The results obtained from BET for the prepared heteropoly acid catalysts are shown in Tables 3.3 and 3.4. Table 3.3 shows how oxide supports can increase the surface area with porosity of HPA catalysts in contrast to bulk HPA catalysts. These catalysts have pore sizes greater than 50 nm, which are classified as macropores. In addition, this table compares the surface area and porosity of $Cs_{2.5}$ and $Cs_{2.25}$ acidic salts of HPW,

indicating that $Cs_{2.5}$ has a higher surface area and pore size. These catalysts have pore sizes between 2-50 nm, hence are mesoporous. Table 3.4 illustrates that the loading of metal affects the surface area of HPA catalysts. While the CsPW catalyst has a surface area of 139 m^2g^{-1}, it becomes 84 m^2g^{-1} and 105 m^2g^{-1} for 6.0%Pt/CsPW and 5.6%Pt/CsPW, respectively, and 103 m^2g^{-1} for 4.7%Au/CsPW. This effect is much higher with bimetallic PtAu loading as the surface area of 5.9%Pt/4.4%Au/CsPW is 62 m^2g^{-1}, despite the pore size of the particles for the bimetallic catalyst 5.9%Pt/4.4%Au/CsPW (42 Å) being bigger than for 6.0%Pt/CsPW (25 Å). The PtAu catalyst has a smaller surface area (62 m^2g^{-1}) compared to the Pt catalyst (84 m^2g^{-1}), which suggests some blocking of pores. In the case of the activated carbon support, the surface areas of the catalysts are much higher in comparison with HPAs.

Table 3.3 Information about HPA acid catalysts and supports.

Catalysts	S_{BET}[a]	Pore volume[b]	Pore size[c]
	m^2g^{-1}	cm^3g^{-1}	Å
TiO_2 (P25 Degussa)	44	0.10	90
SiO_2 (Aerosil 300)	300[f]		
$H_3PW_{12}O_{40}$ (HPW)	5.6	0.04	81
$H_4SiW_{12}O_{40}$ (HSiW)	9.0	0.02	71
$Cs_{2.5}H_{0.5}PW_{12}O_{40}$ (CsPW)	132	0.10	29
$Cs_{2.25}H_{0.75}PW_{12}O_{40}$	128	0.07	22
15%HPW/SiO_2	202	1.00	169

15%HSiW/SiO_2	221	1.02	185
15%HPW/TiO_2	45	0.20	174

[a]BET surface area. [b]Single point total pore volume at P/P_o = 0.97. [c]Average BET pore diameter. [f]Manufacturer's value.

Table 3.4 Information about Pt and Au catalysts.

Catalyst[a]	S_{BET}[b]	Pore volume[c]	Pore size[d]
	m^2g^{-1}	cm^3g^{-1}	Å
$H_3PW_{12}O_{40}$ (HPW)	7.8	0.012	63
$Cs_{2.5}H_{0.5}PW_{12}O_{40}$ (CsPW)	139	0.079	23
6.0%Pt/CsPW	84	0.052	25
5.6%Pt/CsPW	105	0.068	26
5.9%Pt/4.4%Au/CsPW	62	0.065	42
4.7%Au/CsPW	103	0.048	33
Darco KB-B activated carbon	977	0.89	35
5.0%Au/C	1207	1.00	33

6.2%Pt/C	1224	1.04	34
6.7%Pt/5.0%Au/C	1177	0.98	33

[a]Metal catalysts prepared by impregnating H_2PtCl_6 and $HAuCl_4$ onto CsPW or activated carbon from aqueous medium; metal loading determined from ICP-AES analysis. [b]BET surface area. [c]Single point total pore volume at P/P_o = 0.97. [d]Average BET pore diameter.

Figures 3.4 displays the nitrogen adsorption and desorption isotherms of $Cs_{2.5}H_{0.5}PW_{12}O_{40}$, which represent type IV isotherm with a type H3 hysteresis loop on the basis of IUPAC classification. This loop proves that the material is typically mesoporous (2 nm < pore diameter < 50 nm), with a non-uniform shape and size. Figure 3.5 displays the pore size distribution of $Cs_{2.5}H_{0.5}PW_{12}O_{40}$ obtained from the BJH method, where a sharp peak is at about 40 Å diameter. This is in agreement with previous report [12]. The N_2 adsorption technique employed in this study was not capable to determine micropores in these catalysts.

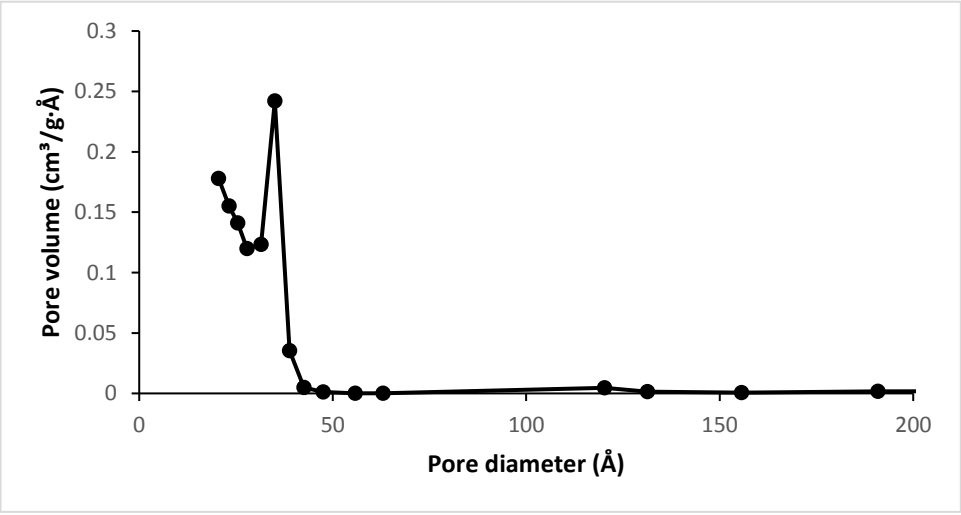

Figure 3.4 Pore size distribution of $Cs_{2.5}H_{0.5}PW_{12}O_{40}$.

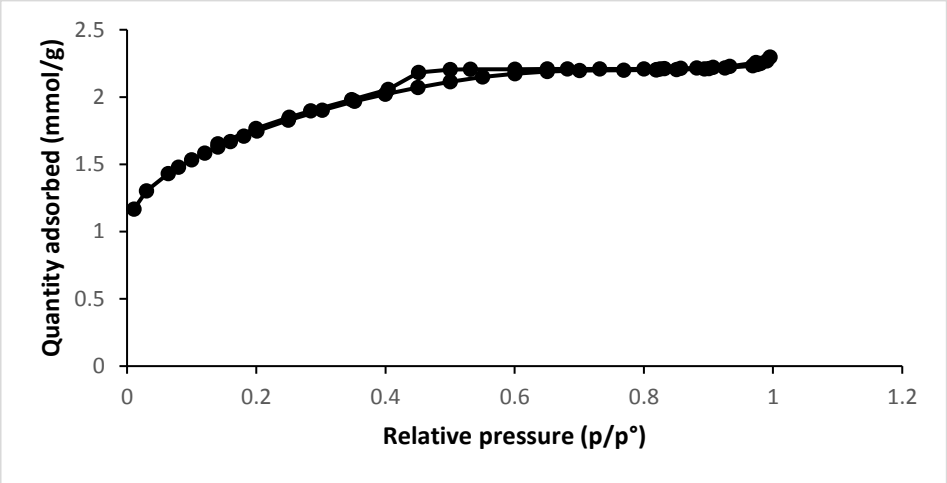

Figure 3.5 N_2 adsorption and desorption isotherms of CsPW.

Figures 3.6-3.9 show the nitrogen adsorption and desorption isotherms for $Pt/Cs_{2.5}H_{0.5}PW_{12}O_{40}$ catalysts prepared from water (using H_2PtCl_6) and benzene (using $Pt(acac)_2$. It can be seen that in spite of different preparation and metal precursors using H_2O and C_6H_6 as solvents, there is no significant effect on the N_2 isotherm profiles. The BET surface areas of Pt/CsPW catalysts were lower than the surface area of bulk CsPW. However, there is no significant effect of Pt loading on the catalyst porosity.

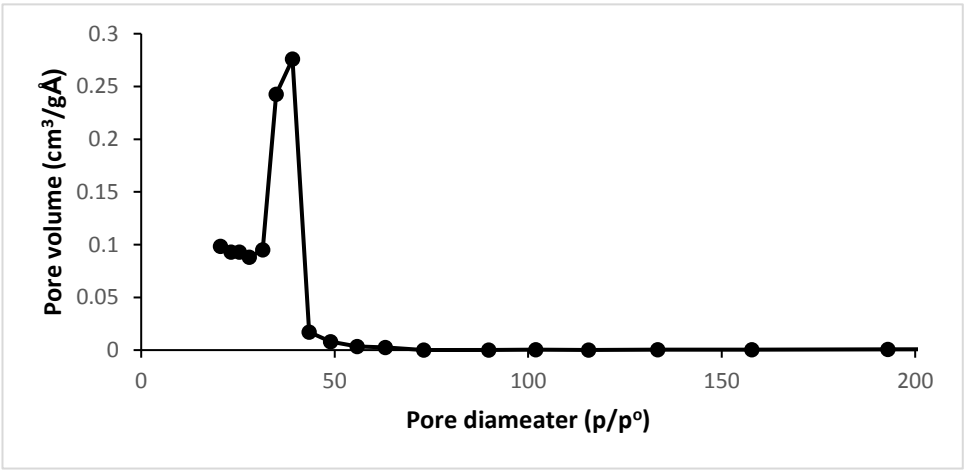

Figure 3.6. Pore size distribution of 6%Pt/CsPW prepared from H_2O.

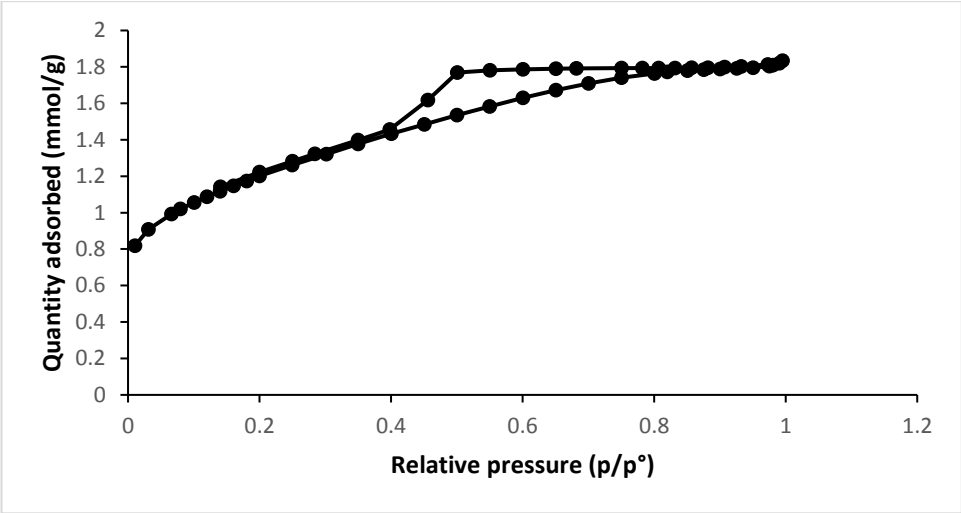

Figure 3.7 N_2 adsorption and desorption isotherms of 6%Pt/CsPW prepared from H_2O.

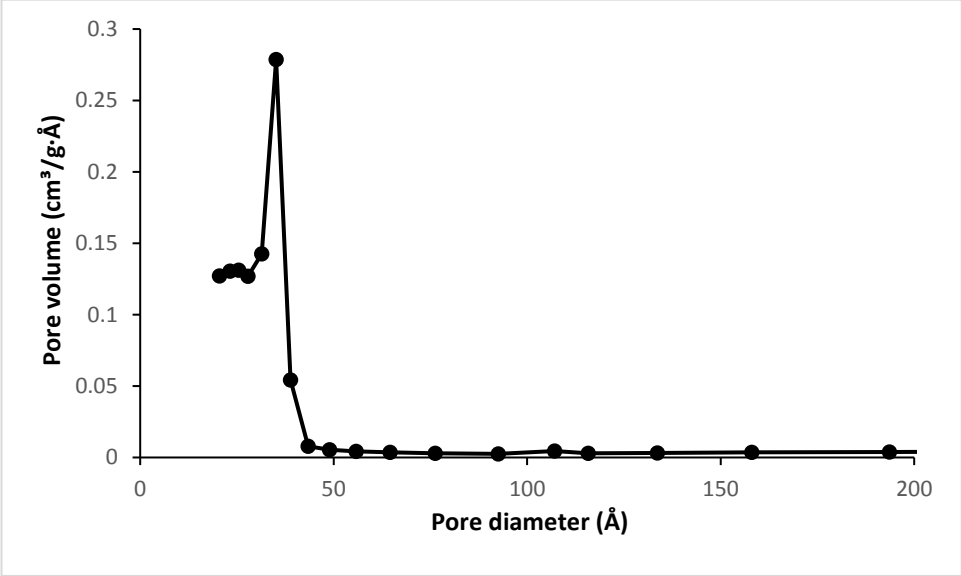

Figure 3.8 Pore size distribution of 5.6%Pt/CsPW prepared from C_6H_6.

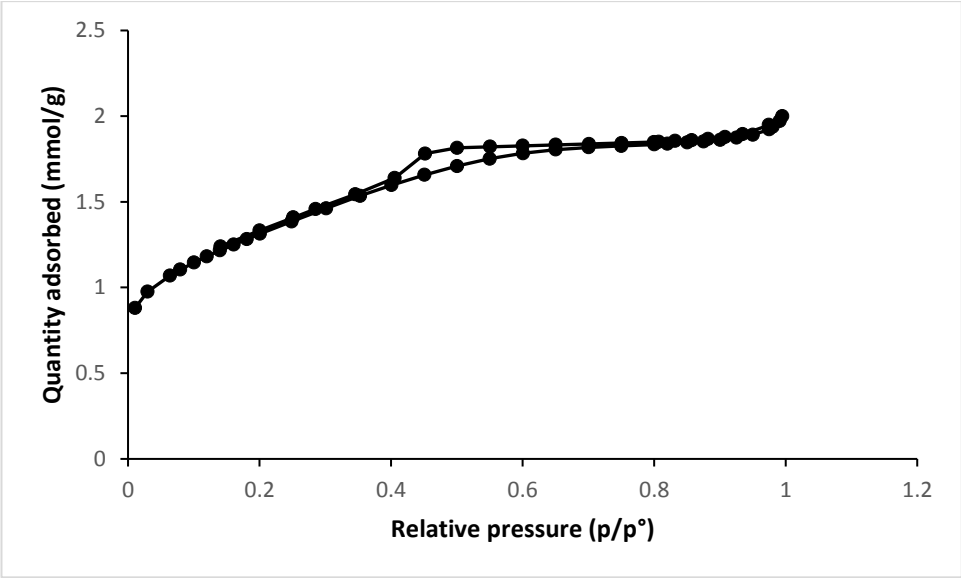

Figure 3.9 N_2 adsorption and desorption isotherms of 5.6%Pt/CsPW prepared from C_6H_6.

Figures 3.10-3.11 exhibit the nitrogen adsorption and desorption isotherms and pore size distribution of Pt/Au/CsPW. These were similar to Pt/CsPW catalysts. Thus, the effect of bimetallic PtAu nanoparticles was the same as the Pt alone.

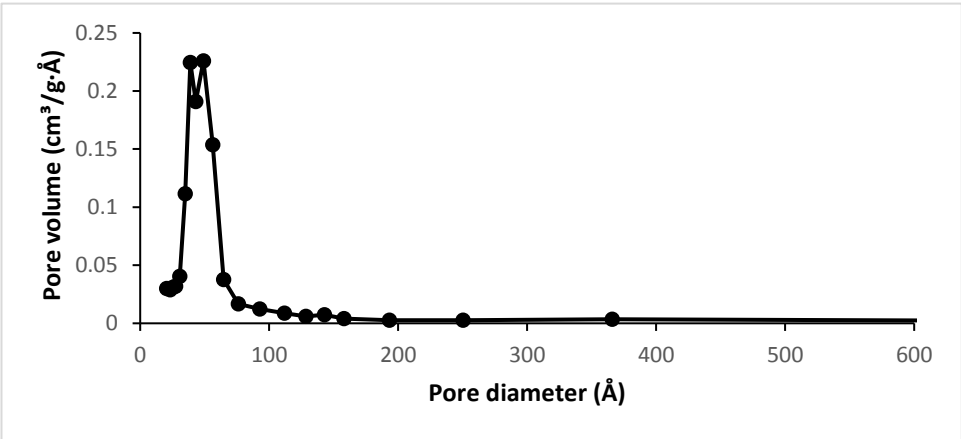

Figure 3.10 Pore size distribution of 5.9%Pt/4.4%Au/CsPW.

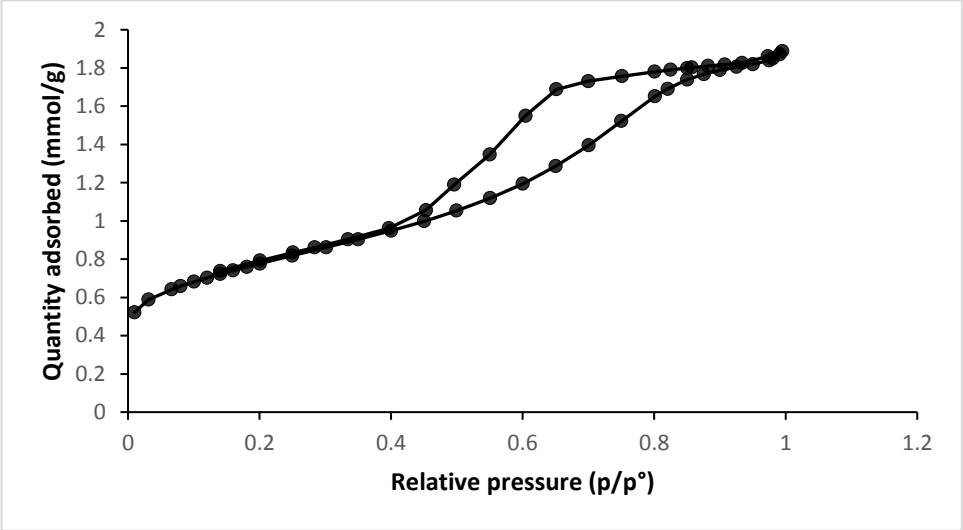

Figure 3.11 N_2 adsorption and desorption isotherms of 5.9%Pt/4.4%Au/CsPW.

3.3 Powder X-ray diffraction (XRD)

Powder X-ray diffraction (XRD) patterns of heteropoly acids and CsPW-modified metal catalysts were recorded on a PANalytical Xpert diffractometer with CuKα radiation (λ = 1.542 Å) and attributed using the JCPDS database. The XRD patterns were studied to estimate the metal particle size applying the Scherer equation, with line broadening assessed as the full width at half maximum intensity (FWHM). All XRD analyses were conducted by the Liverpool University Single Crystal X-ray Diffraction suite.

3.2.1 CsPW-supported metal catalysts

Figure 3.13 shows the XRD pattern of fresh $Cs_{2.5}H_{0.5}PW_{12}O_{40}$, which is in full agreement with the standards in the literature [11, 12].

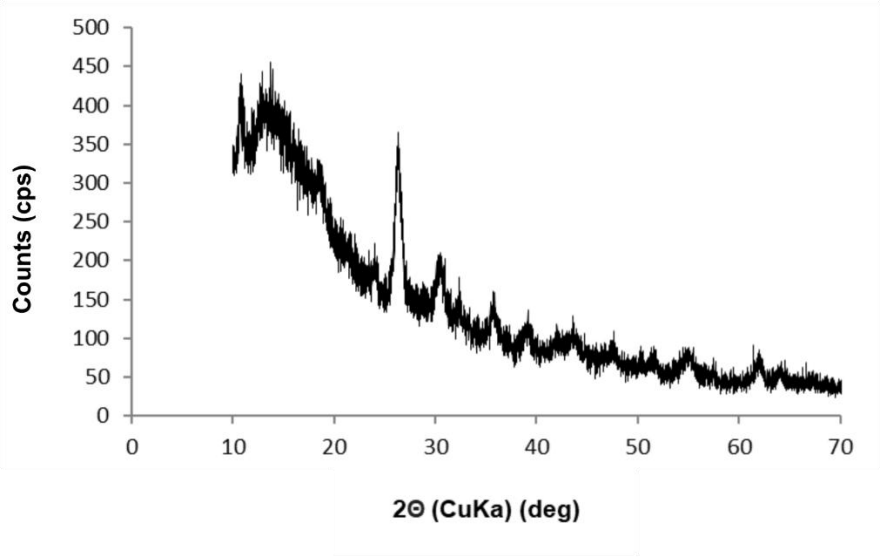

Figure 3.13. XRD pattern with CuKα radiation for fresh $Cs_{2.5}H_{0.5}PW_{12}O_{40}$.

Figure 3.14a shows the XRD patterns of 5.57%Pt/4.25%Au/CsPW and 5.78%Pt/CsPW catalysts, in which the bcc pattern of crystalline CsPW [41] is dominated. Also clearly seen is the fcc pattern of Pt (39.8^o [111] and 46.2^o [200]) and Au (38.2^o [111] and 44.4^o [200]) metal nanoparticles. This confirms coexistence of Pt and Au particles in the PtAu/CsPW catalyst. In addition, PtAu bimetallic particles may be present with diffraction pattern falling in between the corresponding diffractions of the pure metals, which is obscured by the intense pattern of CsPW. Indeed, the close-up normalized difference XRD (Fig. 3.14b) shows a broad diffraction peak in the range of 38-40^o and possibly a weaker [200] peak in the range 44-46^o between the diffractions of pure Pt and Au, which could be attributed to PtAu alloys. In Figure.

3.14a, the Pt peaks appear notably broader than the Au peaks, indicating higher dispersion of Pt particles. Although accurate analysis of metal particle size is difficult due to the prevailing CsPW pattern, rough estimate from the [111] peaks using the Scherrer equation gave 60 and 30 nm volume-average particle size for Au and Pt, respectively. This estimate, however, may be biased towards larger metal particles.

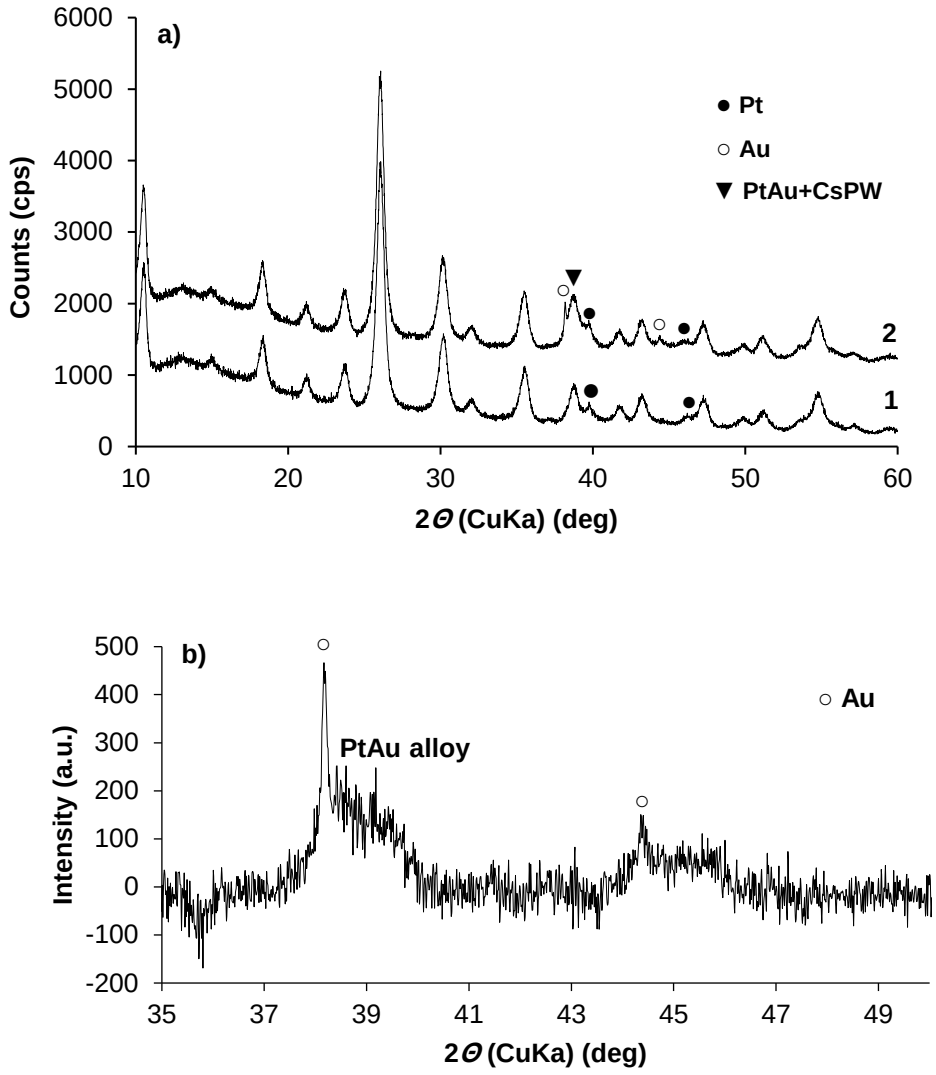

Figure 3.14 Powder XRD patterns: (a) 5.78%Pt/CsPW (1) and 5.57%Pt/4.25%Au/CsPW (2); (b) close-up normalized difference (2) – (1) XRD pattern showing a broad [111] fcc PtAu alloy peak in the range 38-40^{o} and possibly a weaker [200] PtAu alloy peak in the range 44-46^{o}.

3.4 TEM

Transmission electron microscopy (TEM) imaging of catalysts was carried out on FEI Tecnai Spirit BioTWIN instrument at 120 kV operation. For TEM and STEM analysis, the samples were prepared by scooping up the catalyst powder by a TEM grid (holey carbon film on 300 Ni or Cu mesh, Agar Scientific) followed by shaking to remove excess material from the grid. The noticeable difference on the TEM image reflects the interaction between the transmitted electron beam and different atoms involved in the sample. On the basis of atom density, metal has a high electron density comparing to the support, causing darker spots on the TEM image. Figures 3.15-3.16 display the TEM images for carbon-supported monometallic Pt, Au and bimetallic PtAu catalysts together with particle size distributions. From these data, average metal particle size in these catalysts was determined.

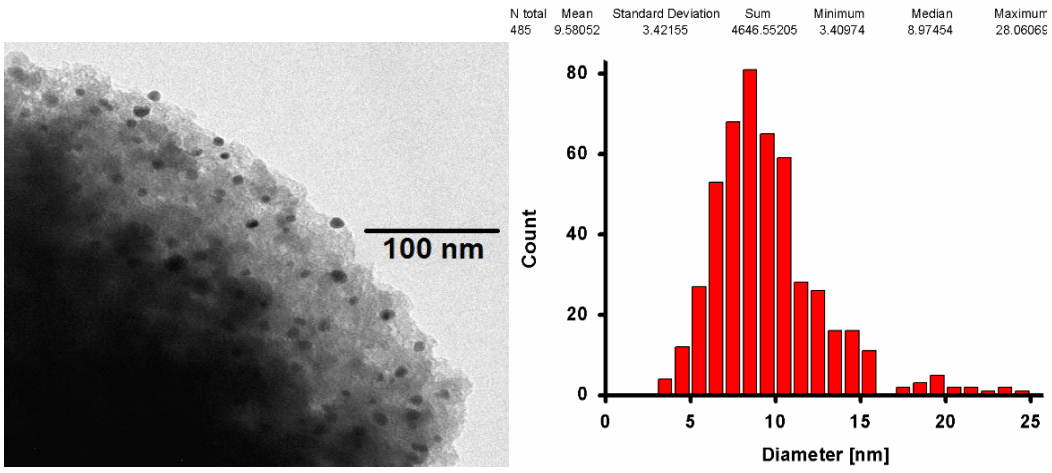

Figure 3.15 TEM image and Au particle size distribution for 5.0%Au/C with a mean Au particle size of 9.6±3.4 nm.

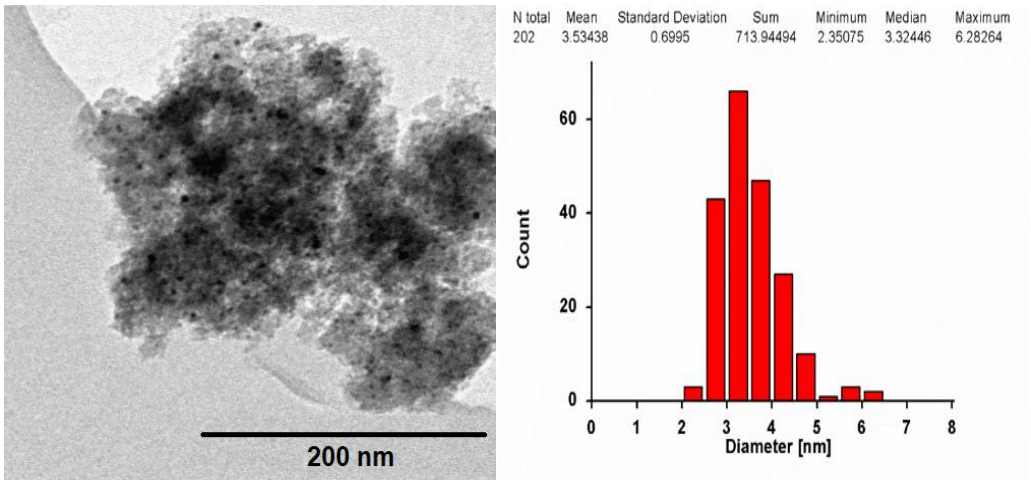

Figure 3.16 TEM image and Pt particle size distribution for 6.2%Pt/C with a mean Pt particle size of 3.5±0.7 nm.

3.5 STEM-EDX

Scanning transmission electron microscopy (STEM) imaging and energy dispersive X-ray spectroscopy (EDX) analysis of catalysts was carried out on an aberration-corrected JEOL JEM 2100FCs instrument operated at 200 kV, equipped with an EDAX Octane T Optima 60 windowless silicon drift detector. For STEM analysis, the samples were prepared by scooping up the catalyst powder by a TEM grid (holey carbon film on 300 Ni mesh, Agar Scientific) followed by shaking to remove excess material from the grid. HAADF-STEM images and STEM-EDX analysis for the Pt, Au and PtAu catalysts are shown in Figures 3.17-3.21. These results are discussed in detail in Chapters 4 and 5.

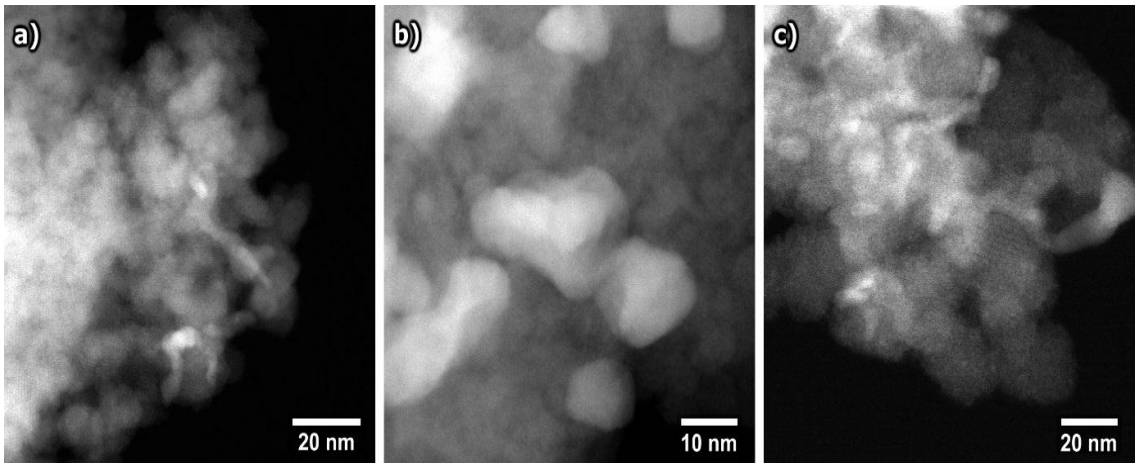

Figure 3.17 HAADF-STEM images of (a) 5.78%Pt/CsPW, (b) 2.62%Au/CsPW and (c) 5.57%Pt/4.25%Au/CsPW catalysts, showing noble metal nanoparticles as bright spots.

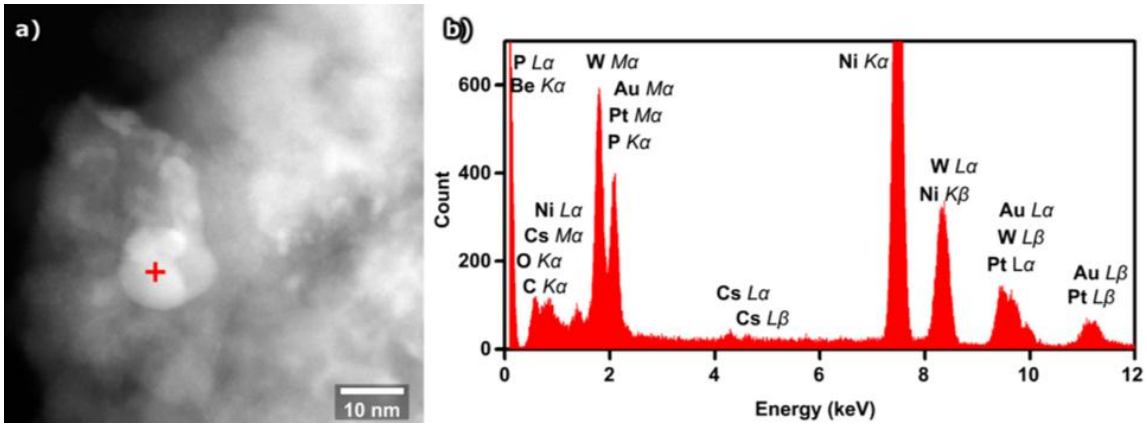

Figure 3.18 (a) HAADF-STEM image of 5.57%Pt/4.25%Au/CsPW catalyst; the cross on a 12 nm PtAu nanoparticle marks the spot where EDX analysis was performed; (b) the EDX spectrum, revealing the atomic ratio Pt/Au = 7.7, indicating that the probed PtAu nanoparticle is Pt-rich.

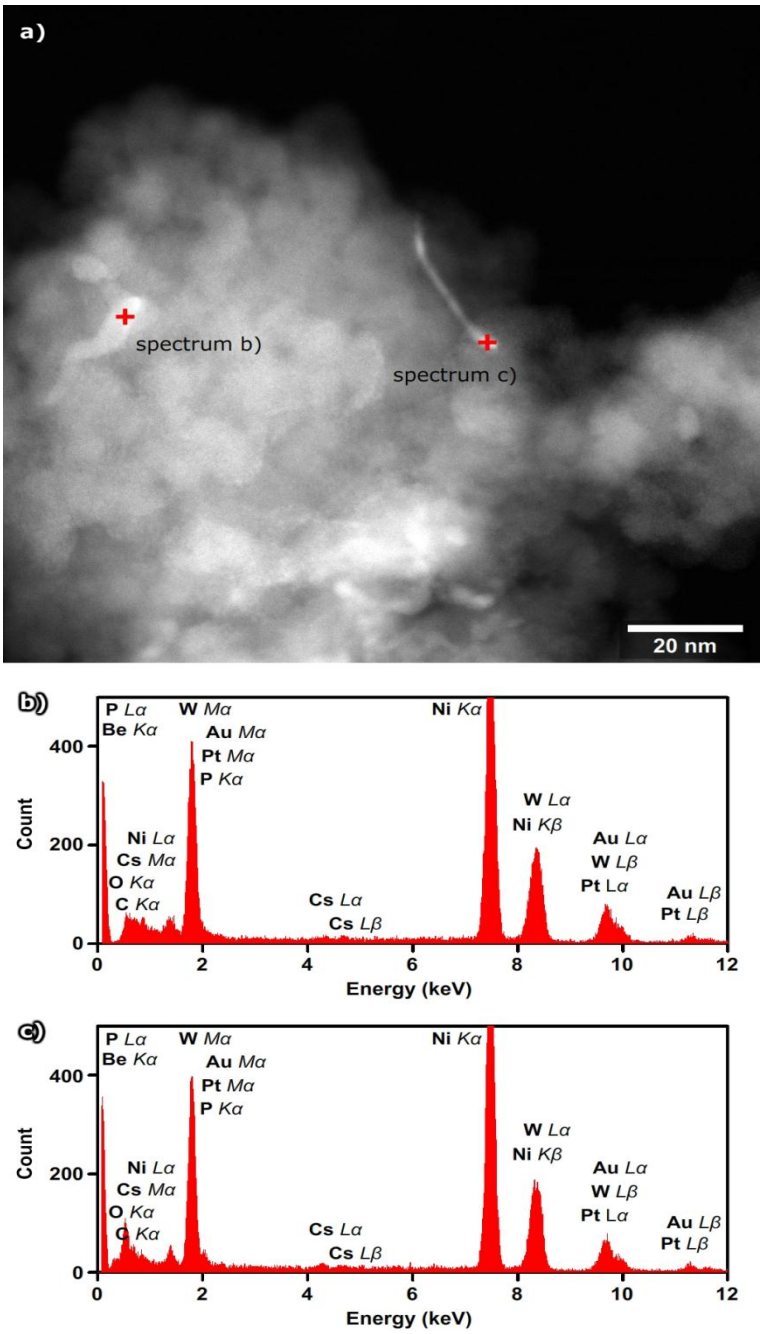

Figure 3.19 STEM-EDX analysis of 5.57%Pt/4.25%Au/CsPW catalyst: (a) HAADF-STEM image showing two PtAu nanoparticles marked with crosses that were investigated by EDX; (b, c) the corresponding EDX spectra, revealing the atomic ratio Pt/Au ≈ 0.5 in both spots.

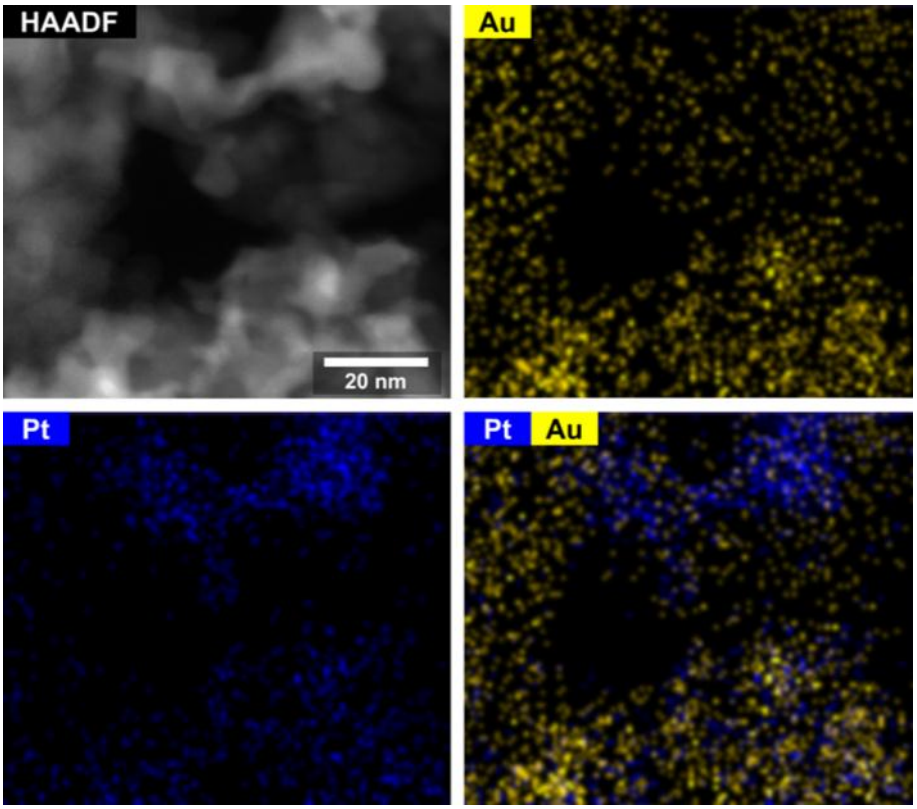

Figure 3.20 HAADF-STEM image of 5.57%Pt/4.25%Au/CsPW catalyst and the corresponding STEM-EDX elemental maps showing the spatial distribution of Au (yellow) and Pt (blue) in the sample. The upper part appears to be relatively Pt rich, whereas the bottom part is Au rich, indicating the presence of non-uniform PtAu nanoparticles.

a)

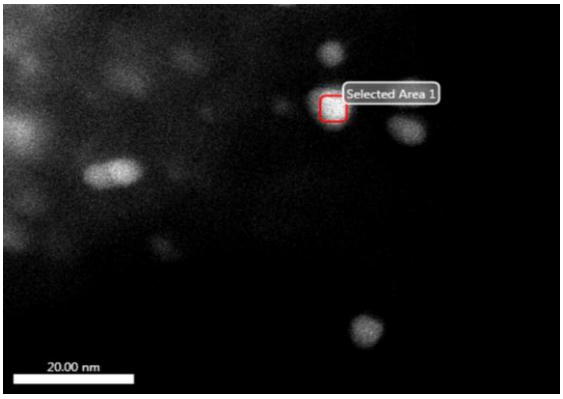

b

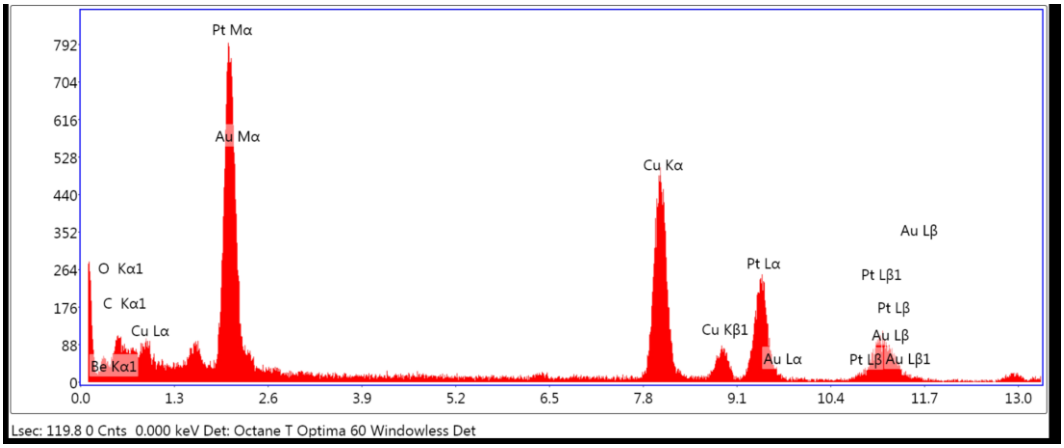

c)

Element	Weight %	Atomic %
Be K (TEM holder)	4.85	36.01
C K (including TEM grid)	0.61	3.41
O K	1.99	8.34
Cu K (TEM grid)	28.89	30.42
Pt L	60.61	20.79
Au L	3.04	1.03

Figure 3.21 STEM-EDX analysis of 6.7%Pt/5.0%Au/C catalyst: (a) HAADF-STEM image showing metal nanoparticles as bright spots; the spot in red square was investigated by EDX; (b) the corresponding EDX spectrum, revealing the atomic ratio Pt/Au = 21; (c) elemental composition of the selected area.

3.6. H_2 chemisorption

Pt dispersion in the catalysts was determined on a Micromeritics TPD/TPR 2900 instrument equipped with a thermal conductivity detector (TCD) using the H_2/O_2 titration pulse method in a flow system at room temperature as described elsewhere [13] using 50-75 mg catalyst samples in N_2 flow (50 mL min^{-1}). The Pt dispersion (defined as the Pt fraction at the surface, $D = Pt_s/Pt_{total}$) was calculated assuming the stoichiometry of H_2 adsorption: $Pt_sO + 1.5\ H_2 \rightarrow Pt_sH + H_2O$ [14, 15]. H_2 adsorption observed on the PtAu catalysts was attributed to platinum as Au/CsPW did not adsorb any hydrogen under such conditions [16]. The average diameter of Pt particles, *d*, was calculated from the empirical equation d (nm) = 0.9/D [14]. Figures 3.22 and 3.23 show examples of pulse chemisorption of H_2 on CsPW supported Pt and PtAu catalysts.

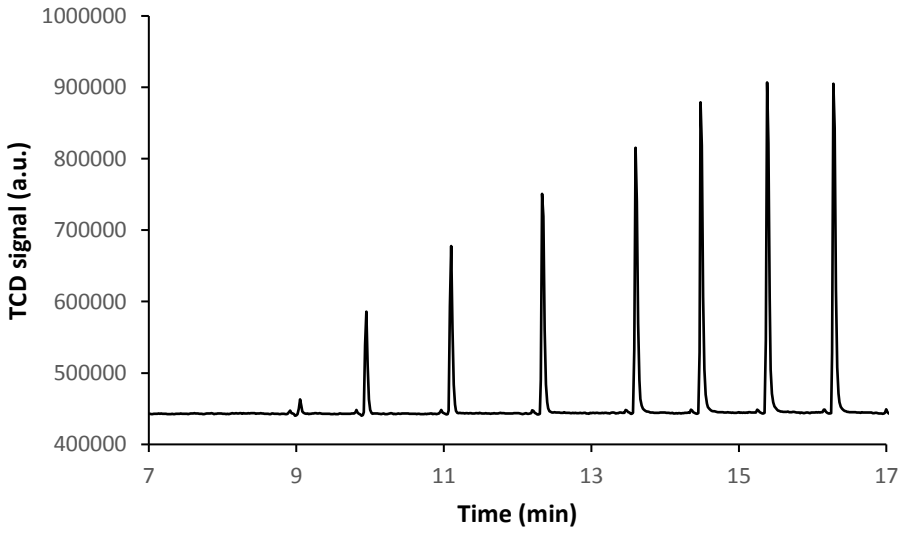

Figure 3.22 H_2 pulse chemisorption on 5.6%Pt/CsPW.

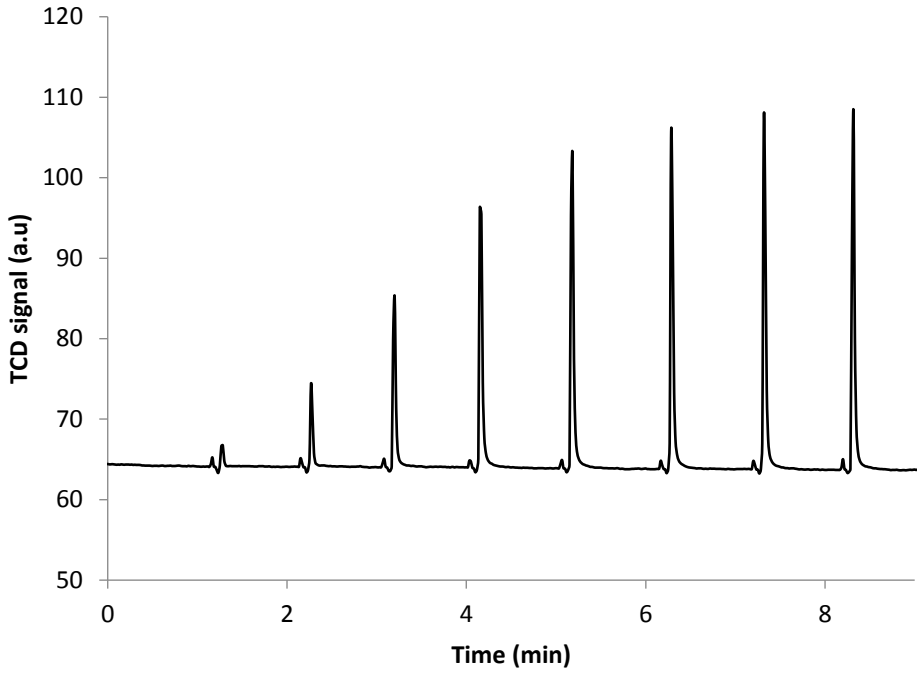

Figure 3.23 Pulse chemisorption of H_2 on 5.6%Pt/4.3%Au/CsPW-CI.

Table 3.5 presents Pt dispersion and particle size for the catalysts prepared. It can be seen that Au additives practically did not change the dispersion of Pt in these catalysts.

Table 3.5 The metal dispersion of catalysts.

Catalyst[a]	D^b	d^c nm
0.11%Pt/CsPW	0.85	1.1
0.23%Pt/CsPW	0.76	1.2
0.32%Pt/CsPW	0.61	1.5
0.71%Pt/CsPW	0.55	1.6
2.45%Pt/CsPW	0.29	3.1
3.56%Pt/CsPW	0.13	6.9
3.76%Pt/CsPW	0.26	3.5
5.78%Pt/CsPW	0.19	4.7
5.87%Pt/CsPW	0.22	4.1
11.5%Pt/CsPW	0.15	6.0
0.28%Pt/0.35%Au/CsPW	0.55	1.6
5.57%Pt/4.25%Au/CsPW	0.17	5.3

[a]Metal loading obtained from ICP-AES analysis. [b]Pt dispersion determined from H_2/O_2 titration; for PtAu catalysts assuming negligible H_2 adsorption on gold. [c]Metal particle diameter: for Pt from the equation d (nm) = 0.9/D, for Au from STEM.

3.7 Temperature programmed desorption

After completion of H_2/O_2 titration, H_2-TPD was measured by increasing the temperature from room temperature to 250 °C at a rate of 10 °C per minute. The H_2/O_2 titration and H_2-TPD procedure is illustrated in Figure 3.24 for Pt/CsPW and in Figure 3.25 for PtAu/CsPW catalyst. For comparison, these results are plotted together in Figure 5.10 (for discussion, see Chapter 5).

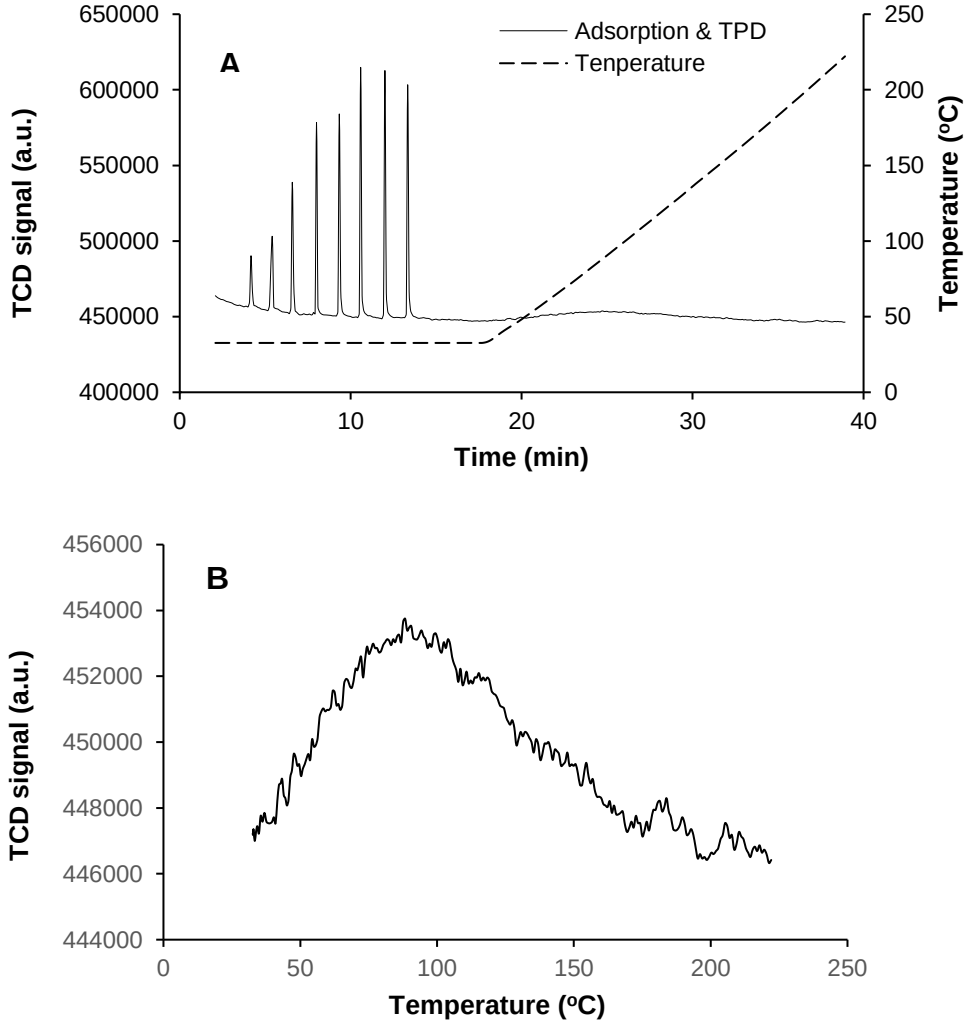

Figure 3. 24 (A) H_2/O_2 titration and H_2-TPD for 5.9%Pt/CsPW (75 mg catalyst sample, 50 µL H_2 pulses, 50 mL min^{-1} N_2 flow rate), (B) H_2-TPD.

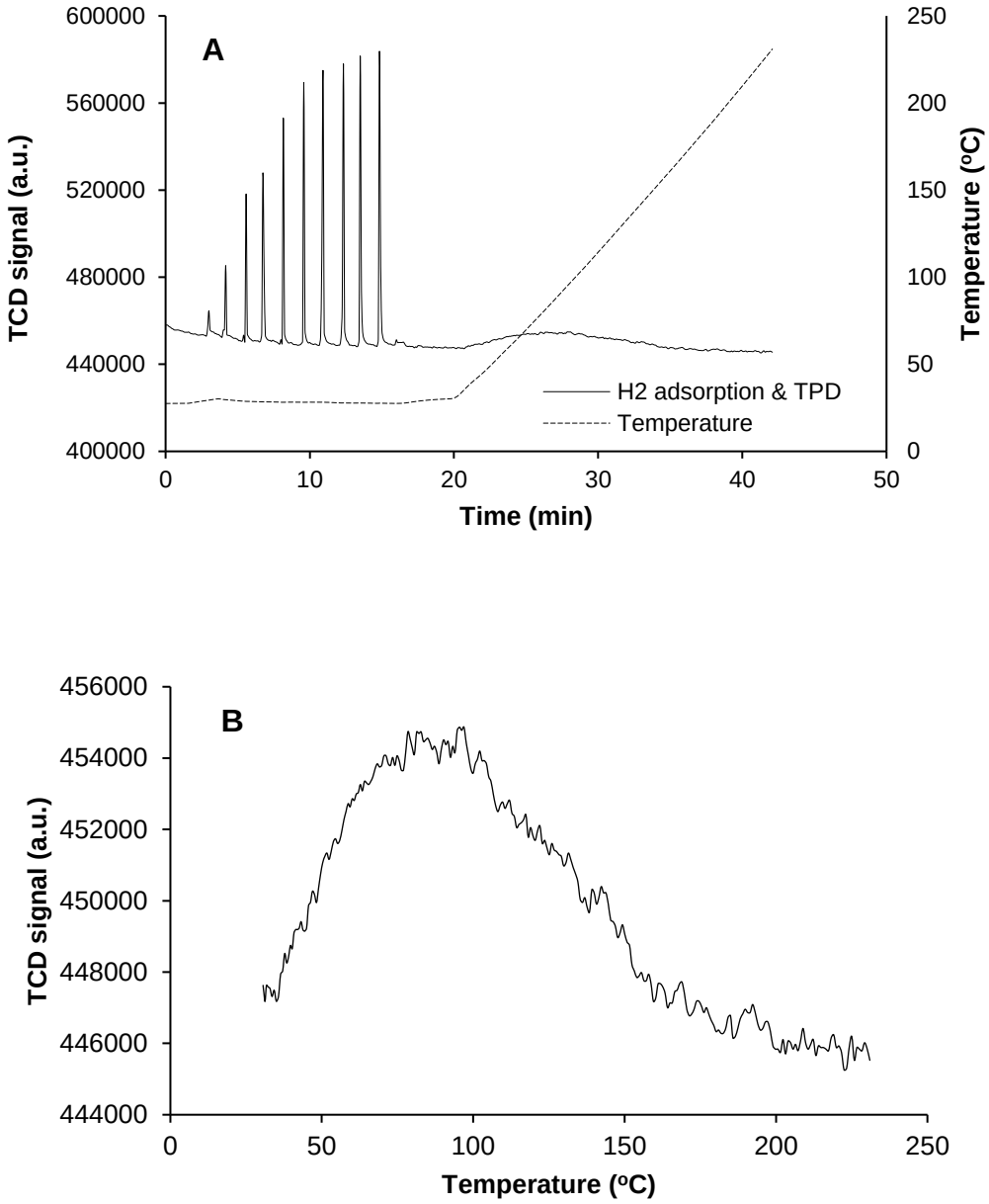

Figure 3.25 (A) H_2/O_2 titration and H_2-TPD for 5.9%Pt/4.4%Au/CsPW (75 mg catalyst sample, 50 µL H_2 pulses, 50 mL min^{-1} N_2 flow rate), (B) H_2-TPD.

3.8 C analysis

Thermo Flash EA 1112 analyser was used to determine carbon content in spent catalysts by combustion chemical analysis. The carbon content in spent catalysts after n-hexane isomerisation is presented in Table 3.6.

Table 3.6 Carbon content in spent catalysts after n-hexane isomerisation.[a]

Catalyst	T. °C	Time on stream h	Conversion[b] %	C. content %
CsPW	180	6.0	2.8-1.2	0.6
0.32%Pt/CsPW	180	6.0	4.5-3.3	0
5.78%Pt/CsPW	180	6.0	8.1-7.4	0
0.28%Pt/0.35%Au/CsPW	180	6.0	9.0-6.1	0
5.57%Pt/4.25%Au/CsPW	180	6.0	11.2-9.6	0.1
2.62%Au/CsPW	180	6.0	1.9-0.9	0.3

[a]0.20 g catalyst, 5.78 kPa n-hexane partial pressure in H_2 flow (20 mL min^{-1}). [b]Initial and final n-hexane conversion over 6 h time on stream.

The amount of coke in spent Pt/CsPW catalysts was below the detection limit after reaction at 180 °C (6 h on stream). No coke was found in spent PtAu/CsPW catalysts, although a small amount of coke (0.3% C) was formed in Au/CsPW catalyst. Nevertheless, the amount of coke in the Au/CsPW was less than that in CsPW (0.6%). This might explain a better performance stability of Au/CsPW compared to CsPW.

References

[1] H. Bönnemann, Gadi Rothenberg. Catalysis Concepts and Green Applications Wiley-VCH, 2008.

[2] G. Leofanti, M. Padovan, G. Tozzola, B. Venturelli, Surface area and pore texture of catalysts, Catalysis Today, 41 (1998) 207-219.

[3] S. Gregg, K. Sing, Adsorption, surface area, and porosity, London: Academic Press, 1982.

[4] L.G. Joyner, E.P. Barrett, R. Skold, The determination of pore volume and area distributions in porous substances. II. Comparison between nitrogen isotherm and mercury porosimeter methods, Journal of the American Chemical Society, 73 (1951) 3155-3158.

[5] S.-S. Chang, B. Clair, J. Ruelle, J. Beauchêne, F. Di Renzo, F. Quignard, G.-J. Zhao, H. Yamamoto, J. Gril, Mesoporosity as a new parameter for understanding tension stress generation in trees, Journal of Experimental Botany, 60 (2009) 3023-3030.

[6] J.M. Thomas, W.J. Thomas, Principles and Practice of Heterogeneous Catalysis, VCH, Weinheim, 1997.

[7] J. Rouquerol, D. Avnir, C. Fairbridge, D. Everett, J. Haynes, N. Pernicone, J. Ramsay, K. Sing, K. Unger, Recommendations for the characterization of porous solids (Technical Report), Pure and Applied Chemistry, 66 (1994) 1739-1758.

[8] G. Rothenberg, Catalysis: concepts and green applications, John Wiley & Sons, 2017.

[9] I.V. Kozhevnikov, Catalysts for fine chemical synthesis, catalysis by polyoxometalates, John Wiley & Sons, 2002.

[10] N. Mizuno, M. Misono, Heterogeneous catalysis, Chemical reviews, 98 (1998) 199-218.

[11] J.A. Dias, E. Caliman, S.C.L. Dias, Effects of cesium ion exchange on acidity of 12-tungstophosphoric acid, Microporous and Mesoporous Materials, 76 (2004) 221-232.

[12] T. Okuhara, H. Watanabe, T. Nishimura, K. Inumaru, M. Misono, Microstructure of cesium hydrogen salts of 12-tungstophosphoric acid relevant to novel acid catalysis, Chemistry of Materials, 12 (2000) 2230-2238.

[13] K. Alharbi, E. Kozhevnikova, I. Kozhevnikov, Hydrogenation of ketones over bifunctional Pt-heteropoly acid catalyst in the gas phase, Applied Catalysis A: General, 504 (2015) 457-462.

[14] J. Benson, H. Hwang, M. Boudart, Hydrogen-oxygen titration method for the measurement of supported palladium surface areas, Journal of Catalysis, 30 (1973) 146-153.

[15] J.E. Benson, M. Boudart, Hydrogen-oxygen titration method for the measurement of supported platinum surface areas, Journal of Catalysis, 4 (1965) 704-710.

[16] O. Poole, K. Alharbi, D. Belic, E.F. Kozhevnikova, I.V. Kozhevnikov, Hydrodeoxygenation of 3-pentanone over bifunctional Pt-heteropoly acid catalyst in the gas phase: Enhancing effect of gold, Applied Catalysis B: Environmental, 202 (2017) 446-453.

Chapter 4. Isomerisation of n-hexane over bifunctional Pt-heteropoly acid catalyst: Enhancing effect of gold

4.1 Introduction

Isomerisation of linear C_5–C_6 alkanes, which are relatively stable toward cracking, is used in industry to produce high octane gasoline. For example, n-hexane isomerisation to 2-methylpentane (2MP) and 3-methylpentane (3MP) increases the research octane number (RON) from 25 to 74. Further branching to 2,2- and 2,3-dimethylbutane isomers (22DMB and 23DMB) increases RON to 96 and 105, respectively [1].

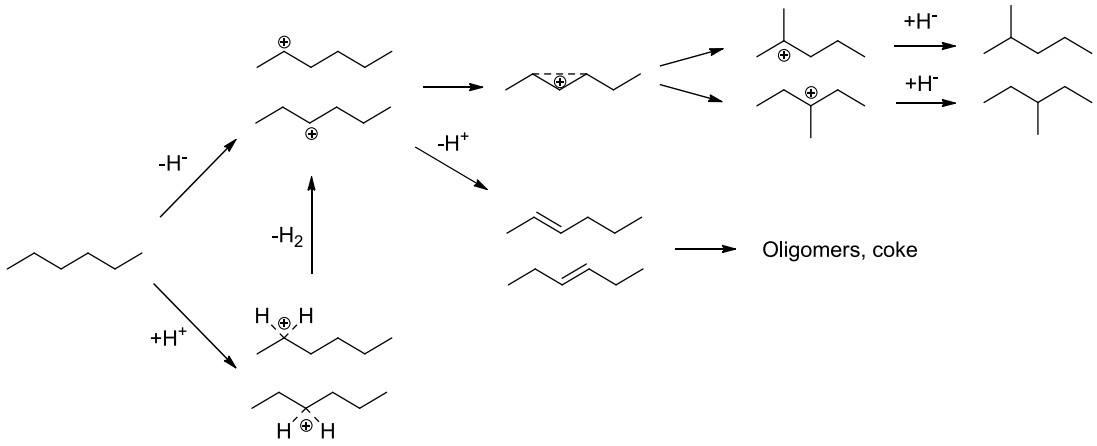

Scheme 4.1 Acid-catalysed pathway for n-hexane isomerisation via monomolecular mechanism.

Alkane isomerisation can occur via an acid-catalysed pathway on strong Lewis and Brønsted acid sites [2, 3] (Scheme 4.1). With Lewis acids, a linear alkane, e.g., n-hexane, can be isomerised through a monomolecular carbenium-ion chain mechanism including carbenium ions produced by H^- abstraction on Lewis acid sites. The carbenium ions then form a protonated cyclopropane intermediate, which undergoes β-migration of methyl group followed by H^- transfer from an n-hexane molecule to give mono-branched 2MP and 3MP as the primary isomerisation products together

with the carbenium ions continuing the chain process (not shown in Scheme 4.1). Subsequent isomerisation of 2MP and 3MP can lead to formation of 23DMB and 22DMB. On strong Brønsted acid sites, carbonium ions are formed by protonation of a C-H bond. The carbonium ions then undergo H_2 elimination to give the carbenium ions leading to the formation of 2MP and 3MP. Proton elimination from the carbenium ions could give alkenes. The latter form oligomers and coke, which cause catalyst deactivation (Scheme 4.1). In addition, C_{6-} hydrocarbons can be formed by cracking of hexane isomers. Also C_{6-} and C_{6+} products can be produced by disproportionation of C_{12} cation intermediates formed from the C_6 carbenium ions and an alkene (bimolecular mechanism) [2, 3].

Industrial isomerisation of linear alkanes is carried out using bifunctional metal-acid catalysts, usually platinum supported on chlorinated alumina or acidic zeolites (e.g., mordenite) in the presence of hydrogen (hydroisomerisation) [1]. The reaction is suggested to proceed in accordance with Scheme 4.2 involving alkane dehydrogenation on Pt sites followed by isomerisation of the alkene formed on acid sites of support [4]. The alkene isomer is then hydrogenated on the platinum to give the branched alkane. The bifunctional pathway (Scheme 4.2) is much more efficient than the acid-catalysed pathway (Scheme 4.1). Platinum in the bifunctional catalyst is important not only in enhancing the isomerisation process, but also in reducing the steady state alkene concentration. The latter increases reaction selectivity due to diminishing the contribution of the bimolecular mechanism [5] and reduces coke formation, thus improving catalyst lifetime [1].

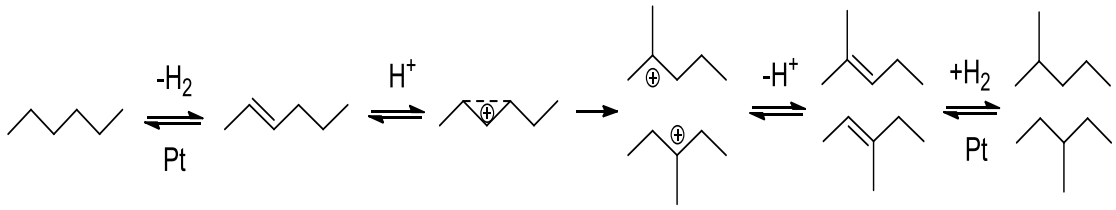

Scheme 4.2 Bifunctional catalysed pathway for n-hexane isomerisation (hydroisomerisation).

Heteropoly acids (HPAs) possessing very strong Brønsted acidity have attracted much interest as acid catalysts, in particular tungsten HPAs with Keggin structure such as $H_3PW_{12}O_{40}$ (HPW) and $H_4SiW_{12}O_{40}$ (HSiW) [6-8]. In recent years, Pt-HPA bifunctional catalysis for alkane isomerisation has been studied extensively to show its high efficiency in this reaction ([[9-12] and references therein).

Here, we investigate the Pt-HPA bifunctional catalysis in the isomerisation of n-hexane, focussing on the use of $Cs_{2.5}H_{0.5}PW_{12}O_{40}$ (CsPW) as the acid component. CsPW is an insoluble acidic salt of 12-tungstophosphoric acid, which has important advantages over the parent HPW in possessing much larger surface area (hence larger surface acidity) and higher thermal stability, while having the Brønsted acid sites almost as strong as in HPW [6,7]. Also, we report here an enhancing effect of Au on n-hexane isomerisation over Pt/CsPW. It is demonstrated that modification of the Pt/CsPW catalyst with gold increases the reaction turnover rate at Pt surface sites more than twofold, although the gold alone without Pt is practically inactive in this reaction. It is suggested that the enhancement is caused by PtAu alloying. STEM-EDX and XRD analysis of the PtAu/CsPW catalysts indicates the presence of bimetallic PtAu nanoparticles with a wide range of Pt/Au atomic ratios.

4.2 Experimental

4.2.1 Isomerisation of n-hexane

Isomerisation of n-hexane was carried out at the gas-solid interface in flowing H_2 at 180-220 °C. The catalysts were tested under atmospheric pressure at a ratio of n-hexane and H_2 partial pressures of 0.06-0.24 in a Pyrex fixed-bed down-flow microreactor (9 mm internal diameter) fitted with an on-line gas chromatograph (Varian Star 3400 CX instrument with a 30 m x 0.25 mm HP INNOWAX capillary column and a flame ionisation detector). For more accurate off-line GC analysis of C_6-hydrocarbon products, a 60 m x 0.32 mm GS-GasPro capillary column was used. The temperature in the reactor was controlled by a Eurotherm controller (±0.5 °C) using a thermocouple placed at the top of the catalyst bed. n-Hexane was fed by passing H_2 flow controlled by a Brooks mass flow controller through a stainless steel saturator, which held n-hexane at 0 °C (ice bath) to maintain the chosen reactant partial pressure of 5.78 kPa (5.8 mol% concentration of n-hexane in H_2 flow) unless stated otherwise. The downstream gas lines and valves were heated to 150 °C to prevent substrate and product condensation. The gas feed entered the reactor from the top at a flow rate of 20 mL min^{-1}. The reactor was packed with 0.20 g catalyst powder of 45-180 μm particle size. Unless stated otherwise, the reaction was carried out at a space time W/F = 69.2 g h mol^{-1}, where W is the catalyst weight (in grams) and F is the inlet molar flow rate of n-hexane (in mol h^{-1}). Prior to reaction, the catalysts were pre-treated in situ for 1 h at the reaction temperature. Once reaction started, the downstream gas flow was analysed by the on-line GC to obtain reactant conversion and product composition. Product selectivity was defined as moles of product formed per one mole of n-hexane converted and quoted in mole per cent. The mean absolute percentage

error in conversion and selectivity was ≤ 5% and the carbon balance was maintained within 95%. Reaction rates (R) were determined as $R = XF/W$ (in mol $g_{cat}^{-1}h^{-1}$), where X is the fractional conversion of n-hexane. In most cases, the reaction was carried out at differential conditions ($X \leq 0.1$), where X is directly proportional to the reaction rate. In some cases, the catalysts were diluted with silica in order to achieve low conversion.

4.3 Results and discussion

4.3.1 Acid-catalysed isomerisation of n-hexane

Bulk and supported heteropoly acids HSiW and HPW were found to have small activity in n-hexane isomerisation. Bulk acidic Cs salts of HPW, i.e. CsPW and $Cs_{2.25}PW$, showed better activities in this reaction (Table 4.2) despite their weaker acidity compared to the bulk HPW (Table 4.1). This can be attributed to the larger surface area hence larger proton site density of the Cs salts (Table 4.1). 2MP and 3MP were the main reaction products, which formed with 65-67% and 29-31% selectivity, respectively, together with 3-5% of cracking products, mainly C_3-C_5 olefins (propene, butenes and pentenes). Double-branched 23DMB isomer was formed in less than 1% selectivity. Strong catalyst deactivation was observed, which can be assigned to coke deposition. Initially white, CsPW catalyst turned black after reaction, with a carbon content of 0.6 wt% as determined by combustion chemical analysis for the reaction at 180 °C after 6 h time on stream (Table 3.6). As seen from the time course of reaction with CsPW at 200 °C (Figure 4.1), n-hexane conversion is strongly affected by catalyst deactivation, however without changing reaction selectivity. Practically the same results were obtained when using N_2 instead of H_2 as the carrier gas.

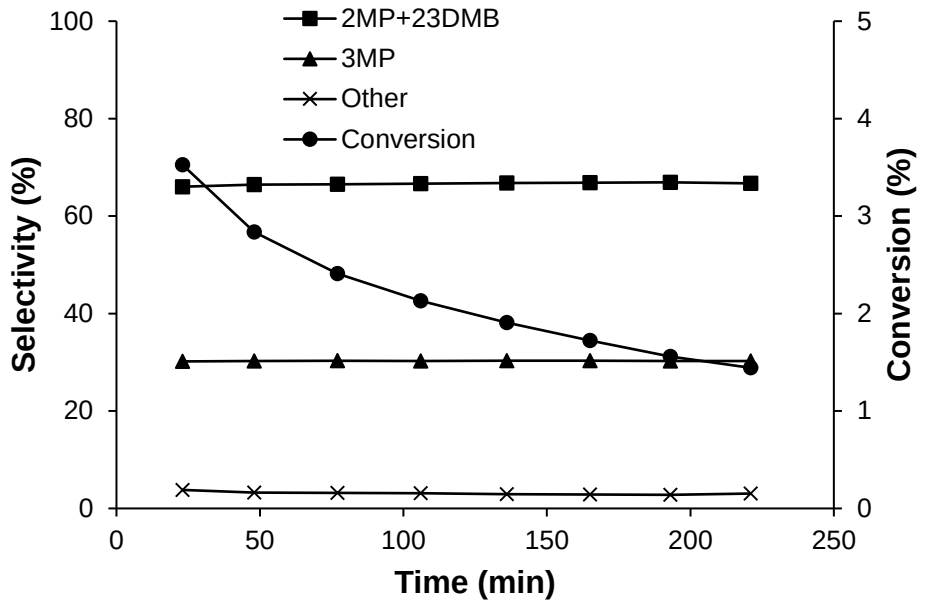

Figure 4.1 Isomerisation of n-hexane catalysed by CsPW (0.20 g) at 200 °C, 5.78 kPa n-hexane partial pressure in H_2 flow (20 mL min^{-1}).

The rates of acid-catalysed isomerisation of n-hexane (*R*) and turnover frequencies (TOF_H) per surface proton site were calculated using the values of n-hexane conversion for 1 h time on stream (Table 4.2). The required densities of surface proton sites are given in Table 4.1; these were estimated as described elsewhere [13, 14]. For supported HPA catalysts, which contained HPW or HSiW at a sub-monolayer loading of 15%, all HPA protons were assumed to be equally available for reaction. For bulk HPW, HSiW and Cs salts of HPW, the number of surface proton sites was calculated using a Keggin unit cross section of 144 $Å^2$ [6, 7] and the catalyst surface areas from Table 4.1.

The TOF_H values obtained ranged from 0.1 h^{-1} for 15%HPW/TiO_2 to 5.2 h^{-1} for bulk HPW (Table 4.2) indicating a strong effect of catalyst acid strength on the reaction turnover rate. Figure 4.2 shows the relationship between the activity of catalysts in n-hexane isomerisation, ln (TOF_H), and their acid strength represented by the initial enthalpy of ammonia adsorption, ΔH_{NH3} (Table 4.1). Although there is considerable scatter of points, which is probably caused by catalyst deactivation, this relationship shows that catalyst activity increases with catalyst acid strength. All these catalysts have predominantly Brønsted acid sites, except the weakest solid acid 15%HPW/TiO_2, which may also have Lewis acid sites originated from TiO_2. Therefore, the relationship (Figure 4.2) indicates that Brønsted acid sites play important role in n-hexane isomerisation over heteropoly acid catalysts as can be anticipated from the reaction mechanism shown in Scheme 4.1.

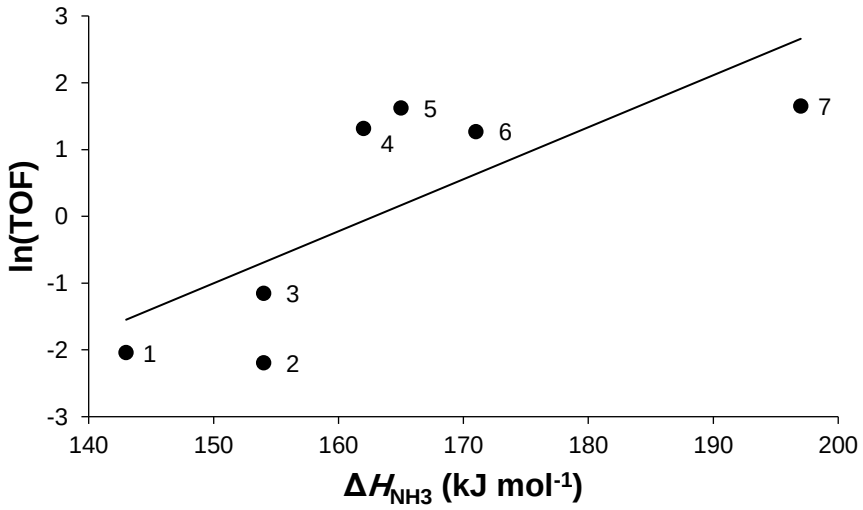

Figure 4.2 Plot of ln(TOF) (TOF in h^{-1}) versus ΔH_{NH3} for n-hexane isomerisation catalysed by HPA catalysts (0.20 g catalyst, 200 °C, 5.78 kPa n-hexane partial pressure, 20 mL min^{-1} H_2 flow rate): 15%HPW/TiO_2 (1), 15%HSiW/SiO_2 (2), 15%HPW/SiO_2 (3), $Cs_{2.25}$PW (4), CsPW (5), HSiW (6), HPW (7) [6, 8, 9, 10].

Table 4.1 Information about acid catalysts [14].

Catalysts	S_{BET}[a] m^2g^{-1}	Pore volume[b] cm^3g^{-1}	Pore size[c] Å	H^+ sites[d] mmol g^{-1}	ΔH_{NH3}[e] kJ mol^{-1}
TiO_2 (P25 Degussa)	44	0.10	90		
SiO_2 (Aerosil 300)	300[f]				
$H_3PW_{12}O_{40}$ (HPW)	5.6	0.04	81	0.019	-197
$H_4SiW_{12}O_{40}$ (HSiW)	9.0	0.02	71	0.042	-171
$Cs_{2.5}H_{0.5}PW_{12}O_{40}$ (CsPW)	132	0.10	29	0.076	-164
$Cs_{2.25}H_{0.75}PW_{12}O_{40}$	128	0.07	22	0.110	-162
15%HPW/SiO_2	202	1.00	169	0.156	-154
15%HSiW/SiO_2	221	1.02	185	0.208	-154
15%HPW/TiO_2	45	0.20	174	0.156	-143

[a]BET surface area. [b]Single point total pore volume at P/P_o = 0.97. [c]Average BET pore diameter. [d]Proton site density (see the text for its calculation). [e]Initial enthalpy of NH_3 adsorption at 150 °C (±3 kJ mol^{-1}). [f]Manufacturer's value.

Table 4.2 Acid-catalysed isomerisation of n-hexane.[a]

Catalyst	Conversion[b]	10^3 R[c]	TOF_H[d]
	%	mol $g^{-1}h^{-1}$	h^{-1}
CsPW	2.7	0.38	5.1
$Cs_{2.25}H_{0.75}PW_{12}O_{40}$ ($Cs_{2.25}PW$)	2.8	0.41	3.7
HPW	0.7	0.10	5.2
HSiW	1.0	0.15	3.6
15%HPW/SiO_2	0.34	0.049	0.32
15%HPW/TiO_2	0.14	0.020	0.13
15%HSiW/SiO_2	0.16	0.023	0.11

[a]200 °C, 0.20 g catalyst, 5.78 kPa n-hexane partial pressure in H_2 flow (20 mL min^{-1}). [b]n-Hexane conversion at 1 h time on stream (mean of two parallel runs). [c]Reaction rate calculated from $R = XF/W$, where X is the fractional conversion of n-hexane, W is the catalyst weight (0.20 g) and F is the molar flow rate of n-hexane (W/F = 69.2 g h mol^{-1}). [d]Turnover frequency per surface proton site; proton site densities are given in Table 4.1.

4.3.2 Bifunctional metal-acid catalysed isomerisation of n-hexane

As expected, Pt/CsPW bifunctional catalysts in the presence of H_2 were more efficient in n-hexane isomerisation than the acid catalyst CsPW. The Pt/CsPW catalysts showed higher catalytic activity and displayed much less catalyst deactivation compared to CsPW (Figure 4.3). The amount of coke in spent Pt/CsPW catalysts was below the detection limit after reaction at 180 °C (6 h on stream) (Table 3.6). When using N_2 as the carrier gas in the absence of H_2, the activity of Pt/CsPW was much lower and strong catalyst deactivation was observed (Figure 4.4). The activity of Pt/CsPW increased with increasing Pt loading (Table 4.3, entries 1-3, 5 and 6). Thus 5.78%Pt/CsPW gave a tenfold higher n-hexane conversion than CsPW at 200 °C (entries 2 and 6). The reaction products included 2MP (64-69% selectivity), 3MP (30-32%) and 23DMB (0.8-1.2%) together with 2-5% of cracking products (mainly C_3-C_5 hydrocarbons) at n-hexane conversion of 4-22%. Similar product selectivity was observed with CsPW without Pt (Table 4.3, entries 1 and 2). This indicates that Pt does not affect β-migration of methyl group in the protonated cyclopropane intermediate (Scheme 4.1 and 4.2). The low 23DMB selectivity can be explained by the low n-hexane conversion under the chosen differential reaction conditions. It should be noted that the conversions and selectivities observed were far from equilibrium values. The equilibrium C_6 alkane isomer mixture at 200 °C contains n-hexane (14%), 2MP (31%), 3MP (20%), 22DMB (26%) and 23DMB (9%), which corresponds to 86% n-hexane conversion [15]. It should be noted that there was no C_{6+} hydrocarbons observed among the reaction products. This indicates the reaction occurring via the monomolecular mechanism (Scheme 4.2) in agreement with the literature [5]. This mechanism involves alkane dehydrogenation on Pt sites followed by isomerisation of the alkene formed on acid sites of support and, finally, hydrogenation of the isoalkene

on Pt sites. Platinum, therefore, reduces the steady state alkene concentration. This increases reaction selectivity due to diminishing the contribution of the bimolecular mechanism. This also reduces coke formation, thus improving catalyst lifetime [1].

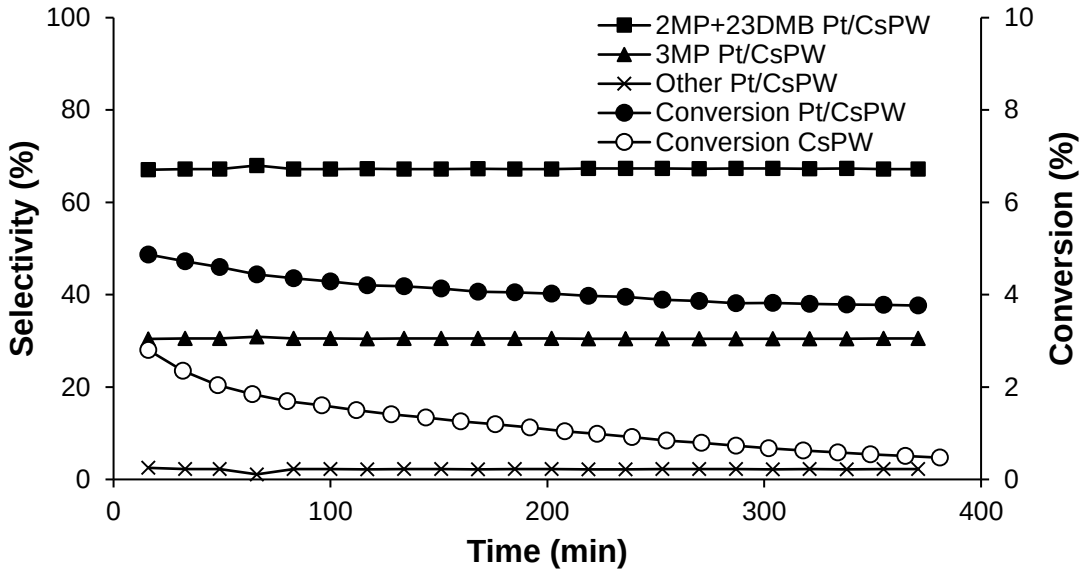

Figure 4.3 Isomerisation of n-hexane catalysed by 0.32%Pt/CsPW (0.20 g) at 180 °C, 5.78 kPa n-hexane partial pressure in H_2 flow (20 mL min^{-1}). Open circles show n-hexane conversion with CsPW catalyst at the same conditions; reaction selectivities are similar in both cases.

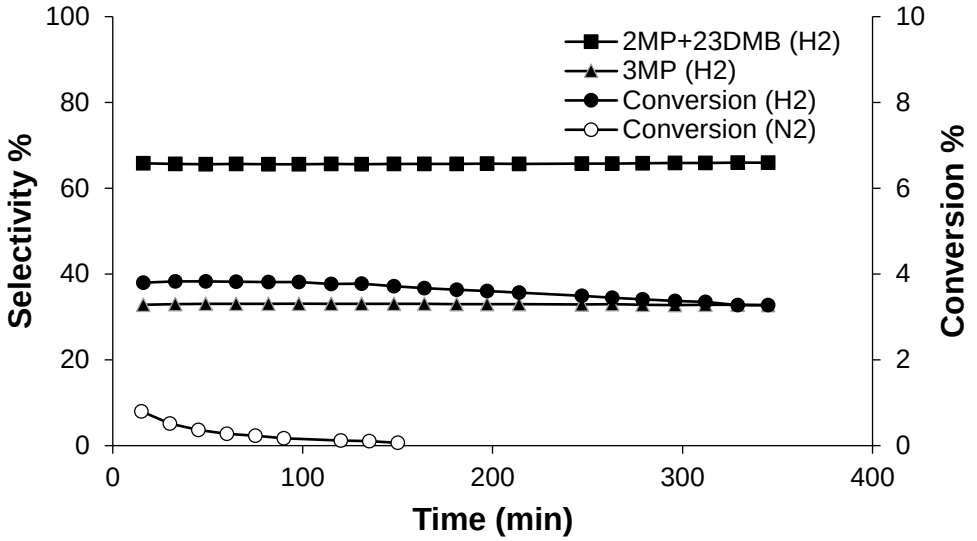

Figure 4.4 n-Hexane isomerisation: 5.78%Pt/CsPW (0.040 g) + SiO_2 (0.160 g), 200 °C, 5.78 kPa n-hexane partial pressure, 20 mL min^{-1} H_2 flow rate. Open circles show n-hexane conversion with N_2 as a carrier gas instead of H_2.

The kinetics of alkane isomerisation over Pt-acid bifunctional catalysts based on zeolites and heteropoly acids has been addressed in previous reports [10, 16, 17]. n-Hexane is relatively stable towards cracking, therefore the rate of isomerisation could be approximated by the rate of n-hexane conversion [17]. When the dehydrogenation reaction step is equilibrated and the isomerisation step is rate limiting (Scheme 4.2) and also the hydrocarbon concentrations inside catalyst pores are in equilibrium with the gas phase, the rate equation of isomerisation can be derived using reaction steps (4.1-4.5) (Scheme 4.3) [16,17]. These steps include n-hexane dehydrogenation (4.1), hexene protonation (4.2), isomerisation of hexyl carbenium ion (4.3), followed by iso-hexyl carbenium ion deprotonation (4.4) and hydrogenation of iso-hexene (4.5), where AH_2 is n-hexane, A is hexene, AH^+ is hexyl carbenium ion, $A'H^+$ is iso-hexyl carbenium ion, A' is iso-hexene, $A'H_2$ is a hexane isomer, K_d is the equilibrium constant of dehydrogenation, K_p is the equilibrium constant of

protonation, k_i is the rate constant of isomerisation, P_{C6} is the partial pressure of n-hexane and P_{H2} is the partial pressure of hydrogen.

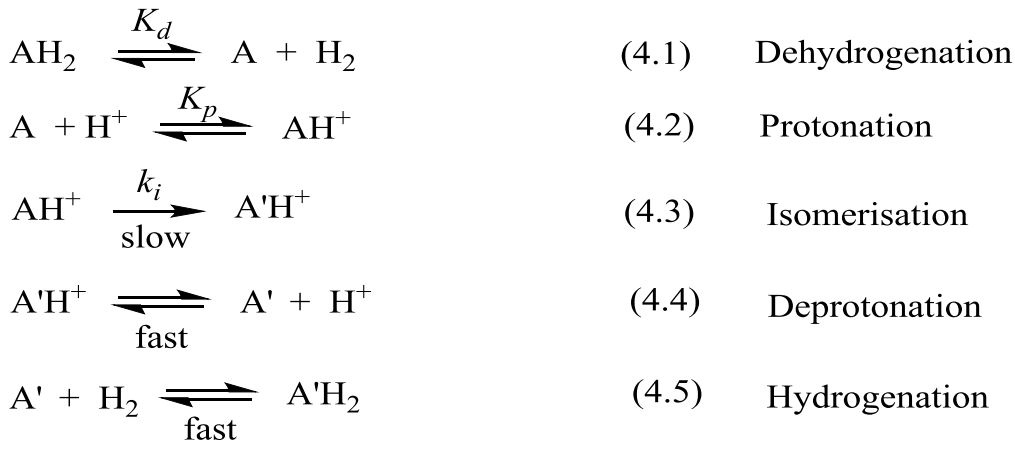

Scheme 4.3 Reaction steps for n-hexane hydroisomerisation over bifunctional metal-acid catalyst Pt–CsPW..

To derive the rate equation, let us assume that dehydration (4.1) and protonation (4.2) are equilibrated and isomerisation (4.3) is the rate limiting step, with K_d and K_p the corresponding equilibrium constants and k_i the isomerisation rate constant. The subsequent steps (4.4) and (4.5) are thought to be kinetically irrelevant. The deprotonation (4.4) is likely to be fast and equilibrated. Since no iso-hexenes were found amongst the products, the hydrogenation (4.5) can be assumed to be fast.

The balance of surface proton sites in CsPW is represented by

$$[H^+]_t = [H^+] + [AH^+] + [A'H^+] \qquad (4.6)$$

where $[H^+]_t$ is the total density of surface proton sites, $[H^+]$, $[AH^+]$ and $[A'H^+]$ is the density of vacant proton sites and adsorbed protonated species AH^+ and $A'H^+$, respectively. At low hexane pressure, the number of $A'H^+$ species should be small compared to AH^+, then

$$[H^+]_t \approx [H^+] + [AH^+] \quad (4.7)$$

From dehydration equilibrium (1), the partial pressure of A is given by

$$P_A = K_d \frac{P_{C6}}{P_{H_2}} \quad (4.8)$$

where P_{C6} is the partial pressure of n-hexane. From protonation equilibrium (4.2)

$$[AH^+] = K_p P_A [H^+] \quad (4.9)$$

Combining (7) and (9) gives

$$[H^+]_t = [H^+] + K_p P_A [H^+] = [H^+]\left(1 + K_p P_A\right) \quad (4.10)$$

The number of vacant H^+ sites is then

$$[H^+] = \frac{[H^+]_t}{1+K_p P_A} \quad (4.11)$$

From step (4.3), n-hexane isomerisation rate is given by equation (4.12).

$$R = k_i [AH^+] \quad (4.12)$$

Combining (9) and (11) with (12) gives

$$R = \frac{k_i K_p P_A [H^+]_t}{(1+K_p P_A)} \quad (4.13)$$

Substituting P_A from equation (4.8) into (4.13) gives the turnover reaction rate

$$\frac{R}{[H^+]_t} = \frac{k_i K_d K_p \left(\frac{P_{C6}}{P_{H_2}}\right)}{1+K_d K_p \left(\frac{P_{C6}}{P_{H_2}}\right)} \approx k_i \left(K_d K_p \frac{P_{C6}}{P_{H_2}}\right)^a \quad (4.14)$$

where α is the reaction order ($\alpha \leq 1$). This rate equation has been reported previously [16,17].

The rate limiting step is determined by the balance between metal and acid functionalities in bifunctional catalyst, i.e., the ratio of accessible surface metal and

acid sites Pt_s/H^+ [4,10,20-22]. In the case of catalysts based on zeolites (e.g., H-MOR, H-BEA, H-USY, etc.), the dehydrogenation step is usually equilibrated at $Pt_s/H^+ < 0.1$, and the isomerisation step becomes rate limiting [17, 18]. For Pt-HPA catalysts based on HPW possessing significantly stronger proton sites compared to zeolites [14], a much higher Pt_s/H^+ ratio may be required to equilibrate the dehydrogenation step [10].

Figure 4.4 shows the plot of n-hexane conversion over Pt/CsPW catalyst as a function of Pt loading. As seen, the conversion increases with increasing the Pt loading, levelling off at ≥ 6% Pt loading. Figure 4.5 shows the same results represented as turnover frequencies TOF_H and TOF_{Pt} versus the Pt_s/H^+ ratio, where the TOF_H and TOF_{Pt} were calculated per surface H^+ and Pt_s site, respectively, using conversion data at 200 °C and the Pt dispersion from Table 4.2. It was also assumed that the proton site density of CsPW (0.076 mmol g^{-1}, Table 4.1) was not affected by Pt loading. The contribution of CsPW (Table 4.3, entry 2) was subtracted from the total conversion when calculating the TOF_{Pt}. As expected from Scheme 4.2, TOF_H increases and TOF_{Pt} decreases with increasing the Pt_s/H^+ ratio, levelling off as the dehydrogenation step reaches quasi-equilibrium (Figure 4.6). These results demonstrate that under the chosen reaction conditions (200°C , P_{C6}/P_{H2} = 0.061), n-hexane dehydrogenation step is equilibrated over Pt/CsPW catalyst at $Pt_s/H^+ \geq 0.8$, which corresponds to a Pt loading of ~6%. This Pt_s/H^+ value is predictably higher than that usually found for Pt/zeolite catalysts, which can be attributed to the stronger acidity of CsPW compared to the conventional zeolites.

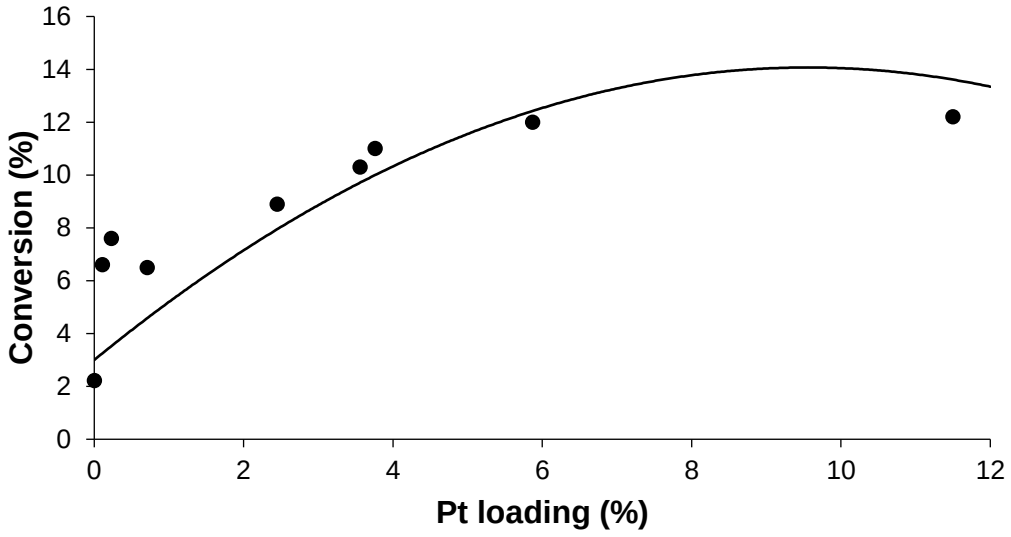

Figure 4.5 Plot of n-hexane conversion versus Pt loading: Pt/CsPW (0.20 g), 200 °C, 5.78 kPa n-hexane partial pressure in H_2 flow (20 mL min^{-1}), 5 h time on stream.

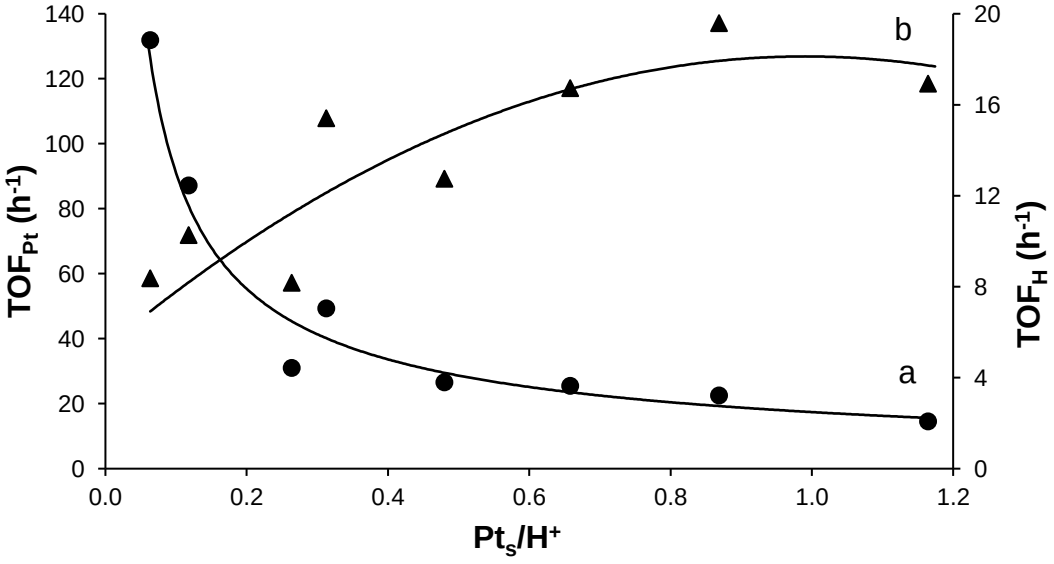

Figure 4.6 Plot of TOF_{Pt} (a) and TOF_H (b) for n-hexane isomerisation over Pt/CsPW (0.20 g) versus atomic ratio of Pt_s and H^+ surface sites: 200 °C, 5.78 kPa n-hexane partial pressure in H_2 flow (20 mL min^{-1}), 5 h time on stream.

The apparent activation energy, E_a, for n-hexane isomerisation over 5.78%Pt/CsPW was found to be 79 kJ mol^{-1} in the temperature range of 180-220 °C. The Arrhenius plot is shown in Figure 4.7; in this plot, the differential conversion of n-hexane X which is directly proportional to the reaction rate is used. The high E_a value obtained indicates no diffusion limitations in the isomerisation reaction over Pt/CsPW.

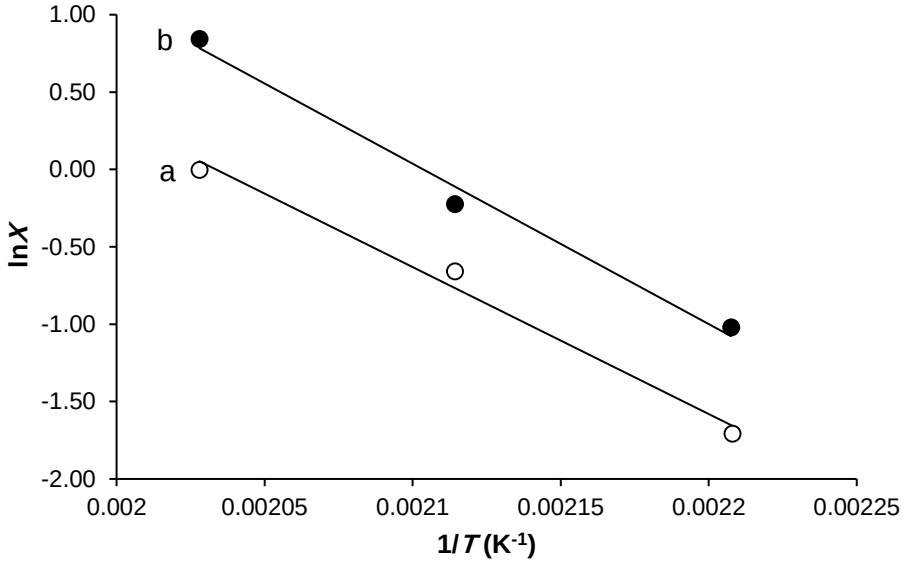

Figure 4.7 Arrhenius plot for n-hexane isomerisation: (a) 5.78%Pt/CsPW (0.04 g) + SiO_2 (0.16 g) (E_a = 79 kJ mol^{-1}); (b) 5.57%Pt/4.25%Au/CsPW (0.04 g) + SiO_2 (0.16 g) (E_a = 86 kJ mol^{-1}); 5.78 kPa n-hexane partial pressure in H_2 flow (20 mL min^{-1}), 6 h time on stream.

The isomerisation reaction is first order in Pt/CsPW catalyst (Figure 4.8). The order in n-hexane was found to be 0.90 in agreement with equation (4.14) (Figure 4.9, where P_{C6} is varied at practically constant P_{H2}). Also in accordance with (Equation 4.14), the reaction rate increases with increasing the partial pressure ratio P_{C6}/P_{H2}; 4- fold increase in P_{C6}/P_{H2} caused a factor of 1.5-1.8 increase in reaction rate for

Pt/CsPW catalysts at 180°C (Table 4.4). Overall, these kinetic results are in good agreement with (Equation 4.14), taking into account that in these reaction systems n-hexane dehydrogenation step was not always fully equilibrated.

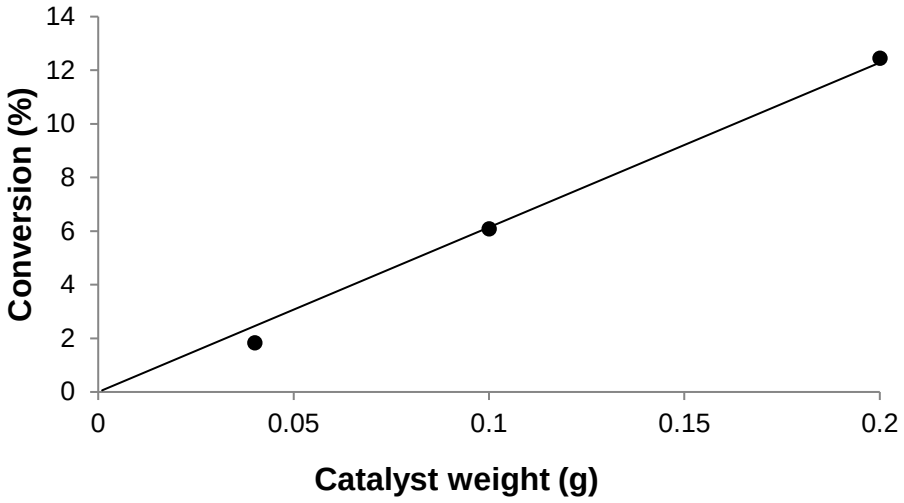

Figure 4.8 Plot of n-hexane conversion versus catalyst weight: 5.87%Pt/CsPW diluted with SiO_2 to 0.20 g, 200 °C, 5.78 kPa n-hexane partial pressure in H_2 flow (20 mL min^{-1}), 6 h time on stream.

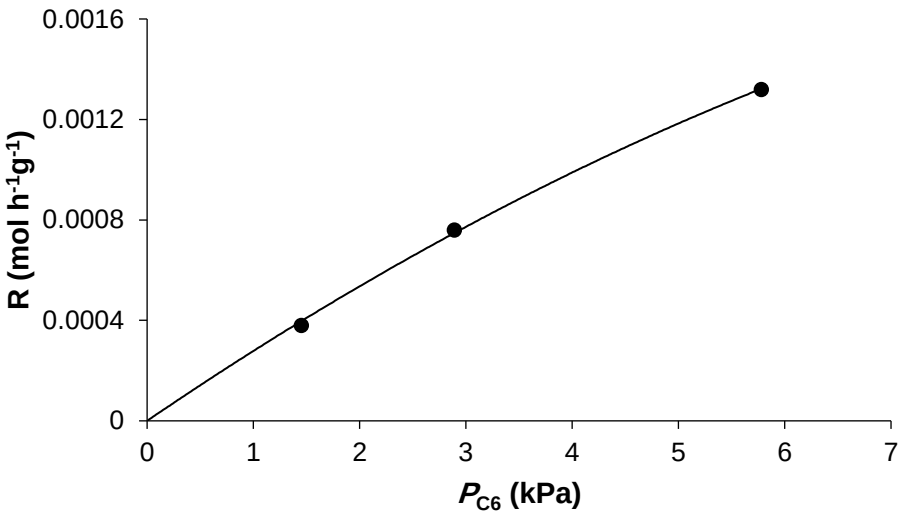

Figure 4.9 Plot of reaction rate versus n-hexane partial pressure: 5.87%Pt/CsPW (0.04 g) + SiO_2 (0.16 g), 200 °C, 20 mL min^{-1} flow rate, 6 h time on stream, P_{H2} = 94-98 kPa (reaction order in n-hexane 0.90).

4.3.3 Effect of gold

It has been well documented that bimetallic PtAu and PdAu catalysts frequently have an enhanced performance in comparison to monometallic Pt and Pd catalysts ([19-29] and references therein), for example in hydrogenation [29], hydrodeoxygenation [19, 24], hydrodesulphurisation [27, 28], oxidation [22-24] and other reactions (for review, see [20, 25, 26]). The enhancement of catalyst performance by addition of gold can be attributed to geometric (ensemble) and electronic (ligand) effects of the constituent elements in PtAu and PdAu bimetallic species [25, 26].

A wide range of bimetallic catalysts have been studied in alkane and cycloalkane reactions such as hydrogenolysis, isomerisation, cyclisation, ring enlargement, etc., dating back to the 1970s [30-35]; these include both supported and alloy film PtAu and PdAu catalysts [30, 33, 35]. A short communication by Fraissard et al. [35] has reported the use of PtAu nanoparticles supported on zeolites (HY and HZSM-5) for hydroisomerisation of n-hexane. It has been found that 1%Pt/0.2%Au/HY and 1%Pt/HY have the same activity and selectivity in this reaction without any Au enhancement; 1%Pt/0.2%Au/HZSM-5 shows good performance stability, but has not been tested against its Pt-only analogue.

Here we looked at the effect of Au additives on the performance of Pt/CsPW catalysts in the isomerisation of n-hexane. In this work, supported bimetallic catalysts PtAu/CsPW were prepared by co-impregnation of platinum and gold precursors onto

CsPW followed by reduction of solid pre-catalysts with H_2 at 250 °C. This method would favour the formation of supported PtAu nanoparticles of a random composition together with various Pt and Au nanoparticles, rather than more uniform bimetallics that can be prepared in solution [26]. Information about the PtAu/CsPW catalysts studied (catalyst texture and metal dispersion) is given in Table 3.5.

STEM-EDX analysis indicated the presence of bimetallic nanoparticles in the PtAu/CsPW catalysts. The high-angle annular dark field (HAADF) STEM images of 5.78%Pt/CsPW, 2.62%Au/CsPW and 5.57%Pt/4.25%Au/CsPW catalysts are shown in Figure 3.17, with metal nanoparticles indicated as bright spots on the darker background.

These STEM images are difficult to analyse due to W, Pt and Au having similar large atomic numbers *Z* (74, 78, and 79, respectively). CsPW containing 70 wt% of W displays a strong background which makes it difficult to distinguish smaller Pt and Au particles from the *Z*-contrast HAADF images and determine accurately metal particle size distribution. Nevertheless, in Figure 3.19a (5.78%Pt/CsPW catalyst), one can see platinum particles of ≤ 12 nm in size. The image of 2.62%Au/CsPW (Figure 3.19b) shows oval shaped gold particles sized up 4 to 25 nm, with an average gold particle size ≤ 10 nm. Particles of a similar size and shape can be also seen in Figure 3.19c (5.57%Pt/4.25%Au/CsPW), which indicates a PtAu alloying on the catalyst surface (see EDX analysis below).

The EDX analysis of a large number of metal nanoparticles in the 5.57%Pt/4.25%Au/CsPW catalyst showed that all these particles contained both Pt and Au in Pt/Au atomic ratios varying from 0.5 to 7.7 (Figure 3.20 and Figure 3.21). EDX elemental mapping (Figure 3.22) shows that Pt and Au maps cover the same areas of

PtAu/CsPW catalyst particles, indicating formation of a non-uniform PtAu particles (alloys), with local variations in Pt/Au atomic ratio.

Figure 3.14a shows the XRD patterns of 5.57%Pt/4.25%Au/CsPW and 5.78%Pt/CsPW catalysts, in which the bcc pattern of crystalline CsPW [36] is dominated. Also clearly seen is the fcc pattern of Pt (39.8^{o} [111**]** and 46.2^{o} [200]) and Au (38.2^{o} [111] and 44.4^{o} [200]) metal nanoparticles. This confirms coexistence of Pt and Au particles in the PtAu/CsPW catalyst. In addition, PtAu bimetallic particles may be present with diffraction pattern falling in between the corresponding diffractions of the pure metals [26], which is obscured by the intense pattern of CsPW. Indeed, the close-up normalized difference XRD (Figure 3.20b) shows a broad diffraction peak in the range of 38-40^{o} and possibly a weaker [200] peak in the range 44-46^{o} between the diffractions of pure Pt and Au, which could be attributed to PtAu alloys. In Figure 3.14b, the Pt peaks appear notably broader than the Au peaks, indicating higher dispersion of Pt particles. Although accurate analysis of metal particle size is difficult due to the prevailing CsPW pattern, rough estimate from the [111] peaks using the Scherrer equation gave 60 and 30 nm volume-average particle size for Au and Pt, respectively. This estimate, however, may be biased towards larger metal particles.

Representative results of PtAu/CsPW catalyst testing are shown in Table 4.3. Addition of gold to the Pt/CsPW catalysts was found to increase n-hexane conversion by a factor of 1.3 to 1.7 (Table 4.3, cf. entry 3 with 7 and 5 with 8), although the Au alone without Pt was inert (cf. entries 9 and 10 with 1). The effect of gold cannot be attributed to any change in Pt dispersion because Au additives practically did not change the dispersion of Pt in these catalysts (Table 3.5).

Table 4.3 n-Hexane isomerisation over bifunctional metal-acid catalysts.[a]

Catalyst	T (^{o}C)	Conv.[b]	Selectivity[c] (%)		
		(%)	2MP+23DMB[d]	MP	other[e]
(1) CsPW	180	1.5 (4)	68.6	1.1	0.3
(2) CsPW	200	2.2 (4)	66.9	0.4	2.7
(3) 0.32%Pt/CsPW	180	3.9 (6)	65.9	1.6	2.5
(4) 5.78%Pt/CsPW	150	1.5 (2)			
(5) 5.78%Pt/CsPW	180	8.0 (6)	65.8	2.0	2.2
(6) 5.78%Pt/CsPW	200	22.3 (4)	64.0	1.9	4.1
(7) 0.28%Pt/0.35%Au/CsPW	180	6.6 (6)	66.8	0.7	2.5
(8) 5.57%Pt/4.25%Au/CsPW	180	10.2 (6)	64.1	4.9	1.0
(9) 2.62%Au/CsPW	180	1.4 (4)	65.1	0.4	4.6
(10) 2.62%Au/CsPW	180	1.3 (6)	65.1	0.4	4.6

[a]0.20 g catalyst, 5.78 kPa n-hexane partial pressure in H_2 flow (20 mL min^{-1}). [b,c]Average n-hexane conversion and product selectivity over the time on stream given in square brackets. [d]2,3-Dimethylbutane (23DMB) selectivity 0.8-1.2%. [e]C_{6-} cracking products, mainly C_3-C_5; no C_{6+} hydrocarbons observed.

As seen from Table 4.4, gold additives, while increasing the conversion, did not affect reaction selectivity. This indicates that the effect of gold is pertinent to the

Pt-catalysed dehydrogenation reaction step and does not affect subsequent reactions of carbenium ions (Scheme 4.2). It is important that the scale of Au effect on catalyst activity depended on the Pt loading, i.e., on the degree of equilibration of the dehydrogenation reaction step. Subtracting the contribution of CsPW (entry 1) from the conversion values in entries 3, 5, 7 and 8 gives the Au enhancement scale of a factor of 2.0 at a low Pt loading (~0.3%) and only a factor of 1.3 at a higher loading (~6%). This implies that the effect of Au is the strongest when alkane dehydrogenation is the rate-limiting step and decreases as alkane dehydrogenation approaches equilibrium.

Figure 4.10 and 4.11 show comparative time courses for PtAu/CsPW versus Pt/CsPW and Au/CsPW versus CsPW, respectively, with n-hexane conversion and product selectivity as a function of the time on stream. Practically no coke was found in spent PtAu/CsPW catalysts, although a small amount of coke (0.3% C) was formed in Au/CsPW catalyst (Table 3.6). Nevertheless, the amount of coke in the Au/CsPW was less than that in CsPW (0.6%). This might explain a better performance stability of Au/CsPW compared to CsPW which can be seen in Figure 4.10.

Kinetically, the reaction with PtAu/CsPW catalyst was found to be very similar to that with the monometallic Pt/CsPW described above. For PtAu/CsPW, the apparent activation energy was found to be 86 kJ mol^{-1} at 180-220 °C (cf. 79 kJ mol^{-1} for Pt/CsPW). As seen from the Arrhenius plot (Figure 4.6), n-hexane conversion for the PtAu catalyst is higher than that for the Pt catalyst with very close Pt loading, thus conforming the Au enhancement in the whole temperature range. Similar to Pt/CsPW, the reaction with PtAu/CsPW is first order in the catalyst (Figure 4.12) and 0.90 order in n-hexane (Figure 4.13). Table 4.5 compares the effect of the P_{C6}/P_{H2} ratio for the

reaction with Pt/CsPW and PtAu/CsPW catalysts. In both cases, the reaction rate increases with increasing the P_{C6}/P_{H2} ratio (a factor of 1.8-1.9 for PtAu/CsPW and 1.5-1.8 for Pt/CsPW when the P_{C6}/P_{H2} ratio was increased from 0.061 to 0.24); this is in agreement with the rate equation (Equation 4.14). These results show that the reaction with both catalysts fits well with this equation.

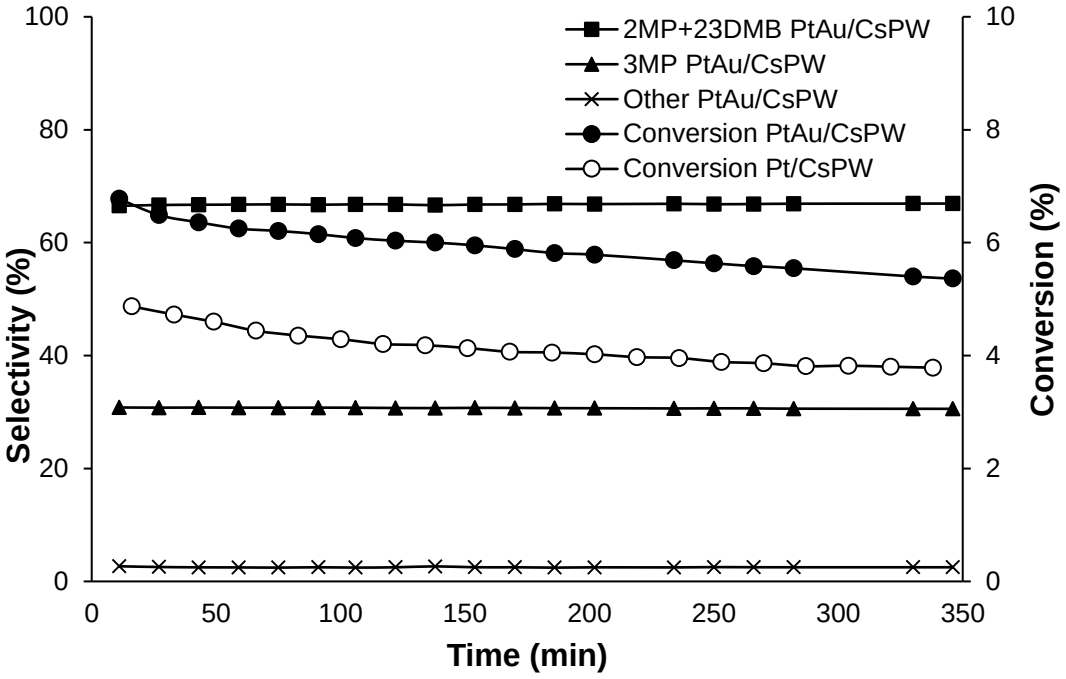

Figure 4.10 n-Hexane isomerisation catalysed by 0.28%Pt/0.35%Au/CsPW (0.20 g) at 180 °C, 5.78 kPa n-hexane partial pressure in H_2 flow (20 mL min^{-1}). Open circles show n-hexane conversion with 0.32%Pt/CsPW catalyst at the same conditions; reaction selectivities are practically the same in both cases

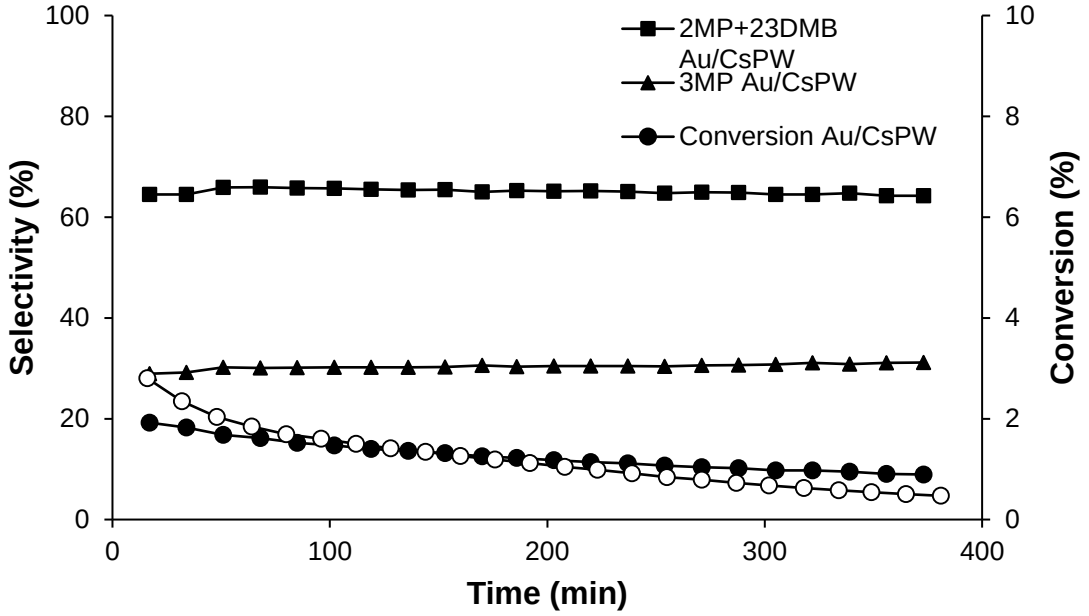

Figure 4.11 n-Hexane isomerisation catalysed by 2.62%Au/CsPW (0.20 g) at 180°C, 5.78 kPa n-hexane partial pressure, 20 mL min^{-1} H_2 flow rate. Open circles show n-hexane conversion with CsPW catalyst at the same conditions; reaction selectivities are practically the same in both cases.

The values of TOF_{Pt} in Table 4.4 give a more accurate estimate of the scale of gold effect. As seen, the gold enhancement of TOF_{Pt} is a factor of 2.2-2.3 for the 0.28-0.32% Pt loading and 1.4-1.7 for the 5.57-5.78% Pt loading. Thus the enhancing effect of gold decreases with increasing the Pt loading as n-hexane dehydrogenation step approaches quasi-equilibrium. It can therefore be anticipated that when the dehydrogenation step is fully equilibrated, the effect of gold will be close to zero.

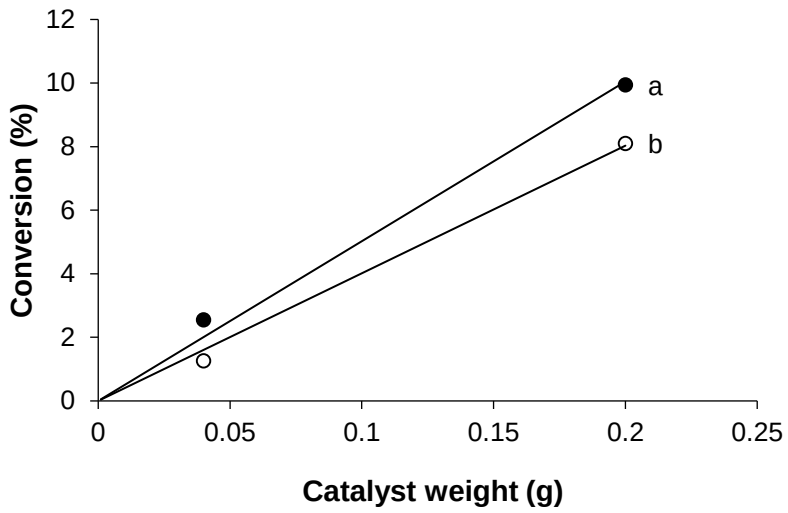

Figure 4.12 Plot of conversion versus catalyst weight: (a) 5.57%Pt/4.25%Au/CsPW + SiO_2; (b) 5.78%Pt/CsPW + SiO_2; 180 °C, 5.78 kPa n-hexane partial pressure in H_2 flow (20 mL min^{-1}), 6 h time on stream.

Therefore, the results obtained demonstrate that gold additives can increase the activity of Pt/CsPW bifunctional catalyst in hydroisomerisation of n-hexane, although the gold alone is not active. More specifically, gold increases the catalytic activity of Pt sites in alkane dehydrogenation step. When alkane dehydrogenation is the rate-limiting step, the enhancing effect on the isomerisation reaction is at its maximum. At such conditions the enhancement of the turnover rate at the Pt surface sites amounts to a factor of ≥ 2 as can be seen from the TOF_{Pt} values in Table 4.4. Conversely, the effect of gold decreases as the dehydrogenation step approaches quasi-equilibrium. As shown above, in n-hexane isomerisation over Pt/CsPW, the dehydrogenation step is equilibrated at a molar ratio of Pt and H^+ surface sites $Pt_s/H^+ \geq 0.8$, corresponding to a Pt loading $\geq 6\%$. As a result, the gold enhancement is observable at $Pt_s/H^+ < 0.8$ in this system. In the case of Pt-zeolite catalysts, the dehydrogenation step is equilibrated at

$Pt_s/H^+ < 0.1$ [16, 18], which is due to the weaker acid strength of zeolites compared to HPA. In this regard, the lack of gold enhancement in n-hexane isomerisation over 1%Pt/0.2%Au/HY as compared to 1%Pt/HY reported by Fraissard et al. [35] can be explained by equilibration of n-hexane dehydrogenation step in this system.

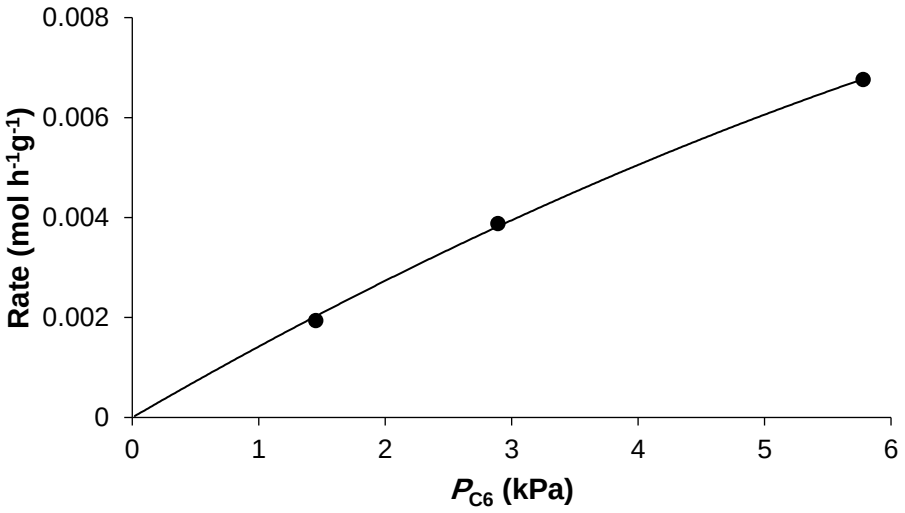

Figure 4.13 Plot of reaction rate versus n-hexane partial pressure: 5.57%Pt/4.25%Au/CsPW (0.04 g) + SiO_2 (0.16 g), 200 °C, 20 mL min^{-1} flow rate, 6 h time on stream, P_{H2} = 94-98 kPa (reaction order in n-hexane 0.90).

Table 4.4 Effect of P_{C6}/P_{H2} partial pressure ratio.[a]

Catalyst	P_{C6}/P_{H2}	Conversion[b]	10^3R[c]	TOF_{Pt}[d]
		%	mol $g^{-1}h^{-1}$	h^{-1}
0.32%Pt/CsPW	0.061	3.89	0.39	24
0.32%Pt/CsPW	0.24	2.50	0.72	44
5.78%Pt/CsPW	0.061	7.95	0.98	3.3
5.78%Pt/CsPW	0.24	4.11	1.5	5.1
0.28%Pt/0.35%Au/CsPW	0.061	6.55	0.77	54
0.28%Pt/0.35%Au/CsPW	0.24	3.86	1.4	96
5.57%Pt/4.25%Au/CsPW	0.01	10.2	1.3	4.6
5.57%Pt/4.25%Au/CsPW	0.24	7.11	2.5	8.6

[a]180 °C, 0.20 g catalyst, 20 mL min^{-1} flow rate. [b]Average conversion over 6 h time on stream (mean of two parallel runs). [c]Reaction rate calculated from $R = XF/W$, where X is the fractional conversion of n-hexane with the contribution of CsPW (0.012 and 0.010 at P_{C6}/P_{H2} = 0.061 and 0.24, respectively) subtracted, W is the catalyst weight (0.20 g) and F is the molar flow rate of n-hexane (W/F = 20.8 and 69.2 g h mol^{-1} at P_{C6}/P_{H2} = 0.24 and 0.061, respectively). [d]Turnover frequency per surface Pt_s site with CsPW contribution subtracted.

The nature of gold enhancement may be attributed to the previously documented electronic (ligand) and geometric (ensemble) effects in bimetallic PtAu species. It is generally suggested that the performance of bimetallic catalysts is mainly determined by the ensemble size effect, although the ligand effect may also contribute [25, 26]. It is thought that the individual surface metal atoms retain their character in bimetallic catalysts, and their catalytic properties are mainly determined by their nearest neighbours. It should be also noted that bimetallic catalysts often show higher activity than either of their constituents due to a lower degree of poisoning. Typically, hydrogenolysis is suppressed by alloying, whereas isomerisation is less affected, which may be beneficial for the selectivity of alkane isomerisation [25, 26].

Our STEM-EDX analysis clearly indicates the presence of bimetallic PtAu nanoparticles in the PtAu/CsPW catalyst. The interaction between Pt and Au in these nanoparticles can lead to the superior catalyst performance in n-hexane isomerisation. Thorough structural characterisation of PtAu/CsPW catalyst complemented by computational studies may provide further insights into the gold effect in this system.

4.4 Conclusions

The isomerisation of n-hexane was carried out using acid and bifunctional metal-acid catalysts based on Keggin-type heteropoly acids at a gas-solid interface at 180-220 °C and ambient pressure in a fixed-bed microreactor. The bifunctional catalysts studied comprised Pt as the metal component and $Cs_{2.5}H_{0.5}PW_{12}O_{40}$ (CsPW), an acidic Cs salt of heteropoly acid $H_3PW_{12}O_{40}$, as the acid component. Addition of gold to the Pt/CsPW catalyst was found to increase the catalytic activity, although the

Au alone without Pt was inert. The enhancement of catalyst performance is suggested to be caused by PtAu alloying. The STEM-EDX and XRD analyses of the PtAu/CsPW catalysts indicate the presence of bimetallic PtAu nanoparticles with a wide range of Pt/Au atomic ratios.

References

[1] L. Lloyd, Handbook of industrial catalysts, Springer Science & Business Media, 2011.

[2] H. Matsuhashi, H. Shibata, H. Nakamura, K. Arata, Skeletal isomerization mechanism of alkanes over solid superacid of sulfated zirconia, Applied Catalysis A: General, 187 (1999) 99-106.

[3] L. Gladen, M. Mantle, A. Sederman, Handbook of Heterogeneous Catalysis, Eds: G. Ertl, H. Knözinger, F. Schüth, J. Weitkamp, Wiley-VCH, Weinheim, 2008.

[4] D. Eley, H. Pines, P.B. Weisz, Advances in catalysis and related subjects, Academic Press, 1963.

[5] A. Miyaji, T. Echizen, L. Li, T. Suzuki, Y. Yoshinaga, T. Okuhara, Selectivity and mechanism for skeletal isomerization of alkanes over typical solid acids and their Pt-promoted catalysts, Catalysis Today, 74 (2002) 291-297.

[6] T. Okuhara, N. Mizuno, M. Misono, Catalytic chemistry of heteropoly compounds, Advances in Catalysis, 4 (1996) 113-252.

[7] I.V. Kozhevnikov, Catalysts for fine chemical synthesis, catalysis by polyoxometalates, Wiley, 2002.

[8] E.F. Kozhevnikov, I.V. Kozhenikov, A calorimetric study of the acidity of bulk and silica-supported heteropoly acid $H_3PW_{12}O_{40}$, Journal of Catalysis, 224 (2004) 164-169.

[9] W.Alharbi, E. Brown, E.F. Kozenikov, I.V. Kozenikov, Dehydration of ethanol over heteropoly acid catalysts in the gas phase, Journal of Catalysis, 319 (2014) 174-181.

[10] A.M. Alsalme, P.V. Wiper, Y.Z. Khimyak, E.F. Kozenikov, I.V. Kozenikov, Solid acid catalysts based on $H_3PW_{12}O_{40}$ heteropoly acid: Acid and catalytic properties at gas-solid interface, Journal of Catalysis, 276 (2010) 181-189.

[11] S.-S. Wang, G.-Y. Yang, Recent advances in polyoxometalate-catalyzed reactions, Chemical Reviews, 115 (2015) 4893-4962.

[12] A. Ivanov, T. Vasina, V. Nissenbaum, L. Kustov, M. Timofeeva, J. Houzvicka, Isomerization of n-hexane on the Pt-promoted Keggin and Dawson tungstophosphoric heteropoly acids supported on zirconia, Applied Catalysis A: General, 259 (2004) 65-72.

[13] W. Knaeble, R.T. Carr, E. Iglesia, Mechanistic interpretation of the effects of acid strength on alkane isomerization turnover rates and selectivity, Journal of Catalysis, 319 (2014) 283-296.

[14] T. Pinto, P. Arquillière, V. Dufaud, F. Lefebvre, Isomerization of n-hexane over Pt-H3PW12O40/SBA-15 bifunctional catalysts: Effect of the preparation method on catalytic performance, Applied Catalysis A: General, 528 (2016) 44-51.

[15] F. Lefebvre, Acid Catalysis by Heteropolyacids: Transformations of Alkanes, Current Catalysis, 6 (2017) 77-89.

[16] Y. Izumi, M. Ono, M. Kitagawa, M. Yoshida, K. Urabe, Silica-included heteropoly compounds as solid acid catalysts, Microporous Materials, 5 (1995) 255-262.

[17] K. Alharbi, W. Alharbi, E.F. Kozhevnikova, I.V. Kozhevnikov, Deoxygenation of Ethers and Esters over Bifunctional Pt–Heteropoly Acid Catalyst in the Gas Phase, ACS Catalysis, 6 (2016) 2067-2075.

[18] T. Pinto, V. Dufaud, F. Lefebvre, Isomerization of n-hexane on heteropolyacids supported on SBA-15. 1. Monofunctional impregnated catalysts, Applied Catalysis A: General, 483 (2014) 103-109.

[19] F. Ribeiro, C. Marcilly, M. Guisnet, Hydroisomerization of n-hexane on platinum zeolites: I. Kinetic study of the reaction on platinum/Y-zeolite catalysts: Influence of the platinum content, Journal of Catalysis, 78 (1982) 267-274.

[20] A. Van de Runstraat, J. Kamp, P. Stobbelaar, J. Van Grondelle, S. Krijnen, R. Van Santen, Kinetics of hydro-isomerization ofn-hexane over platinum containing zeolites, Journal of Catalysis, 171 (1997) 77-84.

[21] P.S. Mendes, F.M. Mota, J.M. Silva, M.F. Ribeiro, A. Daudin, C. Bouchy, A systematic study on mixtures of Pt/zeolite as hydroisomerization catalysts, Catalysis Science & Technology, 7 (2017) 1095-1107.

[22] O. Poole, K. Alharbi, D. Belic, E.F. Kozhevnikova, I.V. Kozhevnikov, Hydrodeoxygenation of 3-pentanone over bifunctional Pt-heteropoly acid catalyst in the gas phase: Enhancing effect of gold, Applied Catalysis B: Environmental, 202 (2017) 446-453.

[23] G.J. Hutchings, Nanocrystalline gold and gold palladium alloy catalysts for chemical synthesis, Chemical Communications, (2008) 1148-1164.

[24] K. Sun, A.R. Wilson, S.T. Thompson, H.H. Lamb, Catalytic deoxygenation of octanoic acid over supported palladium: effects of particle size and alloying with gold, ACS Catalysis, 5 (2015) 1939-1948.

[25] Y.-F. Han, J.-H. Wang, D. Kumar, Z. Yan, D. Goodman, A kinetic study of vinyl acetate synthesis over Pd-based catalysts: kinetics of vinyl acetate synthesis over Pd–Au/SiO_2 and Pd/SiO_2 catalysts, Journal of Catalysis, 232 (2005) 467-475.

[26] E.K. Hanrieder, A. Jentys, J.A. Lercher, Impact of alkali acetate promoters on the dynamic ordering of PdAu catalysts during vinyl acetate synthesis, Journal of Catalysis, 333 (2016) 71-77.

[27] J. Xu, T. White, P. Li, C. He, J. Yu, W. Yuan, Y.-F. Han, Biphasic Pd− Au alloy catalyst for low-temperature CO oxidation, Journal of the American Chemical Society, 132 (2010) 10398-10406.

[28] B. Coq, F. Figueras, Bimetallic palladium catalysts: influence of the co-metal on the catalyst performance, Journal of Molecular Catalysis A: Chemical, 173 (2001) 117-134.

[29] F. Gao, D.W. Goodman, Pd–Au bimetallic catalysts: understanding alloy effects from planar models and (supported) nanoparticles, Chemical Society Reviews, 41 (2012) 8009-8020.

[30] A. Venezia, V. La Parola, V. Nicolı, G. Deganello, Effect of gold on the HDS activity of supported palladium catalysts, Journal of Catalysis, 212 (2002) 56-62.

[31] A. Venezia, V. La Parola, G. Deganello, B. Pawelec, J. Fierro, Synergetic effect of gold in Au/Pd catalysts during hydrodesulfurization reactions of model compounds, Journal of Catalysis, 215 (2003) 317-325.

[32] T.J. Schwartz, S.D. Lyman, A.H. Motagamwala, M.A. Mellmer, J.A. Dumesic, Selective hydrogenation of unsaturated carbon–carbon bonds in aromatic-containing platform molecules, ACS Catalysis, 6 (2016) 2047-2054.

[33] J.R.H. Van Schaik, R. Dessing, V. Ponec, Reactions of alkanes on supported Pt-Au alloys, Journal of Catalysis, 38 (1975) 273-282.

[34] Z. Karpiński, J.K. Clarke, Reactions of alkanes on iridium and iridium-gold catalysts, Journal of the Chemical Society, Faraday Transactions 1: Physical Chemistry in Condensed Phases, 71 (1975) 2310-2318.

[35] J. Clarke, A. Kane, T. Baird, Reaction of alkanes and cycloalkanes on silica-supported platinum and platinum-gold alloy catalysts, Journal of Catalysis, 64 (1980) 200-212.

[36] J. Clarke, A. Creaner, T. Baird, Preparation of supported platinum-gold catalysts and alkane reactions on selected platinum and platinum-gold supported “clusters”, Applied Catalysis, 9 (1984) 85-108.

[37] B.D. Chandler, A.B. Schabel, L.H. Pignolet, Preparation and characterization of supported bimetallic Pt–Au and Pt–Cu catalysts from bimetallic molecular precursors, Journal of Catalysis, 193 (2000) 186-198.

[38] J. Fraissard, V. Gerda, K.I. Patrylak, Y.G. Voloshyna, Isomerization of hexane on PtAu nanoparticles supported on zeolites, Catalysis Today, 122 (2007) 338-340.

[39] T. Okuhara, H. Watanabe, T. Nishimura, K. Inumaru, M. Misono, Microstructure of cesium hydrogen salts of 12-tungstophosphoric acid relevant to novel acid catalysis, Chemistry of Materials, 12 (2000) 2230-2238.

Chapter 5. Isomerisation of cyclohexane over bifunctional Pt-, Au- and PtAu-heteropoly acid catalysts

5.1 Introduction

Skeletal isomerisation of alkanes is the basis for several important industrial processes. Isomerisation of linear C_5–C_6 alkanes is used in industry for the production of high octane gasoline, whereas longer-chain alkane isomerisation is important for lowering pour point of lubricants and jet and diesel fuels [1, 2]. Isomerisation of cycloalkanes is of interest for the reduction of toxic aromatics, especially benzene, in gasoline to protect the environment [2]. Benzene, while possessing high octane number (research octane number, RON, 100), is carcinogenic to humans. Reduction of benzene in gasoline may be achieved practically without a loss in gasoline octane rating by hydrogenation of benzene to cyclohexane (RON 84) followed by isomerisation to methylcyclopentane (RON 96) [3, 4].

The isomerisation of cyclohexane can proceed via an acid catalysed route on strong Lewis and Brønsted acid sites (Scheme 5.1) or via bifunctional metal-acid catalysis (Scheme 5.2). The acid catalysed isomerisation of alkanes can occur via a monomolecular carbenium-ion chain mechanism [2, 5]. With Lewis acids, cyclohexyl carbenium ion is produced by H^- abstraction on a Lewis acid site. This ion then undergoes methyl group migration through a protonated cyclopropane intermediate, which is followed by H^- transfer from a cyclohexane molecule to give methylcyclopentane (MCP) isomerisation product together with cyclohexyl carbenium ion continuing the chain process. On strong Brønsted acid sites, a carbonium ion is initially formed by C-H bond protonation in cyclohexane. This ion eliminates H_2 to form the cyclohexyl carbenium ion and further MCP. Proton elimination from intermediate carbenium ions produces alkenes, which can build coke, causing

deactivation of catalyst (Scheme 5.1). Besides, C_{6-} hydrocarbons can be produced by cracking of C_6 isomers. In addition, C_{6-} and C_{6+} hydrocarbons can be formed via disproportionation of C_{12} cations originated from alkenes and C_6 carbenium ions (bimolecular mechanism) [2, 5].

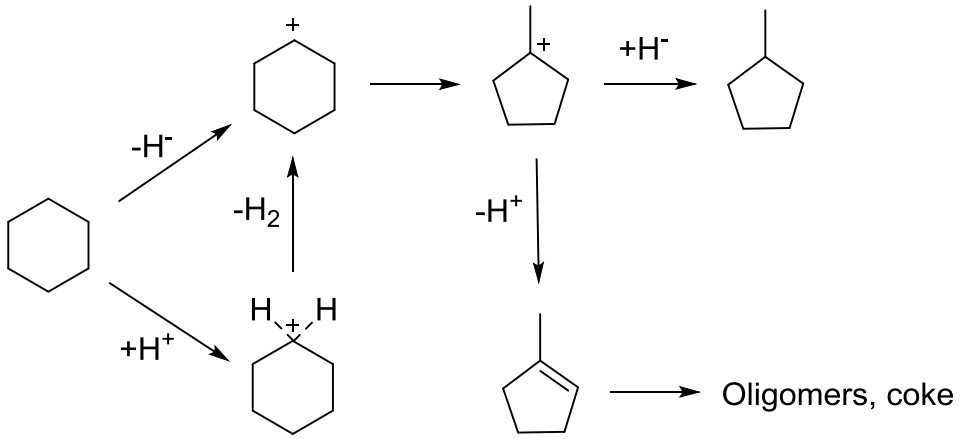

Scheme 5.1 Acid-catalysed isomerisation of cyclohexane via monomolecular mechanism.

With bifunctional metal-acid catalysts, typically containing platinum on acidic supports, for example, Pt/zeolite, alkane isomerisation proceeds in the presence of hydrogen (often referred to as hydroisomerisation) [1]. The reaction can be assumed to occur via (Scheme 5.2) involving cyclohexane dehydrogenation on metal sites followed by isomerisation of cyclohexene formed to methylcyclopentene on acid sites of support [6]. The latter is hydrogenated on the metal sites to give MCP. In general, the bifunctional route is more efficient than the acid catalysed route. In the bifunctional catalyst, Pt not only enhances the isomerisation process, but also reduces the steady

state alkene concentration. This increases reaction selectivity due to suppressing the bimolecular mechanism [5] and diminishes coke formation [1].

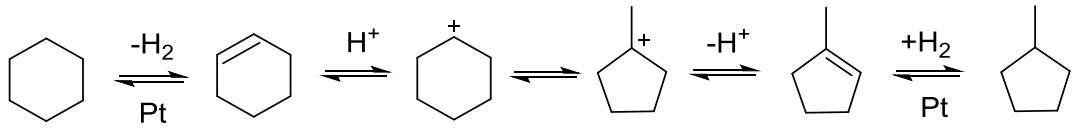

Scheme 5.2 Isomerisation of cyclohexane via bifunctional route.

Keggin-type heteropoly acids (HPAs), in particular tungsten HPAs possessing very strong Brønsted acidity, have attracted much interest as acid catalysts. These include primarily HPAs such as $H_3PW_{12}O_{40}$ and $H_4SiW_{12}O_{40}$ as well as their acidic Cs salts such as $Cs_{2.5}H_{0.5}PW_{12}O_{40}$ (CsPW) [7-9]. Pt–HPA bifunctional catalysis has been extensively studied in alkane isomerisation, and its effectiveness has been demonstrated ([4, 10-18] and references therein). Pt–HPA catalysts have been reported for the isomerisation of cycloalkanes such as cyclohexane [4] and methylcyclohexane [15] .

Alkane isomerisation via bifunctional metal-acid catalysis can be further enhanced using bimetallic PtAu catalysts. This has been reported for methylcyclopentane isomerisation over PtAu/HY and PdAu/HY by Fraissard et al. [19] and more recently for n-hexane isomerisation over PtAu/CsPW by ourselves [17].

In this work, we investigate the metal–HPA bifunctional catalysis for the isomerisation of cyclohexane, focussing on CsPW as the acid component and Pt and Au as the metal components. Insoluble acidic salt CsPW has important advantages

over the parent $H_3PW_{12}O_{40}$ (HPW). It has a higher thermal stability and much larger surface area (therefore larger surface site density), with the proton sites almost as strong as those in HPW [7, 20]. We also investigate the enhancing effect of Au on cyclohexane isomerisation and on the accompanying dehydrogenation of cyclohexane to benzene over Pt/CsPW. It is shown that the addition of gold to Pt/CsPW gives a significant increase in catalytic activity. The gold enhancement is attributed to PtAu bimetallic particles, which is supported by STEM-EDX.

5.2 Experimental

5.2.1 Chemicals and catalyst

Bifunctional catalysts Pt/CsPW and Au/CsPW were prepared by wet impregnation of CsPW with aqueous solutions of H_2PtCl_6 or $HAuCl_4$, as described previously [23-25]. The preparation involved stirring the aqueous slurry at 50 °C for 2 h, rotary evaporation to dryness and reduction with H_2 flow at 250 °C for 2 h. PtAu/CsPW bimetallic catalysts were prepared similarly via co-impregnation of CsPW with H_2PtCl_6 and $HAuCl_4$ from aqueous solution with reduction by H_2 as above. Another Pt/CsPW catalyst, hereafter referred to as Pt/CsPW-b, was prepared using a water- and chloride-free procedure by impregnating $Pt(acac)_2$ onto CsPW from benzene solution. This was done by stirring CsPW with 0.02 M $Pt(acac)_2$ benzene solution at room temperature for 1 h, followed by rotoevaporation of benzene at room temperature, drying under vacuum at 150 °C/10^{-3} kPa and reduction by hydrogen as above. Pt and Au loading in these catalysts was determined by ICP-AES. Physical mixtures of bifunctional catalysts with CsPW an d SiO_2 were prepared by grinding the catalysts with CsPW and Aerosil 300 silica.

Pt/C and Au/C catalysts were prepared by impregnating Darco KB-B activated carbon with aqueous solutions of H_2PtCl_6 and $HAuCl_4$ at 50 °C for 2 h followed by rotary evaporation to dryness and reduction with H_2 as above [25]. PtAu/C bimetallic catalysts were prepared similarly by co-impregnating the carbon support with H_2PtCl_6 and $HAuCl_4$. Physically mixed bifunctional catalysts Pt/C + CsPW, Au/C + CsPW and PtAu/C + CsPW were prepared by grinding a mixture of the corresponding components.

Information about the catalysts prepared in presented in Table 5.1. Other experimental details regarding catalyst characterisation and testing in cyclohexane isomerisation are given in Chapter 3.

5.2.2 Isomerisation of cyclohexane

The isomerization of cyclohexane was carried out in a H_2 flow at 180-300 °C. The catalysts were tested under ambient pressure at a ratio of cyclohexane and H_2 partial pressures of 0.04-0.14 in a Pyrex fixed-bed down-flow microreactor (9 mm internal diameter) fitted with an on-line gas chromatograph (Varian 3800 instrument with a 30 m x 0.25 mm x 0.5 μm HP INNOWAX capillary column and a flame ionisation detector). The temperature in the reactor was controlled by a Eurotherm controller (±0.5 °C) using a thermocouple placed at the top of the catalyst bed. Cyclohexane was fed by passing H_2 flow controlled by a Brooks mass flow controller through a stainless-steel saturator, which held cyclohexane at 0 °C (ice bath) to maintain the chosen reactant partial pressure of 3.4 kPa (3.4 mol% concentration of cyclohexane in H_2 flow). The concentration of cyclohexane was varied by diluting the

gas flow with H_2. The downstream gas lines and valves were heated to 150 °C to prevent substrate and product condensation. The gas feed entered the reactor from the top at a flow rate of 20 mL min^{-1}. The reactor was packed with 0.20 g catalyst powder of 45-180 μm particle size. Prior to reaction, the catalysts were pre-treated in situ for 1 h at the reaction temperature in H_2 flow. The reaction was carried out at a space time W/F = 24 – 118 g h mol^{-1}, where W is the catalyst weight and F is the inlet molar flow rate of cyclohexane. Product selectivity was defined as moles of product formed per one mole of cyclohexane converted and quoted in mole per cent. The mean absolute percentage error in conversion and selectivity was ≤ 5% and the carbon balance was maintained within 95%. Reaction rates (R) were determined as $R = XF/W$ (in mol $g_{cat}^{-1}h^{-1}$), where X is the fractional conversion of cyclohexane. Generally, the reaction was carried out at differential conditions ($X \leq 0.1$), where X is directly proportional to the reaction rate. Whenever required, the catalysts were diluted with silica in order to achieve a low conversion. Pt/CsPW and Au/CsPW catalysts showed stable performance in cyclohexane isomerization, reaching steady state within 30 – 70 min time on stream (TOS). Generally, their deactivation did not exceed 10-15% of the initial conversion rate over 12 h TOS. For calculating the reaction rates, initial conversion values X at 70 – 100 min TOS were used.

Table 5.1 Information about catalysts.

Catalyst[a]	S_{BET}[b]	Pore volume[c]	Pore size[d]	D[e]	d[f]
	m^2g^{-1}	cm^3g^{-1}	Å		nm
$H_3PW_{12}O_{40}$ (HPW)	7.8	0.012	63		
$Cs_{2.5}H_{0.5}PW_{12}O_{40}$ (CsPW)	139	0.079	23		
6.0%Pt/CsPW	84	0.052	25	0.17[h]	4.7[i]
5.6%Pt/CsPW-b[g]	105	0.068	26	0.15[h]	6.0[i]
5.9%Pt/4.4%Au/CsPW	62	0.065	42	0.27[h]	5.3[i]
4.7%Au/CsPW[j]	103	0.048	33	≥0.09[i]	≤10[k]
Darco KB-B activated carbon	977	0.89	35		
5.0%Au/C	1207	1.00	33	0.094[i]	9.6[k]
6.2%Pt/C	1224	1.04	34	0.26[i]	3.5[k]; 3.0[l]
6.7%Pt/5.0%Au/C	1177	0.98	33	0.21[i]	4.2 Pt[l]
				0.02[i]	54 Au[l]

[a]Metal catalysts prepared by impregnating H_2PtCl_6 and $HAuCl_4$ onto CsPW or activated carbon from aqueous medium; metal loading determined from ICP-AES analysis. [b]BET surface area. [c]Single point total pore volume at P/P_o = 0.97. [d]Average BET pore diameter. [e]Metal dispersion. [f]Metal particle size. [g]The catalyst prepared by impregnating $Pt(acac)_2$ onto CsPW from benzene solution. [h]Pt dispersion from H_2/O_2 titration; for PtAu catalysts, assumed negligible H_2 adsorption on gold. [i]Calculated from the equation d (nm) = 0.9/D. [j]No H_2 adsorption observed on the Au/CsPW catalyst. [k]Metal particle diameter from TEM and STEM. [l]Metal particle diameter from powder XRD (Scherrer equation).

5.3 Results and discussion

5.3.1 Thermodynamics of isomerisation of cyclohexane

The thermodynamic analysis (Scheme 5.3) includes calculation of the Gibbs free energy and equilibrium conversion for the isomerisation of cyclohexane in the ideal gas system at 473.15 K (200 °C) and 1 bar pressure. Initial thermodynamic data including the formation functions $\Delta_f G^o$ and $\Delta_f H^o$ together with S^o and C_p at standard conditions (298.15 K and 1 bar) are presented in Table 5.2 [21, 22].

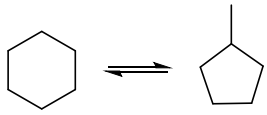

Scheme 5.3 Thermodynamics of isomerisation of cyclohexane.

Table 5.2 Initial thermodynamic data (298.15 K, 1 bar, ideal gas).

Compound	$\Delta_f H^o$	S^o	C_p
	kJ/mol	J/mol K	J/mol K
Cyclohexane	-123.1	298.2	105.3
Methylcyclopentane	-106.6	339.7	109.7

The equations used for the calculations are given below, where K_p is the equilibrium constant and x is the equilibrium conversion of cyclohexane. These are practically independent of the pressure and dilution as the total number of reactant and

product molecules does not change in the reaction ("volume neutral" reaction). ΔC_p was assumed to be independent of temperature, i.e., $\Delta C_p = \Delta C_p^o$. The results are presented in Table 5.3. The equilibrium conversion of cyclohexane was calculated to be 70% at 200 °C and 1 bar pressure,

$$\Delta H = \Delta H^o + \Delta C_p^o (T - 298.15)$$

$$\Delta S = \Delta S^o + \Delta C_p^o \ln(T/298.15)$$

$$\Delta G = \Delta H - T\Delta S$$

$$K_p = exp(-\Delta G/RT) \quad (R = 8.314 \text{ J/mol K})$$

$$K_p = \frac{x}{1 - x}$$

$$x = \frac{K_p}{1 + K_p}$$

Table 5.3 Thermodynamics of cyclohexane isomerisation at 200 °C (473.15 K) and 1 bar pressure.

ΔH^o	ΔS^o	ΔC_p^o	ΔG^o	ΔH^{473}	ΔS^{473}	ΔG^{473}	K_p	x
kJ/mol	J/mol K	J/mol K	kJ/mol	kJ/mol	J/mol K	kJ/mol		
16.5	41.5	4.4	4.1	17.3	43.5	-3.3	2.3	0.70

5.3.2 Acid-catalysed isomerisation of cyclohexane over CsPW

Bulk heteropoly acid HPW had small activity in cyclohexane isomerisation (Table 5.4) despite its very strong Brønsted acidity [26]. This can be explained by the low surface area of HPW (7.8 m^2g) (Table 5.1), hence low density of surface proton sites in the catalyst. In contrast, CsPW, despite its somewhat weaker acidity compared to the bulk HPW [26], showed relatively high initial activity in this reaction, although suffered from strong deactivation, as seen in Figure 5.1. The higher activity of CsPW can be attributed to its larger surface area (139 m^2g), hence larger (about 3-fold) density of surface proton sites, as compared to HPW. Similar results have been reported for the isomerisation of n-hexane [17]. The strong catalyst deactivation can be attributed to coke deposition originated from alkene oligomerisation (Scheme 5.1). CsPW, initially white, turned black after reaction (200 °C, 18 h on stream, Figure 5.1). From combustion chemical analysis, the spent catalyst contained 0.76 wt% of carbon. Methylcyclopentane (MCP) was the main product of cyclohexane isomerisation: 98% selectivity, with 2% of cracking products (mainly C_3-C_4 hydrocarbons). C_{6+} hydrocarbons were not observed in reaction products, which indicates the monomolecular mechanism of cyclohexane isomerisation over CsPW (Scheme 5.1). It should be noted that the selectivity did not change over entire range of the time on stream despite strong catalyst deactivation. Besides, the results practically did not change when using N_2 instead of H_2 as the carrier gas.

5.3.3 Isomerisation of cyclohexane over bifunctional metal-acid catalysts

CsPW-supported and physically mixed bifunctional metal-acid catalysts in the presence of H_2 were much more efficient in cyclohexane isomerisation than CsPW

alone. All bifunctional catalysts showed similar initial deactivation profiles – a sharp initial drop in cyclohexane conversion (probably due to deactivation of the strongest proton sites in CsPW) followed by steady-state course. As expected, Pt/CsPW (prepared from H_2PtCl_6 in aqueous medium) showed much higher catalytic activity than CsPW (Table 5.4) and a very good performance stability during 12 h on stream (Figure 5.1). Pt/CsPW-b catalyst prepared from $Pt(acac)_2$ in benzene with similar Pt loading and dispersion (Table 5.1) was twice as active as Pt/CsPW (Table 5.4) and showed stable performance during 20 h on stream (Figure 5.1). The higher activity of Pt/CsPW-b may be explained by stronger acidity of the CsPW support due to the water-free preparation procedure. At about 6% Pt loading, cyclohexane dehydrogenation step is likely to be equilibrated (see below), and the isomerisation of cyclohexyl carbenium ion becomes the rate-limiting step (Scheme 5.2). Consequently, the rate of the isomerisation step should increase with increasing catalyst acid strength, leading to an increase in the overall reaction rate as observed in the case of Pt/CsPW-b in comparison to Pt/CsPW. The amount of coke in spent Pt/CsPW and Pt/CsPW-b catalysts was below detection limit. However, in the absence of H_2 when using N_2 as the carrier gas, Pt/CsPW and Pt/CsPW-b catalysts predictably suffered strong deactivation just as CsPW alone did. Unexpectedly, Au/CsPW showed a relatively high activity (Table 5.4) and excellent performance stability during 20 h on stream (Figure 5.1). This is different from n-hexane isomerisation, where Au/CsPW was virtually inactive

Table 5.4 Isomerisation of cyclohexane over acid and bifunctional metal-acid catalysts.[a]

Catalyst	T (°C)	TOS[b] (h)	Conv.[c] (%)	Select.[c] (%)	
				C_6H_6	MCP
HPW	200	2.5	0.5	0	>99
CsPW	200	6.0	3.0	0	98
6.0%Pt/CsPW	200	6.0	15	0	>99
5.6%Pt/CsPW-b	200	6.0	27	0	>99
4.7%Au/CsPW	200	6.0	7.1	0	>99
6.2%Pt/C+CsPW(1:5w/w, 1.0%Pt)[d]	200	4.0	12	0	>99
6.2%Pt/C+CsPW (1:5 w/w, 1.0%Pt)[d]	250	4.0	26	15	85
6.2%Pt/C+CsPW (1:5 w/w, 1.0%Pt)[d]	300	4.0	55	62	38

[a]0.20 g catalyst, 3.4 kPa cyclohexane partial pressure, 20 mL min^{-1} H_2 flow, 200 °C, W/F = 118 g h mol^{-1}, catalyst pretreatment at 200 °C/1h in H_2 flow. [b]Time on stream. [c]Cyclohexane conversion and methylcyclopentane selectivity at the TOS given; C_3-C_4 cracking by-products also formed, but no C_{6+} hydrocarbons observed. [d]Physical mixture of 6.2%Pt/C and CsPW (0.20 g in total).

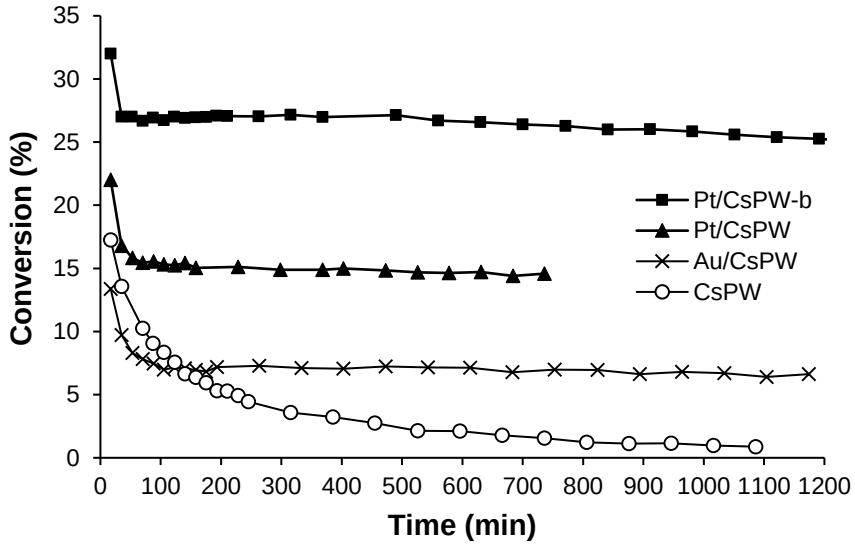

Figure 5.1 Time course for cyclohexane isomerisation in the presence of CsPW, 4.7%Au/CsPW, 6.0%Pt/CsPW and 5.6%PtCsPW-b catalysts (0.20 g) at 200 °C, 3.4 kPa cyclohexane pressure, 20 mL min^{-1} H_2 flow rate, W/F = 118 g h mol^{-1}. For all catalysts, MCP selectivity ≥99% over entire range of TOS.

Physically mixed Pt/C + CsPW bifunctional catalysts had activities comparable to those of the CsPW-supported catalysts Pt/CsPW (Table 5.4). This suggests that the reaction is not limited by migration of alkene intermediates between the metal and acid sites in bifunctional catalysts since in the mixed catalysts their H^+ and Pt surface sites are far apart compared to the supported Pt/CsPW catalysts (micrometer versus nanometer distance).

Both Pt and Au bifunctional catalysts had very high selectivity to MCP (>99%) at least up to 27% cyclohexane conversion at 200 °C (Table 5.4). It should be pointed out that under the chosen reaction conditions, cyclohexane-to-MCP isomerisation was far from equilibrium and occurred under kinetic control. The equilibrium conversion

of cyclohexane to MCP at 200 °C was calculated to be 70% (Supporting Information), in agreement with the literature [4]. The absence of C_{6+} hydrocarbons in reaction products suggests the reaction occurring via the monomolecular mechanism as shown in Scheme 5.2. At higher temperatures, 250-300 °C, benzene was also formed at the expense of MCP by dehydrogenation of cyclohexane on Pt sites. As expected, the selectivity to benzene increased with increasing the temperature, reaching 62% at 300 °C (Table 5.4).

The kinetics of alkane isomerisation in the presence of bifunctional Pt-acid catalysts based on heteropoly acids and zeolites has been discussed previously [15, 16, 27, 28]. Since cyclohexane is stable toward cracking (Table 5.4), the rate of its isomerisation can be approximated by the rate of cyclohexane conversion (in the absence of benzene formation). It has been shown that when the dehydrogenation step is at equilibrium and the isomerisation step is rate limiting (Scheme 5.2), the isomerisation turnover rate obeys Equation 5.1, where K_d is the equilibrium constant of dehydrogenation, K_p is the equilibrium constant of protonation, k_i is the isomerisation rate constant, P_{C6} is the cyclohexane partial pressure, P_{H2} is the hydrogen partial pressure and α is the reaction order ($\alpha \leq 1$) [27, 28]. This equation was derived in Chapter 4 (Equation 4.14)

$$\frac{R}{[H^+]_t} = \frac{k_i K_d K_p \left(\frac{P_{C6}}{P_{H_2}}\right)}{1+K_d K_p \left(\frac{P_{C6}}{P_{H_2}}\right)} \approx k_i \left(K_d K_p \frac{P_{C6}}{P_{H_2}}\right)^a \qquad (5.1)$$

It has been shown that the rate limiting step is determined by the molar ratio of surface metal and acid sites Pt_s/H^+ [[4, 15, 17, 27-29]. In the case of Pt–zeolite catalysts, including H-MOR, H-BEA, H-USY, etc., the alkane dehydrogenation step

is typically equilibrated at $Pt_s/H^+ < 0.1$, so that the isomerisation step becomes rate limiting [27, 29]. In the case of Pt-HPA catalysts having stronger proton sites than those in zeolites [30], a higher Pt_s/H^+ molar ratio is required for the dehydrogenation step to attain equilibrium [15, 17]. In the isomerisation of n-hexane over Pt/CsPW, the dehydrogenation step has been found to equilibrate at $Pt_s/H^+ \geq 0.8$ [17].

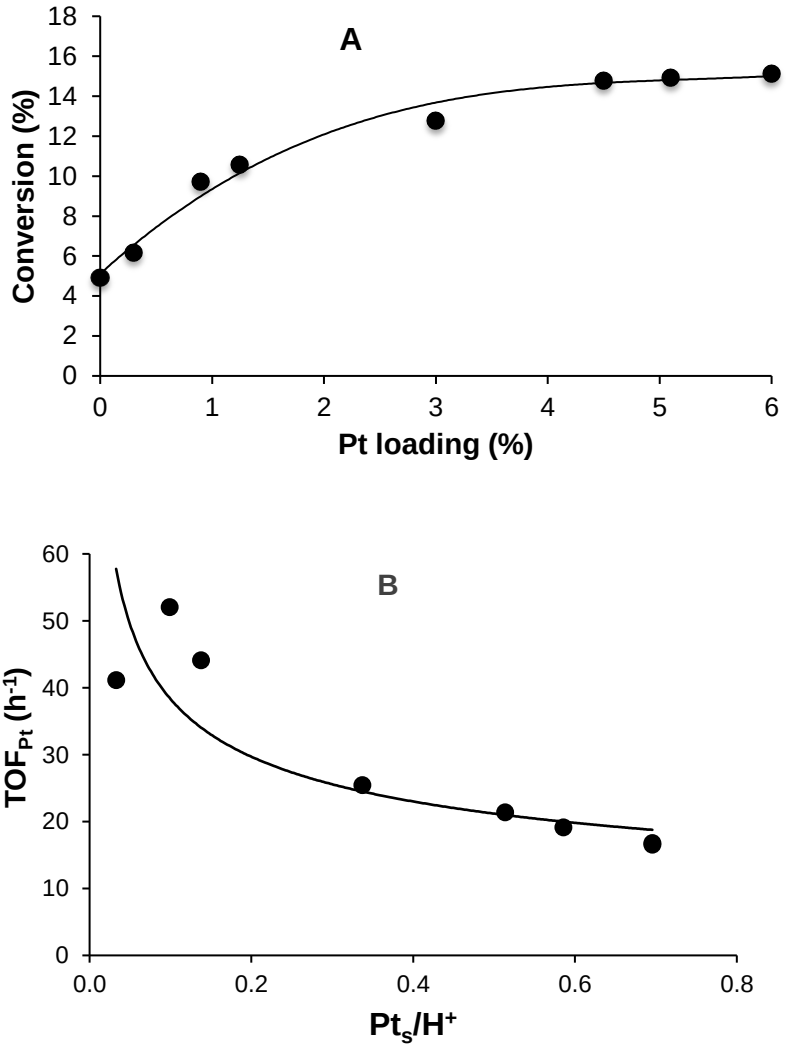

Figure 5.2 Plot of cyclohexane conversion versus Pt loading (A) and plot of TOF_{Pt} versus molar ratio of Pt_s and H^+ surface sites (B) for cyclohexane isomerisation over 6.0%Pt/CsPW: varied amount of 6.0%Pt/CsPW diluted by CsPW to 0.20 g, 200 °C, 3.4 kPa cyclohexane partial pressure, 20 mL min^{-1} H_2 flow rate.

Figure 5.2A shows a plot of cyclohexane conversion over Pt/CsPW versus Pt loading. It can be seen that the conversion increases with the Pt loading, plateauing out at about 6% Pt loading. The same data are presented in Figure 5.2B as turnover frequency TOF_{Pt} versus the Pt_s/H^+ ratio; the TOF_{Pt} values were calculated per surface Pt atom using the cyclohexane conversion data at 200 °C and Pt dispersion from Table 5.1. When calculating TOF_{Pt}, the minor contribution of CsPW was subtracted from the total conversion. The density of surface proton sites in CsPW was calculated using a cross section of 144 $Å^2$ for the Keggin heteropoly anion [7, 20] and the CsPW surface area of 139 m^2g^{-1} (Table 5.1) supposing that the number of accessible protons was 0.5 per Keggin unit at the surface; this gave a proton site density of 0.080 mmol g^{-1}. Also it was suggested that the H^+ surface density was not affected by Pt. As anticipated from Scheme 5.2, TOF_{Pt} diminishes as the Pt_s/H^+ ratio increases, reaching a plateau as the dehydrogenation step attains quasi-equilibrium (Figure 5.2B). This demonstrates that over Pt/CsPW catalyst, cyclohexane dehydrogenation step is equilibrated at $Pt_s/H^+ \geq 0.7$, corresponding to a Pt loading ≥ 6%. As expected, this Pt_s/H^+ value is higher than that for Pt/zeolite catalysts due to the stronger acidity of CsPW in comparison to zeolites. Similar results were also obtained for the Pt/CsPW-b prepared using the chloride-free anhydrous procedure (Figure 5.3).

The apparent activation energy, E_a, for cyclohexane isomerisation over 6.0%Pt/CsPW and 5.6%Pt/CsPW-b was found 131 and 120 kJ mol^{-1}, respectively, in 180-220 °C temperature range. The corresponding Arrhenius plots are shown in Figure 5.4 (these plots use the differential conversion of cyclohexane X, which is directly proportional to the reaction rate). These high E_a values indicate no diffusion limitations in cyclohexane isomerisation over these catalysts.

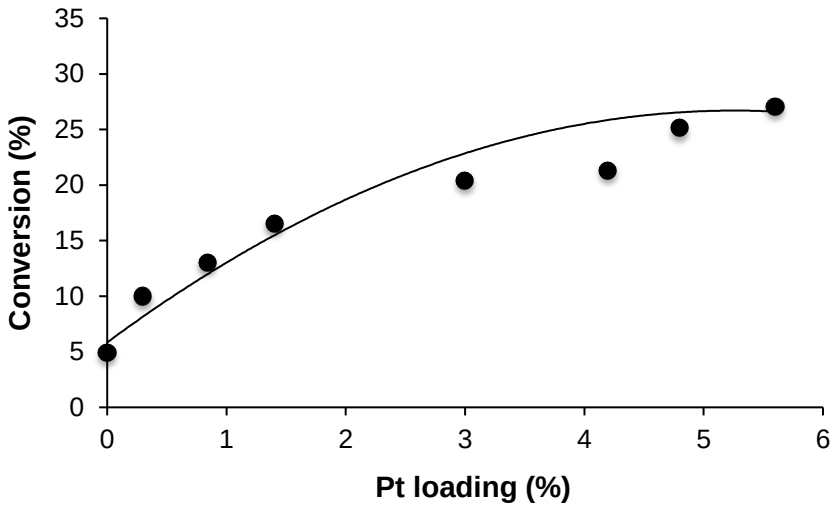

Figure 5.3 Plot of cyclohexane conversion versus Pt loading: varied amount of 5.9%Pt/CsPW-b catalyst diluted by CsPW to 0.20 g, 200 °C, 3.4 kPa cyclohexane partial pressure in H_2 flow (20 mL min^{-1}), W/F = 118 g h mol^{-1}.

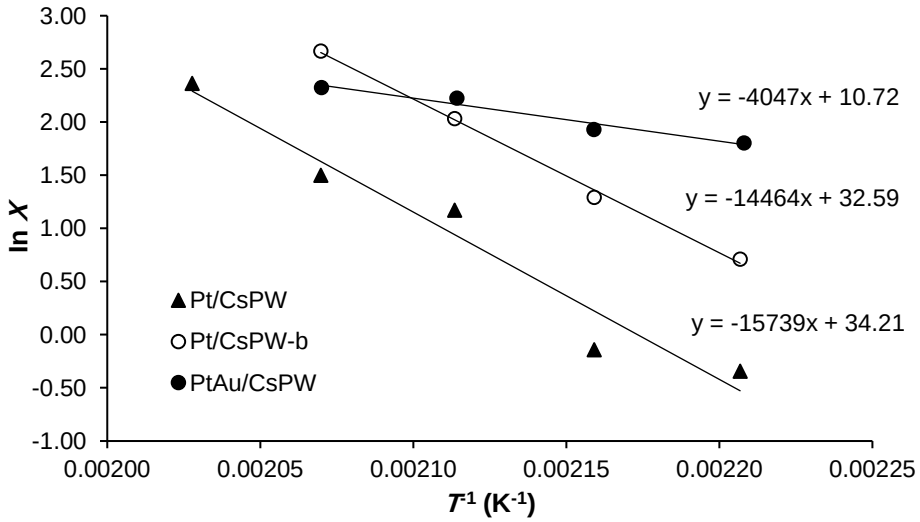

Figure 5.4 Arrhenius plot for cyclohexane isomerisation: 6.0%Pt/CsPW (0.04 g) + SiO_2 (0.16 g) (E_a = 131 kJ mol^{-1}); 5.6%Pt/CsPW-b (0.04 g) + SiO_2 (0.16 g) (E_a = 120 kJ mol^{-1}); 5.9%Pt/4.4%Au/CsPW (0.04 g) + SiO_2 (0.16 g) (E_a = 34 kJ mol^{-1}); 3.4 kPa cyclohexane partial pressure, 20 mL min^{-1} H_2 flow rate; X is the differential fractional conversion.

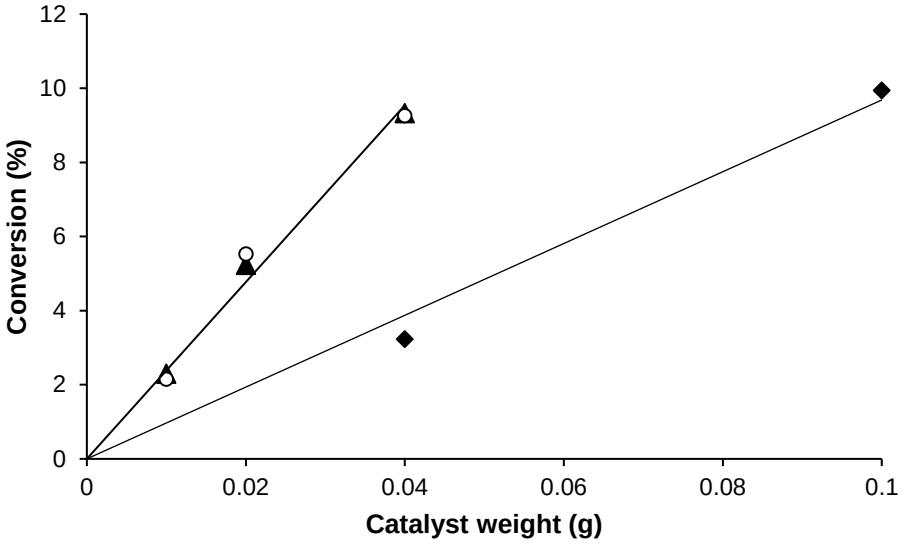

Figure 5.5 Plot of cyclohexane conversion (differential data) versus catalyst weight: 6%Pt/CsPW (diamonds), 5.6%Pt/CsPW-b (circles), 5.9%Pt/4.4%Au/CsPW (triangles); varied amount of catalysts diluted with SiO_2 to 0.20 g; 200 °C, 3.4 kPa cyclohexane partial pressure, 20 mL min^{-1} H_2 flow rate.

The isomerisation reaction order in Pt/CsPW and Pt/CsPW-b catalysts was close to 1 (Figure 5.5). The order in cyclohexane was found to be 0.49 and 0.55 for Pt/CsPW and Pt/CsPW-b, respectively (Figure 5.6, where P_{C6} is varied at practically constant P_{H2}). These results comply with Equation 5.1. Also in agreement with Equation 5.1, the initial rate of reaction over Pt/CsPW increased with decreasing the hydrogen pressure P_{H2} (Table 5.3); simultaneously increased the rate of catalyst deactivation, as seen from the reaction course at longer times on stream (Figure 5.7). Therefore, the kinetics is in fairly good agreement with the rate equation (Equation 5.1), considering that cyclohexane dehydrogenation step was not always at equilibrium in these reaction systems.

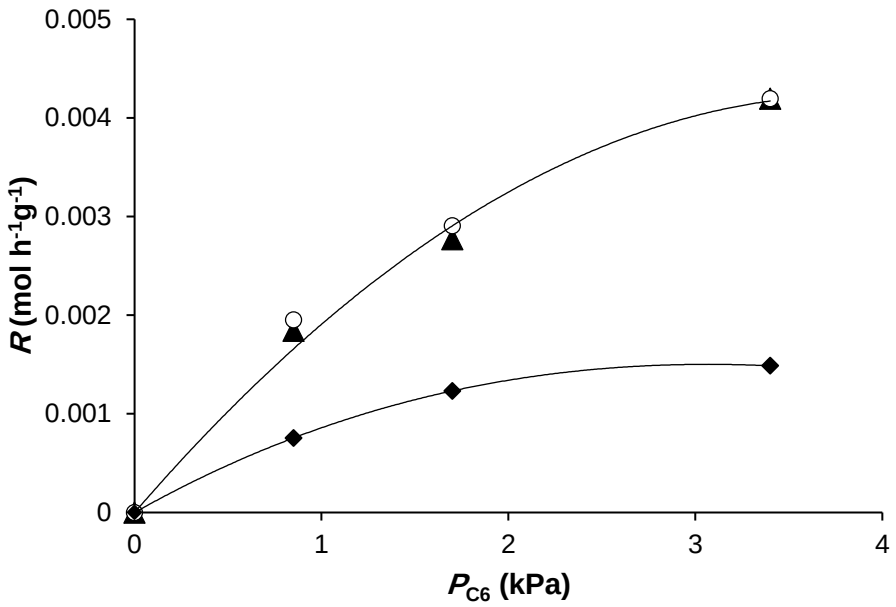

Figure 5.6 Plot of reaction rate versus cyclohexane partial pressure: 5.9%Pt/4.4%Au/CsPW (0.04 g) + SiO_2 (0.16 g) (triangles, order in cyclohexane 0.59), 5.6%Pt/CsPW-b (0.04 g) + SiO_2 (0.16 g) (circles, order in cyclohexane 0.55), 6.0%Pt/CsPW (0.04 g) + SiO_2 (0.16 g) (diamonds, order in cyclohexane 0.49); 200 °C, 20 mL min^{-1} flow rate, P_{H2} = 96–99 kPa.

Table 5.5 Effect of hydrogen pressure on the rate of cyclohexane isomerisation.[a]

H_2 pressure (kPa)	97	73	48	24
Initial conversion (%)	3.9	5.5	4.4	4.0
10^3 Initial rate (mol $g^{-1}h^{-1}$)[b]	1.6	2.3	1.9	1.7

[a] Catalyst 6.0%Pt/CsPW (0.04 g) + SiO_2 (0.16 g), 3.4 kPa cyclohexane partial pressure, 200 °C, 20 mL min^{-1} rate of H_2 + N_2 flow at different H_2/N_2 volume ratios. [b]Reaction rate calculated from $R = XF/W$, where X is the initial fractional conversion of cyclohexane and the space time W/F = 24 mol $g^{-1}h^{-1}$.

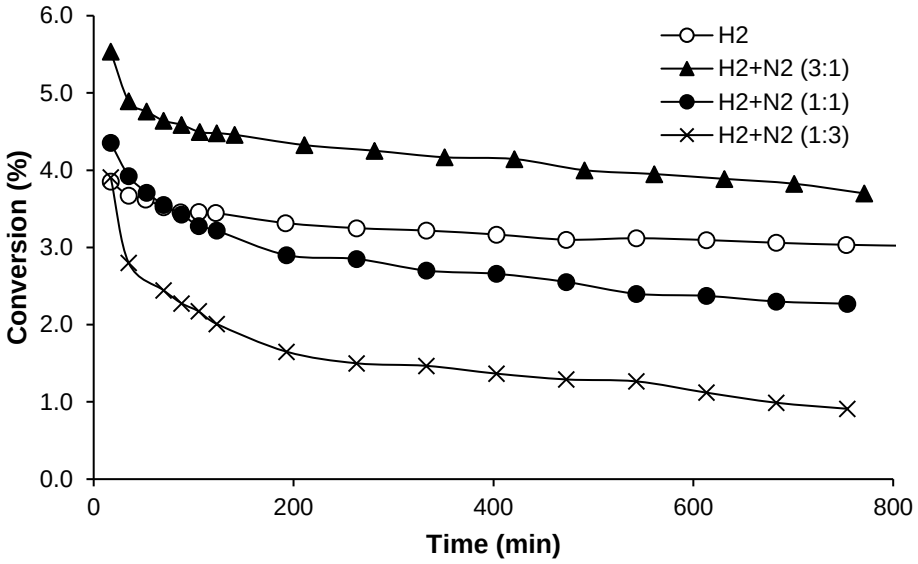

Figure 5.7 Effect of hydrogen pressure on activity of 6.0%Pt/CsPW catalyst (3.4 kPa cyclohexane partial pressure, 200 °C, 20 mL min^{-1} rate of H_2 + N_2 flow at different H_2/N_2 volume ratios).

5.3.4 Effect of gold

There has been a continued interest in bimetallic catalysis since the discovery of superior properties of PtSn, PtIr and PtRe catalysts in petrochemistry and petroleum reforming in the 1960s ([30, 31] and references therein). Bimetallic catalysts often exhibit higher catalytic activity than either of their components due to a better stability to deactivation. Typically, hydrogenolysis of C-C bond is suppressed in favour of reactions such as hydrogenation, dehydrogenation and isomerisation, leading to an increase in reaction selectivity. It is suggested that the enhanced performance of bimetallic catalysts is mainly determined by the geometric ensemble size effect, and an electronic ligand effect may also take place [30,31].

PtAu and PdAu bimetallic catalysts often exhibit an enhanced activity in comparison to monometallic Pt and Pd catalysts ([17, 25, 30-49]), for example in hydrogenation [50], hydrodeoxygenation [24, 34], hydrodesulfurisation [40, 41], oxidation [35-37] and other reactions [30, 31, 33, 38, 39]. PdAu/HY and PtAu/HY have been used for isomerisation of methylcyclopentane [17] and n-hexane [49]. For the methylcyclopentane isomerisation, the PdAu/HY and PtAu/HY catalysts exhibited an increase in activity and selectivity in comparison with the corresponding Pd/HY and Pt/HY catalysts. No such effect has been observed for the n-hexane isomerisation, though. Previously, we have reported an Au enhancement for the isomerisation of n- hexane catalysed by PtAu/CsPW and attributed it to PtAu bimetallics [17].

In this work, we examined the effect of gold on the activity and selectivity of Pt/CsPW and Pt/C + CsPW physically mixed catalysts in the isomerisation of cyclohexane as well as in the accompanying dehydrogenation of cyclohexane to benzene and attempted to assess the effect of gold on the turnover reaction rate at Pt sites. The supported bimetallic catalysts 5.9%Pt/4.4%Au/CsPW and 6.7%Pt/5.0%Au/C were prepared by co-impregnation of H_2PtCl_6 and $HAuCl_4$ precursors onto CsPW and activated carbon, respectively, from aqueous medium followed by reduction with H_2 at 250 °C. This preparation is likely to give supported bimetallic PtAu particles of a random composition together with monometallic Pt and Au particles, rather than relatively uniform bimetallics that can be obtained by size-controlled synthesis in solution [39]. Table 5.1 presents the texture and metal dispersion for these catalysts. Notably, the addition of Au to Pt/CsPW catalyst increased the Pt dispersion from 0.17±0.02 to 0.27±0.02% (average values from four H_2/O_2 titrations); in contrast, Au addition to Pt/C virtually did not alter Pt dispersion.

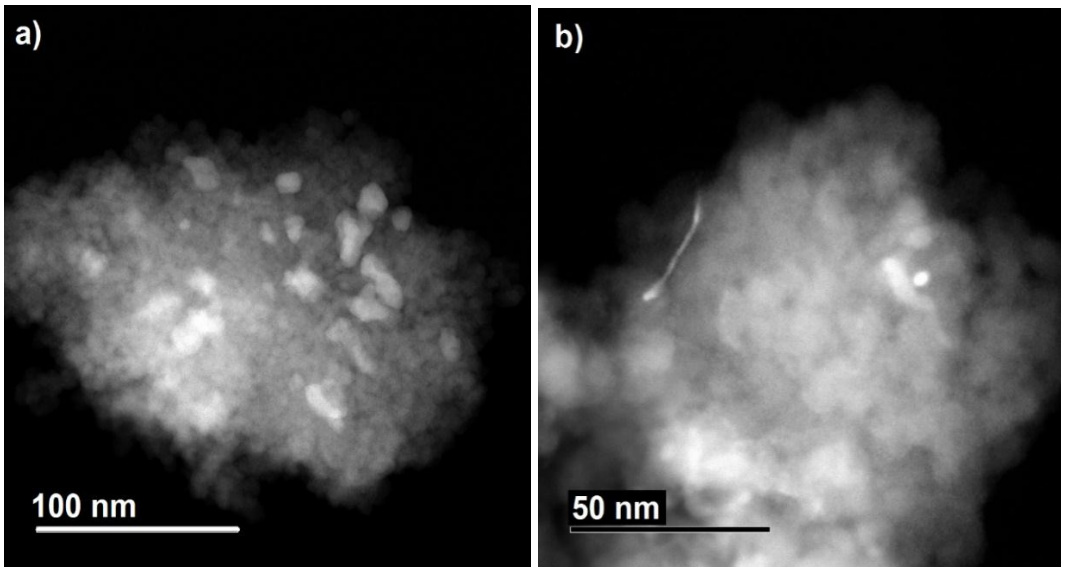

Figure 5.8 HAADF-STEM images of (a) 5.0%Au/CsPW and (b) 5.6%Pt/4.3%Au/CsPW catalysts, displaying noble metal particles as bright spots. Elongated PtAu nanostructures can be seen in image (b).

Previously, PtAu/CsPW, Pt/CsPW and Au/CsPW catalyst have been characterised by STEM-EDX and powder XRD [16, 24]. These catalysts consist of 10-20 nm CsPW particles (*bcc* crystal structure with a lattice constant of 12 Å) and contain noble metal particles from ~20 nm down to metal atoms. Au/CsPW has larger Au particles up to ~20 nm, whereas Pt/CsPW has smaller particles, less than 5 nm. The bimetallic PtAu/CsPW catalyst shows a similar content and, in addition to monometallic Pt and Au particles, contains non-uniform bimetallic PtAu particles with a Pt/Au atomic ratio varying from 0.5 to 7.7 (Figure 3.19). The appearance of the PtAu nanostructures is frequently more elongated than those in Au/CsPW, as can be seen in Figure 3.19and Figure 5.8. It should be noted that the STEM images of PtAu/CsPW are difficult to examine because W, Pt and Au have similar large atomic numbers *Z* (74, 78, and 79, respectively). Besides, CsPW containing ca. 70 wt% of tungsten

exhibits a strong background which obscures smaller Pt and Au particles in the *Z*- contrast high-angle annular dark field (HAADF) images which makes it difficult to determine precisely metal particle size distribution. XRD analysis of metal particle size is also difficult due to the dominated pattern of the crystalline CsPW.

Representative results of catalyst testing at 200 °C and 6 h TOS are shown in Table 5.4. These include two sets of testing of Pt/CsPW, Au/CsPW, Pt/CsPW + Au/CsPW and PtAu/CsPW catalysts with the same Pt and Au content in each set: 0.59-0.60% Pt and 0.44-0.47% Au in the first set and 1.2% Pt and 0.88-0.94% Au in the second. The content of CsPW was also kept constant in each set. The full reaction time courses (12-14 h TOS) for the first set are shown in Figure 5.9. The time courses for the second set were similar, but with higher conversion rates, as expected. These reactions notably exhibit a stronger catalyst deactivation than the reactions shown in Figure 5.1 because of the lower metal content. Under such conditions, Au and CsPW made very small contributions to the cyclohexane conversion. As seen in Table 5.6, the bimetallic PtAu/CsPW catalyst is more active than the either of Pt/CsPW and Au/CsPW catalysts and the two of them together (cf. entry 4 with 5 and 9 with 10). With PtAu/CsPW catalyst, cyclohexane conversion increased by a factor of 2.2 at 0.6% Pt content and by a factor of 1.7 at 1.2% Pt content in comparison with the combined activity of Pt/CsPW + Au/CsPW at 200 °C (note that the compared catalysts in entries 4 and 5 as well as 9 and 10 have the same Pt, Au and CsPW content). Evidently, the scale of gold effect on catalyst activity depends on the Pt content, that is on the extent of equilibration of cyclohexane dehydrogenation step (Scheme 5.2). The effect of gold is stronger when the dehydrogenation step is the rate-limiting one and decreases as this step approaches equilibrium

Table 5.6 Effect of gold on isomerisation of cyclohexane over Pt/CsPW bifunctional catalysts.[a]

Catalyst[b]	Conv.[c] (%)
1) CsPW + SiO_2 (2:8 w/w)	0.5
2) 4.7%Au/CsPW + CsPW + SiO_2 (1:1:8 w/w, 0.47%Au)	0.9
3) 6.0%Pt/CsPW + CsPW + SiO_2 (1:1:8 w/w, 0.60%Pt)	3.3
4) 5.9%Pt/4.4%Au/CsPW + CsPW + SiO_2 (1:1:8 w/w, 0.59%Pt, 0.44%Au)	7.4
5) 6.0%Pt/CsPW + 4.7%Au/CsPW + SiO_2 (1:1:8 w/w, 0.60%Pt, 0.47%Au)	3.3
6) CsPW + SiO_2 (2:3 w/w)	0.8
7) 4.7%Au/CsPW + CsPW + SiO_2 (1:1:3 w/w, 0.94%Au)	1.1
8) 6.0%Pt/CsPW + CsPW + SiO_2 (1:1:3 w/w, 1.2%Pt)	6.1
9) 5.9%Pt/4.4%Au/CsPW + CsPW + SiO_2 (1:1:3 w/w, 1.2%Pt, 0.88%Au)	11.0
10) 6.0%Pt/CsPW + 4.7%Au/CsPW + SiO_2 (1:1:3 w/w, 1.2%Pt, 0.94%Au)	6.8

[a] 200 °C, 3.4 kPa cyclohexane partial pressure, 20 mL min^{-1} H_2 flow rate, 6 h time on stream, *W/F* = 24 g h mol^{-1} (entries 1-5) and 47 g h mol^{-1} (entries 6-10), catalyst pretreatment at 200 °C/1h in H_2 flow. [b]Catalysts (0.20 g) were physical mixtures prepared by grinding all components together. [c]Cyclohexane conversion at 6 h TOS; MCP selectivity >98% with C_3-C_4 cracking by-products formed; no C_{6+} hydrocarbons observed.

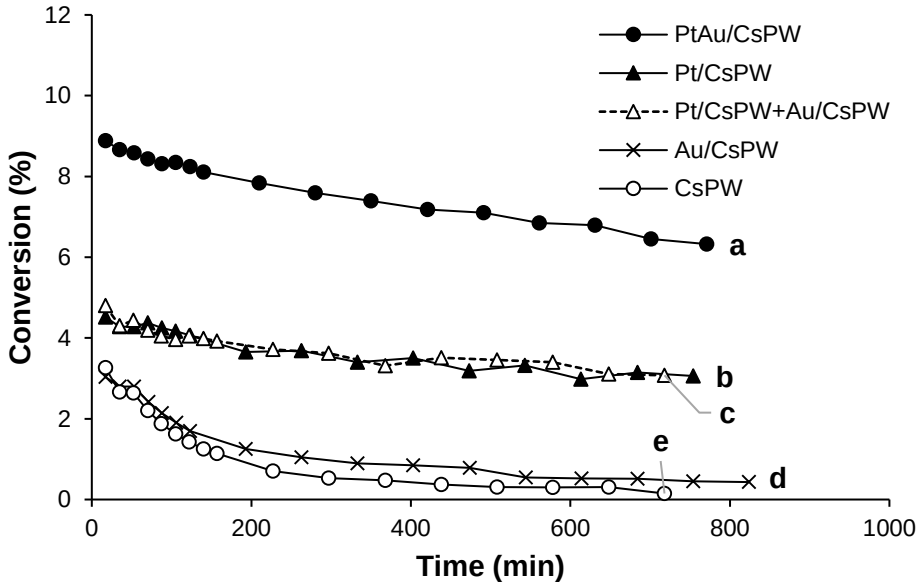

Figure 5.9 Time course for cyclohexane isomerisation in the presence of CsPW-supported bifunctional catalysts physically mixed with CsPW and SiO_2 (0.20 g total weight) with comparable metal and CsPW content. From top to bottom: (a) 5.9%Pt/4.4%Au/CsPW (0.02 g) + CsPW (0.02 g) + SiO_2 (0.16 g); (b) 6.0%Pt/CsPW (0.02 g) + CsPW (0.02 g) + SiO_2 (0.16); (c) 6.0%Pt/CsPW (0.02 g) + 4.7%Au/CsPW (0.02 g) + SiO_2 (0.16 g); (d) 4.7%Au/CsPW (0.02 g) + CsPW (0.02 g) + SiO_2 (0.16 g); (e) CsPW (0.04 g) + SiO_2 (0.16 g); 200 °C, 3.4 kPa cyclohexane pressure, 20 mL min^{-1} H_2 flow rate, W/F = 24 g h mol^{-1}, catalyst pre-treatment at 200 °C/1h in H_2 flow.

While enhancing cyclohexane conversion, gold additives did not influence reaction selectivity. This suggests that the gold affects the metal-catalysed dehydrogenation reaction step, not the subsequent transformations of carbenium ions (Scheme 5.2). Although Au shows some activity, it is most likely that it is the Pt that plays a major role [16]. The effect of gold on the turnover rate at a surface Pt site was estimated by subtracting the contribution of CsPW (entries 1 and 6) and using the Pt

dispersion for PtAu/CsPW (D = 0.27) and Pt/CsPW (D = 0.17) (Table 5.1). This gave a 1.6-fold increase in the turnover rate at Pt sites at 0.6% Pt content and a tiny (1.1-fold) increase for the PtAu/CsPW catalyst at 1.2% Pt content. Since, the turnover rate at Pt sites is only moderately affected by gold additives, the Au enhancement observed can be attributed primarily to the geometric effect due to the increase in the Pt dispersion in the bimetallic PtAu/CsPW catalyst

The electronic state of Pt in PtAu/CsPW is probably unaffected by the gold as evidenced by H_2-TPD (Figure 5.10). It can be seen that H_2 desorption occurs at the same temperature, ca. 90 °C, for both Pt/CsPW and PtAu/CsPW catalysts, with suggests the lack of ligand effect of gold on Pt sites.

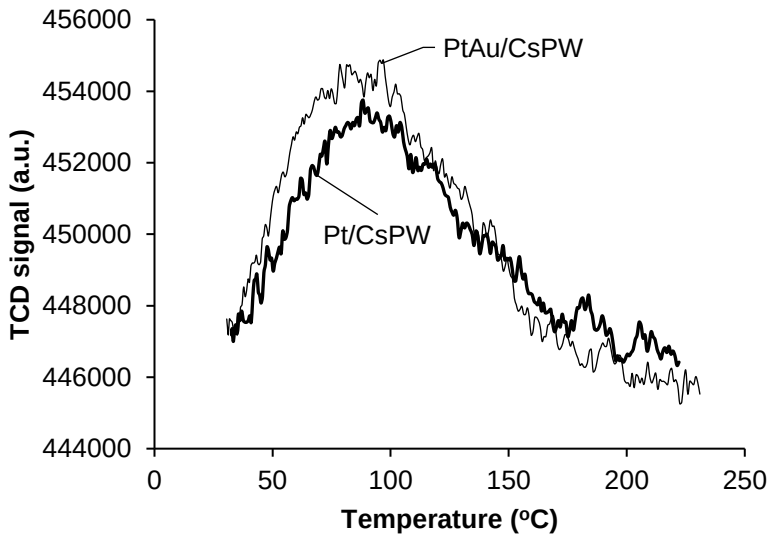

Figure 5.10 H_2-TPD for 6.0%Pt/CsPW (64 mg) and 5.9%Pt/4.4%Au/CsPW (75 mg) at 10 °C min^{-1} temperature ramp rate and 50 mL min^{-1} N_2 flow rate.

Reaction kinetics with PtAu/CsPW was found similar to that with monometallic Pt/CsPW. It was first order in the catalyst (Figure 5.5) and 0.59 order in

cyclohexane (Figure 5.6), in agreement with the rate (Equation 5.1). Important difference is that the reaction with PtAu/CsPW occurred with much lower activation energy of 34 kJ mol^{-1} than with Pt/CsPW (131 kJ mol^{-1}). It should be noted that for n-hexane isomerisation these activation energies have been found quite close [16]. This may be rationalised considering the different geometry of cyclohexane and n-hexane adsorption on platinum. Cyclohexane will probably require a larger surface Pt ensemble (e.g., Balandin's sextet [51]), whereas there is no such requirement for n-hexane adsorption. As can be seen from the Arrhenius plot (Figure 5.4), cyclohexane conversion with PtAu/CsPW is higher than with Pt/CsPW, which confirms the gold enhancement for the whole 180-220 °C temperature range.

At higher reaction temperatures (250-300 °C), cyclohexane isomerisation was accompanied by cyclohexane dehydrogenation to benzene (Table 5.4). This dehydrogenation reaction was also found to exhibit significant Au enhancement, especially regarding the selectivity to benzene (Table 5.5). At 280 °C, the bimetallic PtAu/CsPW catalyst gave an initial cyclohexane conversion 1.3-fold higher and benzene selectivity 3.5-fold higher than the Pt/CsPW + Au/CsPW physical mixture. Although these reactions suffered stronger deactivation than those at 200 °C, showing a 3-fold decrease in conversion in 4 h TOS (Figure 5.11 and 5.12), their selectivity pattern remained stable over the entire time course. The average enhancement factors (1.5- and 2.4-fold, respectively) were close to the above initial figures. The smaller Au effect on cyclohexane conversion (compared to 2.2-fold at 200 °C) is in agreement with the lower activation energy of cyclohexane isomerisation with PtAu/CsPW in comparison with Pt/CsPW. Besides, at 280 °C, the reaction may be limited by the isomerisation step rather than the dehydrogenation step (Scheme 5.2). The effect of

Au on cyclohexane isomerisation stems from the Au enhancement of partial dehydrogenation of cyclohexane to cyclohexene (Scheme 5.2)

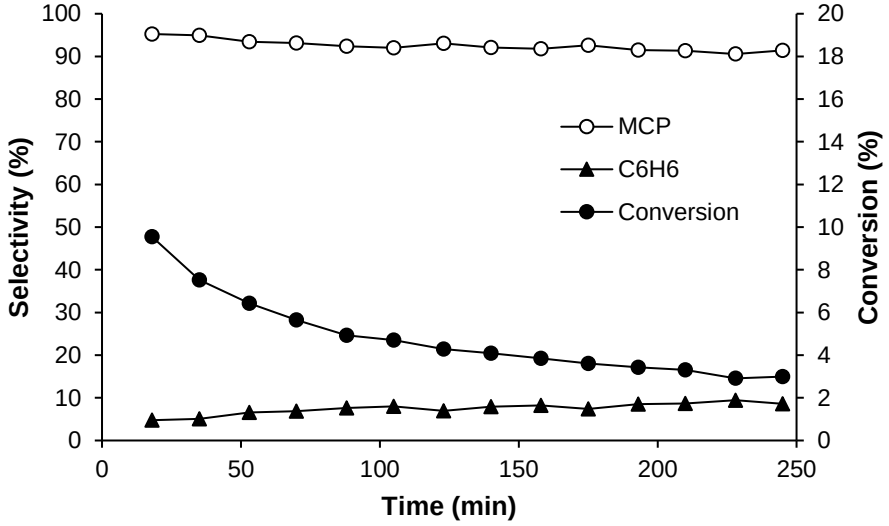

Figure 5.11 Time course for cyclohexane isomerisation in the presence of catalyst 6.0%Pt/CsPW + 4.7%Au/CsPW + SiO_2 (1:1:3 w/w, 1.2%Pt, 0.94%Au) at 200 °C, 3.4 kPa cyclohexane pressure, 20 mL min^{-1} H_2 flow rate, *W/F* = 47 g h mol^{-1}.

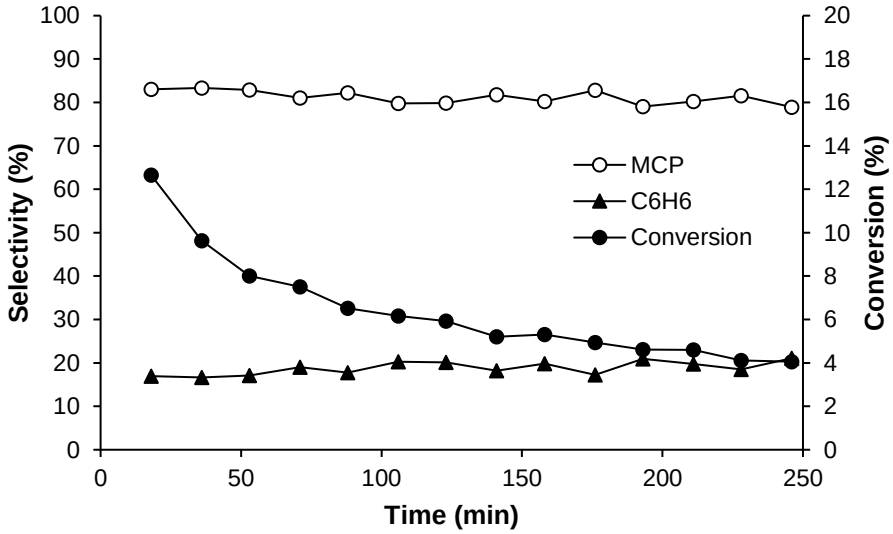

Figure 5.12 Time course for cyclohexane isomerisation in the presence of catalyst 5.9%Pt/4.4%Au/CsPW + CsPW + SiO_2 (1:1:3 w/w, 1.2%Pt, 0.88%Au) at 200 °C, 3.4 kPa cyclohexane pressure, 20 mL min^{-1} H_2 flow rate, *W/F* = 47 g h mol^{-1}.

As the complete cyclohexane dehydrogenation to benzene is more thermodynamically feasible, a greater Au effect on this reaction may be expected, which indeed proved to be the case. Previously, the Au enhancement of dehydrogenation of methylcyclohexane to toluene over $PtAu/Al_2O_3$ has been reported [52].

Table 5.7 Effect of gold on benzene selectivity over Pt/CsPW bifunctional catalysts.[a]

Catalyst	Conversion (%)	Selectivity (%)	
		Methylcyclopntane	Benzene
Pt + Au[b]	9.6	95	5.0
PtAu[c]	13	83	17

[a] 280 °C, 3.4 kPa cyclohexane partial pressure, 20 mL min^{-1} H_2 flow rate, 18 min time on stream, W/F = 47 g h mol^{-1}, catalyst pre-treatment at 280 °C/1h in H_2 flow. [b] Catalyst: 6.0%Pt/CsPW + 4.7%Au/CsPW + SiO_2 (1:1:3 w/w, 1.2%Pt, 0.94%Au). [c] Catalyst: 5.9%Pt/4.4%Au/CsPW + CsPW + SiO_2 (1:1:3 w/w, 1.2%Pt, 0.88%Au).

It was interesting to examine the effect of support on the gold enhancement. In this regard, we tested carbon-supported physically mixed catalysts, namely PtAu/C + CsPW against Pt/C + CsPW. The Pt/C + CsPW catalyst showed a high activity, which was comparable to that of Pt/CsPW (Table 5.4). The representative results are shown in Table 6. It can be seen that Au/C has much lower activity than Pt/C based on the metal loading (cf. entry 2 and 3, with CsPW contribution to be subtracted). The values

of TOF_{Pt} and TOF_{Au} are 110 and 21 h^{-1} at 200 °C, respectively (calculated using the metal dispersion from Table 5.1). This means that the turnover activity of Au, although lower than that of Pt, is not negligible. It is due to the low dispersion of Au (Table 5.1, Figure 3.16) that it has low activity based on the total metal weight. From the data shown in Table 5.6, it is evident that there is no Au enhancement in this system since the Pt/C and PtAu/C catalysts have the same activity (cf. entries 3 and 4).

Table 5.8 Effect of gold on isomerisation of cyclohexane over Pt/C + CsPW bifunctional catalysts.[a]

Catalyst[b]	Conversion[c] (%)
1) CsPW	3.0
2) 5.0%Au/C + CsPW (1:11 w/w, 0.42%Au)	3.5
3) 6.2%Pt/C + CsPW (1:11 w/w, 0.52%Pt)	12
4) 6.7%Pt/5.0%Au/C+CsPW (1:11 w/w, 0.56%Pt, 0.42%Au)	12

[a] 200 °C, 3.4 kPa cyclohexane partial pressure, 20 mL min^{-1} H_2 flow rate, 6 h time on stream, W/F = 118 g h mol^{-1}, catalyst pre-treatment at 200 °C /1h in H_2 flow. [b] Catalysts (0.20 g) were physical mixtures prepared by grinding all components together. [c] Cyclohexane conversion at 6 h TOS; MCP selectivity >98% with C_3-C_4 cracking by- products formed; no C_{6+} hydrocarbons observed.

Further, our STEM-EDX analysis of PtAu/C failed to reveal the presence of Au-reach bimetallic PtAu particles, only Pt-reach particles with atomic ratios Pt/Au ≥ 15 were found (Figure 3.21). The XRD (Figure 5.12) shows that Au is present on the

carbon surface in the form of large particles of 50-60 nm volume average size, whereas Pt is in a highly dispersed state (4.2 nm particle size). There is hardly any PtAu alloying to be seen in these patterns. TEM images of PtAu/C (Figure 5.13) show an array of finely dispersed particles (2-8 nm), presumed to be Pt, and very large Au particles of 40-80 nm in size. The large particles observed in PtAu/C samples resemble those seen in Au/C samples (9.6±3.4 nm mean size, Figure 3.16), but are strikingly different in size to Pt/C (3.5±0.7 nm mean size, Figure 3.17). Therefore, there is no evidence for any significant modification of Pt sites with Au on the carbon surface. This explains the lack of Au enhancement of activity of the carbon-supported Pt catalyst.

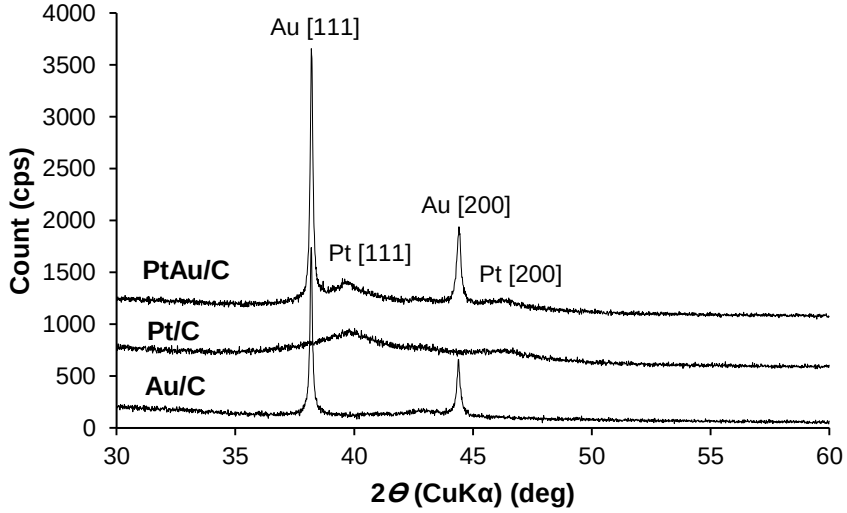

Figure 5.12 Powder XRD patterns for 5.0%Au/C (Au particle size 62 nm from the Scherrer equation), 6.2%Pt/C (Pt particle size 3.0 nm) and 6.7%Pt/5.0%Au/C (metal particle size: Pt 4.2 nm and Au 54 nm).

The results obtained in this work demonstrate that Au additives enhance the activity of bifunctional Pt/CsPW catalyst in isomerisation of cyclohexane by enhancing the alkane dehydrogenation step. The effect of Au can be accredited

primarily to the increase in Pt dispersion in the bimetallic PtAu/CsPW catalyst. The Au effect on cyclohexane isomerisation is at its maximum when the dehydrogenation is the rate-limiting step. The effect of Au declines as the dehydrogenation step draws nearer quasi-equilibrium. In the isomerisation of cyclohexane over Pt/CsPW catalyst, the dehydrogenation step is equilibrated at a surface sites molar ratio $Pt_s/H^+ \geq 0.7$. Therefore, in this system, the Au effect is observable at $Pt_s/H^+ < 0.7$. For Pt/zeolite catalysts, the dehydrogenation step approaches quasi-equilibrium at $Pt_s/H^+ < 0.1$ [26,28] due to the weaker acidity of zeolites in comparison to CsPW [7, 20]. In this case, the gold enhancement should be expected at $Pt_s/H^+ << 0.1$.

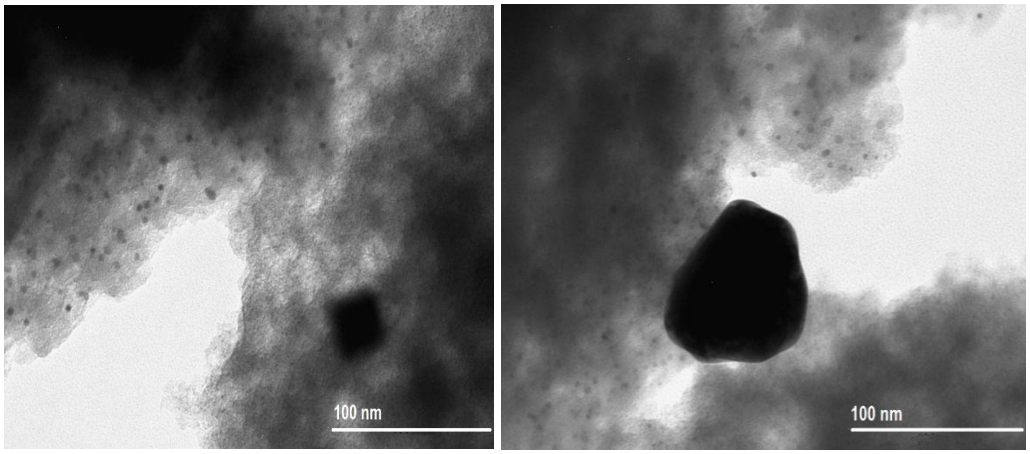

Figure 5. 13 TEM images of 6.7%Pt/5.0%Au/C showing an array of relatively small (2 – 8 nm) metal particles, mostly Pt, and very large Au particles 40 – 80 nm in size.

From the data obtained, the origin of Au enhancement can be assigned to the geometric ensemble size effect in PtAu bimetallic species [30,31]. STEM-EDX and XRD indicate the presence of PtAu bimetallic particles in the PtAu/CsPW catalyst [16, 24]. The geometric effect may be rationalised in terms of Balandin's theory of catalysis

[51] assuming a gold-induced geometric adjustment of the Pt sextet active site required for adsorption of cyclohexane [51]. This is supported by the increase in Pt dispersion in the PtAu/CsPW catalyst (Table 5.1). The gold effect appears to be dependent on the nature of support. Thus, the carbon-supported catalyst PtAu/C lacks any performance enhancement by the gold, and there is no evidence of modification of the Pt sites with Au in this catalyst. Further insights into the Au effect may be gained through in-depth structural characterisation of PtAu/CsPW catalyst supplemented by computational analysis.

5.4 Conclusions

Isomerisation of cycloalkanes is of interest for the reduction of carcinogenic aromatic compounds in gasoline. The isomerisation of cyclohexane was studied in the presence of metal-acid bifunctional catalysts based on Keggin heteropoly salt $Cs_{2.5}H_{0.5}PW_{12}O_{40}$ (CsPW) using Pt and Au as the metal components. The bifunctional pathway involves cyclohexane dehydrogenation on metal sites followed by isomerisation of cyclohexene formed to methylcyclopentene on acid sites; the latter is finally hydrogenated on metal sites to produce methylcyclopentane with high selectivity (>99%). With Pt/CsPW, cyclohexane dehydrogenation step reaches quasi-equilibrium at a molar ratio of Pt_s and H^+ surface sites $Pt_s/H^+ \geq 0.7$, which is much higher than for Pt/zeolite catalysts. PtAu/CsPW bimetallic catalyst exhibited a 2-fold higher activity in cyclohexane isomerisation and a 3.5-fold higher activity in the accompanying dehydrogenation of cyclohexane to benzene than the mixture of Pt/CsPW and Au/CsPW with the same metal loading. The effect of gold is assigned to the increase in Pt dispersion in PtAu bimetallic particles. STEM-EDX revealed PtAu

bimetallic particles in PtAu/CsPW with a wide range of Pt/Au atomic ratios from 0.5 to 7.7. No enhancing effect of Au was found in the case of carbon-supported Pt catalyst.

References

[1] L. Lloyd, Handbook of industrial catalysts, Springer Science & Business Media, 2011.

[2] H. Arnold, F. Dobert, J. Gaube, G. Ertl, H. Knozinger, J. Weitkempl, Handbook of heterogeneous catalysis, Wiley-VCH, 2008.

[3] R. I. Watanabe, T. Suzuki, T. Okuhara, Skeletal isomerization of alkanes and hydroisomerization of benzene over solid strong acids and their bifunctional catalysts, Catalysis Today, 66 (2001) 123-130.

[4] A. Miyaji, T. Echizen, L. Li, T. Suzuki, Y. Yoshinaga, T. Okuhara, Selectivity and mechanism for skeletal isomerization of alkanes over typical solid acids and their Pt-promoted catalysts, Catalysis Today, 74 (2002) 291-297.

[5] H. Matsuhashi, H. Shibata, H. Nakamura, K. Arata, Skeletal isomerization mechanism of alkanes over solid superacid of sulfated zirconia, Applied Catalysis A: General, 187 (1999) 99-106.

[6] D. Eley, H. Pines, P.B. Weisz, Advances in catalysis and related subjects, Academic Press, 21,1963.

[7] T. Okuhara, N. Mizuno, M. Misono, Catalytic chemistry of heteropoly compounds, Advances in Catalysis, 4 (1996) 113-252.

[8] I.V. Kozhevnikov, Catalysts for fine chemical synthesis, catalysis by polyoxometalates, Wiley, 2002.

[9] S.-S. Wang, G.-Y. Yang, Recent advances in polyoxometalate-catalyzed reactions, Chemical reviews, 115 (2015) 4893-4962.

[10] A. Ivanov, T. Vasina, V. Nissenbaum, L. Kustov, M. Timofeeva, J. Houzvicka, Isomerization of n-hexane on the Pt-promoted Keggin and Dawson tungstophosphoric

heteropoly acids supported on zirconia, Applied Catalysis A: General, 259 (2004) 65-72.

[11] B. Gagea, Y. Lorgouilloux, Y. Altintas, P. Jacobs, J. Martens, Bifunctional conversion of n-decane over HPW heteropoly acid incorporated into SBA-15 during synthesis, Journal of Catalysis, 265 (2009) 99-108.

[12] J. Macht, R.T. Carr, E. Iglesia, Consequences of acid strength for isomerization and elimination catalysis on solid acids, Journal of the American Chemical Society, 131 (2009) 6554-6565.

[13] F. Lefebvre, Acid Catalysis by Heteropolyacids: Transformations of Alkanes, Current Catalysis, 6 (2017) 77-89.

[14] W. Knaeble, R.T. Carr, E. Iglesia, Mechanistic interpretation of the effects of acid strength on alkane isomerization turnover rates and selectivity, Journal of Catalysis, 319 (2014) 283-296.

[15] W. Knaeble, E. Iglesia, Acid strength and metal-acid proximity effects on methylcyclohexane ring contraction turnover rates and selectivities, Journal of Catalysis, 344 (2016) 817-830.

[16] A. Alazman, D. Belic, E.F. Kozhevnikova, I.V. Kozhevnikov, Isomerisation of n-hexane over bifunctional Pt-heteropoly acid catalyst: Enhancing effect of gold, Journal of Catalysis, 357 (2018) 80-89.

[17] G. Riahi, D. Guillemot, M. Polisset-Thfoin, A. Khodadadi, J. Fraissard, Preparation, characterization and catalytic activity of gold-based nanoparticles on HY zeolites, Catalysis Today, 72 (2002) 115-121.

[18] T. Pinto, P. Arquillière, V. Dufaud, F. Lefebvre, Isomerization of n-hexane over Pt-H3PW12O40/SBA-15 bifunctional catalysts: Effect of the preparation method on catalytic performance, Applied Catalysis A: General, 528 (2016) 44-51.

[19] Y. Izumi, M. Ono, M. Kitagawa, M. Yoshida, K. Urabe, Silica-included heteropoly compounds as solid acid catalysts, Microporous Materials, 5 (1995) 255-262.

[20] I.V. Kozhevnikov, Catalysts for fine chemical synthesis, Catalysis by polyoxometalates, Wiley, 2002.

[21] P. Linstrom, W. Mallard, NIST Chemistry Webbook (http://webbook. nist. gov/chemistry), NIST Standard Reference Database.

[22] D. Scott, W. Berg, J. McCullough, Chemical thermodynamic properties of methylcyclopentane and 1-cis-3-dimethylcyclopentane, The Journal of Physical Chemistry, 64 (1960) 906-908.

[23] K. Alharbi, W. Alharbi, E.F. Kozhevnikova, I.V. Kozhevnikov, Deoxygenation of Ethers and Esters over Bifunctional Pt–Heteropoly Acid Catalyst in the Gas Phase, ACS Catalysis, 6 (2016) 2067-2075.

[24] O. Poole, K. Alharbi, D. Belic, E.F. Kozhevnikova, I.V. Kozhevnikov, Hydrodeoxygenation of 3-pentanone over bifunctional Pt-heteropoly acid catalyst in the gas phase: Enhancing effect of gold, Applied Catalysis B: Environmental, 202 (2017) 446-453.

[25] K. Alharbi, E. Kozhevnikova, I. Kozhevnikov, Hydrogenation of ketones over bifunctional Pt-heteropoly acid catalyst in the gas phase, Applied Catalysis A: General, 504 (2015) 457-462.

[26] F. Ribeiro, C. Marcilly, M. Guisnet, Hydroisomerization of n-hexane on platinum zeolites: I. Kinetic study of the reaction on platinum/Y-zeolite catalysts: Influence of the platinum content, Journal of Catalysis, 78 (1982) 267-274.

[27] A. Van de Runstraat, J. Kamp, P. Stobbelaar, J. Van Grondelle, S. Krijnen, R. Van Santen, Kinetics of hydro-isomerization ofn-hexane over platinum containing zeolites, Journal of Catalysis, 171 (1997) 77-84.

[28] P.S. Mendes, F.M. Mota, J.M. Silva, M.F. Ribeiro, A. Daudin, C. Bouchy, A systematic study on mixtures of Pt/zeolite as hydroisomerization catalysts, Catalysis Science & Technology, 7 (2017) 1095-1107.

[29] W. Alharbi, E.F. Kozhevnikova, I.V. Kozhevnikov, Dehydration of methanol to dimethyl ether over heteropoly acid catalysts: the relationship between reaction rate and catalyst acid strength, ACS Catalysis, 5 (2015) 7186-7193.

[30] L. Guczi, Z. Schay, Role of bimetallic catalysts in catalytic hydrogenation and hydrogenolysis, Studies in Surface Science and Catalysis, 27 (1986) 313-335.

[31] G.C. Bond, Metal-catalysed reactions of hydrocarbons, Springer, 2005.

[32] B.D. Chandler, L.I. Rubinstein, L.H. Pignolet, Alkane dehydrogenation with silica supported platinum and platinum–gold catalysts derived from phosphine ligated precursors, Journal of Molecular Catalysis A: Chemical, 133 (1998) 267-282.

[33] G.J. Hutchings, Nanocrystalline gold and gold palladium alloy catalysts for chemical synthesis, Chemical Communications, (2008) 1148-1164.

[34] K. Sun, A.R. Wilson, S.T. Thompson, H.H. Lamb, Catalytic deoxygenation of octanoic acid over supported palladium: effects of particle size and alloying with gold, ACS Catalysis, 5 (2015) 1939-1948.

[35] Y.-F. Han, J.-H. Wang, D. Kumar, Z. Yan, D. Goodman, A kinetic study of vinyl acetate synthesis over Pd-based catalysts: kinetics of vinyl acetate synthesis over Pd–Au/SiO2 and Pd/SiO2 catalysts, Journal of Catalysis, 232 (2005) 467-475.

[36] E.K. Hanrieder, A. Jentys, J.A. Lercher, Impact of alkali acetate promoters on the dynamic ordering of PdAu catalysts during vinyl acetate synthesis, Journal of Catalysis, 333 (2016) 71-77.

[37] J. Xu, T. White, P. Li, C. He, J. Yu, W. Yuan, Y.-F. Han, Biphasic Pd− Au alloy catalyst for low-temperature CO oxidation, Journal of the American Chemical Society, 132 (2010) 10398-10406.

[38] B. Coq, F. Figueras, Bimetallic palladium catalysts: influence of the co-metal on the catalyst performance, Journal of Molecular Catalysis A: Chemical, 173 (2001) 117-134.

[39] F. Gao, D.W. Goodman, Pd–Au bimetallic catalysts: understanding alloy effects from planar models and (supported) nanoparticles, Chemical Society Reviews, 41 (2012) 8009-8020.

[40] A. Venezia, V. La Parola, V. Nicolı, G. Deganello, Effect of gold on the HDS activity of supported palladium catalysts, Journal of Catalysis, 212 (2002) 56-62.

[41] A. Venezia, V. La Parola, G. Deganello, B. Pawelec, J. Fierro, Synergetic effect of gold in Au/Pd catalysts during hydrodesulfurization reactions of model compounds, Journal of Catalysis, 215 (2003) 317-325.

[42] J.R.H. Van Schaik, R. Dessing, V. Ponec, Reactions of alkanes on supported Pt-Au alloys, Journal of Catalysis, 38 (1975) 273-282.

[43] Z. Karpiński, J.K. Clarke, Reactions of alkanes on iridium and iridium-gold catalysts, Journal of the Chemical Society, Faraday Transactions 1: Physical Chemistry in Condensed Phases, 71 (1975) 2310-2318.

[44] J. Clarke, A. Kane, T. Baird, Reaction of alkanes and cycloalkanes on silica-supported platinum and platinum-gold alloy catalysts, Journal of Catalysis, 64 (1980) 200-212.

[45] A.F. Kane, J.K. Clarke, Reactions of alkanes and cycloalkanes on platinum–gold alloy films, Journal of the Chemical Society, Faraday Transactions 1: Physical Chemistry in Condensed Phases, 76 (1980) 1640-1651.

[46] J. Clarke, A. Creaner, T. Baird, Preparation of supported platinum-gold catalysts and alkane reactions on selected platinum and platinum-gold supported “clusters”, Applied Catalysis, 9 (1984) 85-108.

[47] Z. Karpiński, W. Juszczyk, J. Stachurski, Isomerization of alkanes on epitaxially oriented (111) Pd–Cu and Pd–Ag alloy films, Journal of the Chemical Society, Faraday Transactions 1: Physical Chemistry in Condensed Phases, 81 (1985) 1447-1454.

[48] B.D. Chandler, A.B. Schabel, L.H. Pignolet, Preparation and characterization of supported bimetallic Pt–Au and Pt–Cu catalysts from bimetallic molecular precursors, Journal of Catalysis, 193 (2000) 186-198.

[49] J. Fraissard, V. Gerda, K.I. Patrylak, Y.G. Voloshyna, Isomerization of hexane on PtAu nanoparticles supported on zeolites, Catalysis Today, 122 (2007) 338-340.

[50] T.J. Schwartz, S.D. Lyman, A.H. Motagamwala, M.A. Mellmer, J.A. Dumesic, Selective hydrogenation of unsaturated carbon–carbon bonds in aromatic-containing platform molecules, ACS Catalysis, 6 (2016) 2047-2054.

[51] A.A. Balandin, The multiplet theory of catalysis. Structural factors in catalysis, Russian Chemical Reviews, 31 (1962) 589.

[52] D. Rouabah, J. Fraissard, Pt-Au/Al2O3 Catalysts: Preparation, Characterization, and Dehydrogenation Activity, Journal of Catalysis, 144 (1993) 30-37.

Chapter 6. Conclusions

Isomerisation of alkanes and cycloalkanes in the presence of bifunctional metal-acid catalysts is an important process for the synthesis of high-octane fuel components. The aim of this study was to gain a better understanding of bifunctional metal-acid catalysis for the isomerisation of n-hexane and cyclohexane. We investigated vital reaction pathways of the gas-phase isomerisation of n-hexane and cyclohexane in the presence of bifunctional metal-acid catalysts based on Keggin heteropoly acids using a fixed-bed continuous flow reactor. The HPAs chosen as acid components for this study were tungstophosphoric acid $H_3PW_{12}O_{40}$ and its acidic caesium salt $Cs_{2.5}H_{0.5}PW_{12}O_{40}$ (CsPW), with the main focus on CsPW as the acidic support. Pt, Au and bimetallic PtAu were chosen the metal components. Also we investigated the effect of Au additives to Pt in the bifunctional metal-acid catalysts on the performance of Pt active sites with respect to catalyst stability, reaction selectivity and turnover reaction rate. Furthermore, kinetics of n-hexane and cyclohexane isomerisation over bifunctional metal-acid catalysts was studied in order to elucidate the effect of reaction parameters such as the temperature, pressure and catalyst loading.

The catalysts were prepared following conventional procedures and characterised using various techniques such as X-ray diffraction (XRD), surface area and porosity analysis (BET), inductively coupled plasma atomic emission spectroscopy (ICP-AES), , hydrogen and CO chemisorption, temperature programmed desorption (H_2-TPD) and scanning transmission electron microscopy with energy dispersive X-ray spectroscopy analysis (STEM-EDX).

It was demonstrated that isomerisation of both n-hexane and cyclohexane over a Pt–heteropoly acid catalysts is an effective pathway to produce branched isomers.

The results obtained in this study were disseminated in two papers published in catalysis journals of high international standing (Journal of Catalysis 357 (2018) 80–89 and ACS Catalysis 9 (2019) 5063−5073).

Isomerisation of n-hexane over Pt–CsPW bifunctional catalysts was studied using a fixed-bed microreactor under differential conditions (n-hexane conversion ≤ 10%) at 180-220 °C, ambient pressure and a ratio of n-hexane and H_2 partial pressures of 0.06-0.24. Differential conditions far from equilibrium allowed for accurate determination of reaction turnover rates. First, we looked at the acid-catalysed n-hexane isomerisation in the presence of HPAs as monofunctional acid catalysts in the absence of a metal component. This reaction was found to occur readily to form 2-metylpentane and 3-methylpentane as the main products, although the conversion rate quickly declined due to catalyst deactivation caused by coking. The turnover rate of HPA-catalysed isomerisation was found to correlate with the acid strength of HPA (initial enthalpy of ammonia adsorption). Bifunctional Pt-HPA catalysts were found to be more efficient and stable to deactivation than monofunctional HPA catalysts, although reaction selectivity was practically the same in both cases. In the isomerisation over Pt/CsPW bifunctional catalyst, n-hexane dehydrogenation step was found to equilibrate at a molar ratio of Pt and H^+ surface sites $Pt_s/H^+ \geq 0.8$, corresponding to a Pt loading ≥ 6%. This Pt_s/H^+ value is significantly higher than that for Pt/zeolite catalysts reported in the literature, which can be explained by the stronger acid strength of HPAs compared to zeolites.

Regarding the effect of gold, bimetallic PtAu/CsPW catalyst was found to exhibit higher activity in n-hexane isomerisation than Pt/CsPW, although the Au alone without Pt was inert in this reaction. In the presence of Au, the turnover rate at Pt sites

increased more than twofold. The effect of Au can be attributed to PtAu alloying, which is supported by our catalyst characterisation using STEM-EDX and XRD. Thus STEM-EDX of PtAu/CsPW clearly indicated the presence of bimetallic PtAu nanoparticles with a wide range of Pt/Au atomic ratios.

Further, using similar methodology, we investigated the isomerisation of cyclohexane to methylpentane in the presence of monofunctional acid and bifunctional metal-acid catalysts based on Keggin-type heteropoly acid $H_3PW_{12}O_{40}$ and Pt and Au as the metal components. The reaction was carried out in a differential fixed-bed microreactor at 180-300°C, ambient pressure and a C_6H_{12}/H_2 partial pressure ratio of 0.04-0.14. Again, particular emphasis was placed on the acidic Cs salt, $Cs_{2.5}H_{0.5}PW_{12}O_{40}$ (CsPW) as the acid catalyst and Pt/CsPW, Au/CsPW and PtAu/CsPW as the bifunctional catalysts. As in the case of n-hexane, in cyclohexane isomerisation, Pt/CsPW and Au/CsPW were more efficient than the monofunctional acid catalyst CsPW, and again Pt/CsPW was more active than Au/CsPW, both giving >99% selectivity to methylcyclopentane. It was found that with Pt/CsPW, cyclohexane dehydrogenation step equilibrated at a molar ratio of Pt and H^+ surface sites $Pt/H^+ \geq 0.7$, which is much higher than that for Pt/zeolite. At higher temperatures (>200 ^oC), cyclohexane was found to undergo dehydrogenation to benzene along with the isomerisation to methylcyclopentane. PtAu/CsPW bimetallic catalyst exhibited a 2-fold higher activity in cyclohexane isomerization and a 3.5-fold higher activity in the accompanying dehydrogenation of cyclohexane to benzene in comparison to the mixture of Pt/CsPW and Au/CsPW with the same metal loading. As in the case of n-hexane, the enhancing effect of gold can be assigned to PtAu bimetallic particles.

The origin of Au enhancement can be assigned to the geometric ensemble size effect in PtAu bimetallic species. STEM-EDX and XRD indicate the presence of PtAu bimetallic particles in the PtAu/CsPW catalyst. The geometric effect may be rationalised in terms of Balandin's theory of catalysis assuming a gold-induced geometric adjustment of the Pt sextet active site required for adsorption of cyclohexane. This is supported by the increase in Pt dispersion in the PtAu/CsPW catalyst as compared with the gold-free Pt/CsPW. It should be noted that the gold effect appears to be dependent on the nature of support. Thus, the carbon-supported catalyst PtAu/C lacked any performance enhancement by the gold. Besides, there is no evidence of modification of the Pt sites with Au in this catalyst.

Further insights into the Au effect may be gained through in-depth structural characterisation of PtAu/CsPW catalyst supplemented by computational analysis using the density functional theory (DFT). More detailed STEM-EDX studies on PtAu/CsPW catalysts could provide more information on PtAu alloying in these catalysts. The nature of exposed active metal sites can be monitored by IR spectroscopy using CO and H_2 as the probe molecules to obtain information regarding the relative coverages of the reactive species present on the metal nanoparticles during catalysis. Another interesting question is about the effect of metal loading on the acid properties of the acidic support. This can be monitored using FTIR of adsorption of pyridine and microcalorimetry of adsorbed basic probe molecules such as ammonia and pyridine. Finally, in-depth kinetic studies could provide further knowledge on the mechanism of alkane isomerisation on the Pt/CsPW and PtAu/CsPW catalysts.